WOODHEAD PUBLISHING IN MATERIALS

European Federation of Corrosion Publications Number 42

Corrosion in refineries

Edited by J. D. Harston and F. Ropital

CRC

WP

ISSN 1354-5116

Corrosion in refineries

European Federation of Corrosion Publications
NUMBER 42

Corrosion in refineries

Edited by
J.D. Harston and F. Ropital

**Published for the European Federation of Corrosion
by Woodhead Publishing and Maney Publishing
on behalf of
The Institute of Materials, Minerals & Mining**

**CRC Press
Boca Raton Boston New York Washington, DC**

WOODHEAD PUBLISHING LIMITED
Cambridge England

Woodhead Publishing Limited and Maney Publishing Limited on behalf of
The Institute of Materials, Minerals & Mining

Published by Woodhead Publishing Limited, Abington Hall, Abington,
Cambridge CB21 6AH, England
www.woodheadpublishing.com

Published in North America by CRC Press LLC, 6000 Broken Sound Parkway, NW,
Suite 300, Boca Raton, FL 33487, USA

First published 2007 by Woodhead Publishing Limited and CRC Press LLC

British Library Cataloguing in Publication Data
A catalogue record for this book is available from the British Library.

Library of Congress Cataloging in Publication Data
A catalog record for this book is available from the Library of Congress.

Woodhead Publishing ISBN 978-1-84569-233-9 (book)
Woodhead Publishing ISBN 978-1-84569-324-4 (e-book)
CRC Press ISBN 978-1-4200-5496-5
CRC Press order number WP5496
ISSN 1354-5116

The publishers' policy is to use permanent paper from mills that operate a sustainable forestry policy, and which has been manufactured from pulp which is processed using acid-free and elementary chlorine-free practices. Furthermore, the publishers ensure that the text paper and cover board used have met acceptable environmental accreditation standards.

Typeset by Replika Press Pvt Ltd, India
Printed by TJ International Limited, Padstow, Cornwall, England

Contents

Contributor contact details *ix*

Series introduction *xii*

Volumes in the EFC series *xiv*

1 Carburisation and metal dusting of steels and high-temperature alloys by hydrocarbons 1

H. J. Grabke, Max-Planck-Institut für Eisenforschung GmbH, Germany

1.1 Introduction: Thermodynamics 1
1.2 Carburisation 2
1.3 Metal dusting 9
1.4 References 16

2 Integrity and life assessment of catalytic reformer units 18

J. M. Brear, Stress Engineering Services (Europe) Limited, UK and J. Williamson, Consultant, UK

2.1 Introduction 18
2.2 Background 19
2.3 Risk assessment 20
2.4 Fired heaters 23
2.5 Reactor vessels 30
2.6 Pipework 36
2.7 Heat exchangers 40
2.8 High-temperature hydrogen attack 43
2.9 Conclusions 45
2.10 Acknowledgements 45
2.11 References 45

3 The use of spot hydrogen flux measurements in assessing corrosion and crack risk in refinery applications 47

F. Dean, Ion Science Ltd, UK

3.1 Introduction 47
3.2 Scenarios leading to hydrogen permeation and detection 47
3.3 Measurement of hydrogen activity based on flux measurement 50
3.4 References 56

4 Degradation of carbon steel under the influence of sulfur in a refinery furnace – remaining life prediction 57

J. Hucińska, Gdańsk University of Technology, Poland

4.1 Introduction 57
4.2 Material and service conditions 57
4.3 In-service examinations 58
4.4 After-service examinations 59
4.5 Conclusions 60
4.6 References 63

5 Troubleshooting corrosion problems in HF alkylation units 64

M. Roche, Total S.A., France, C. Grenet and M. Richez, Total France

5.1 Introduction 64
5.2 Corrosion problems in HF alkylation units 64
5.3 Leak prevention in an HF alkylation unit 69
5.4 Protective coatings tests 70
5.5 Conclusions 71
5.6 References 72

6 Corrosion in the overhead system of a sour water stripper 73

O. Forsén and J. Aromaa, Helsinki University of Technology, Finland; T. Hakonen and K. Rintamäki, Neste Oy, Finland

6.1 Introduction 73
6.2 Experimental procedures 75
6.3 Test results 76
6.4 Discussion 77
6.5 References 78

7 Corrosion of aboveground storage tanks for petroleum distillates and choice of coating systems for their protection from corrosion 79

A. Groysman, Oil Refineries Ltd, Israel

7.1 Introduction 79
7.2 Experimental procedures 79
7.3 Calculations 80
7.4 Results and discussion 80
7.5 Examination and choice of coating systems for the protection of the AST from corrosion 83
7.6 Conclusions and recommendations 84
7.7 References 85

8 The use of coatings to prevent corrosion in process vessels operating at elevated temperatures and pressures 86

A. D. Gaskin, Belzona Inc., USA

8.1 Conventional materials of construction and their limitations 86
8.2 Characteristics and limitations of traditional coating systems 87
8.3 Development of high-temperature-resistant coatings 90
8.4 Practical application of the developed coating system 93
8.5 Conclusions 94

9 The Field Signature Method (FSM) of corrosion monitoring 95

H. Horn, CorrOcean ASA, Norway and D. Morton, iicorr Ltd, UK

9.1 Introduction 95
9.2 The FSM technology 95
9.3 The FSM principle 95
9.4 FSM equipment 97
9.5 Case studies 98

10 Disbonding test methodology: Definition of representative test conditions – results of an industry joint research programme 100

L. Coudreuse, CLI, France; B. Cadilhac, Total, France; C. Dumontier, CMP, France; R. Koers, Shell, The Netherlands; G. Riccardi, Nuovo Pignone, Italy; M. Roche, Total S.A. France; F. Ropital, IFP, France

10.1 Introduction 100

10.2 Background 100
10.3 The disbonding phenomenon 101
10.4 Numerical simulation of hydrogen profiles 101
10.5 Experimental approach 104
10.6 Conclusions – definition of representative test conditions 106
10.7 References 106

Index *107*

Contributor contact details

(* = main contact)

Editors

J.D. Harston
Delft House
Horsell Rise
Woking
Surrey
GU21 4BD
UK

Email: john.harston@tiscali.co.uk

F. Ropital
Institut Français du Pétrole
Direction Chimie et Physico
Chimie Appliquées
1 avenue Bois Préau
92852 Rueil-Malmaison Cedex
France

Email: francois.ropital@ifp.fr

Chapter 1

H. J. Grabke
Schinkelstr. 30 c
D-40699 Erkrath
Germany

Email: grabke@mpie.de

Chapter 2

John Williamson*
102 Murray Road
Ottershaw
Chertsey
Surrey
KT16 OHR
UK

Email: williamson.john@ntlworld.com

John M. Brear
Stress Engineering Services (Europe)
Limited
28 Ember Lane
Esher
Surrey
KT10 8EP
UK

Email: john.brear@seseurope.com

Chapter 3

Frank Dean
Ion Science Head Office
The Way
Fowlmere
Cambridge
SG8 7JU
UK

Email: Frank.Dean@ionscience.com

Chapter 4

Joanna Hucińska
Gdańsk University of Technology
Faculty of Mechanical Engineering
G. Narutowicza Str. No. 11
80-952 Gdańsk
Poland

Email: jhucinsk@pg.gda.pl

Chapter 5

Marcel Roche*, Christophe Grenet and Martin Richez
Head of Corrosion Department
Total SA
DGEP/TDO/TEC/COR
Tour Coupole 22D60
92078 Paris la Defense cedex
France

Email: Marcel.Roche@total.com

Chapter 6

Olof Forsén*, Jari Aromaa
Helsinki University of Technology
Laboratory of Corrosion and Materials Chemistry
P.O. Box 6200
02015 TKK
Finland

Email: olof.forsen@hut.fi

Tiina Hakonen
Neste Oil Oy
P.O. Box 310
FIN-06101 Porvoo
Finland

Kirsi Rintamäki
Neste Jacobs Oy
P.O. Box 310 FIN-06101
Porvoo
Finland

Chapter 7

Alec Groysman
Oil Refineries Ltd
P.O. Box 4
Haifa 31000
Israel

Email: galec@orl.co.il

Chapter 8

Alan D. Gaskin
Senior Vice President
Belzona Inc.
Miami
USA

Email: agaskin@belzona.com

Chapter 9

Derek Morton
iicorr Ltd
Greenbank Place
East Tullos Industrial Estate
Aberdeen
Scotland
AB12 3BT

Email: Derek.Morton@iicorr.com

Harald Horn
CorrOcean ASA
Teglgarden
N-7485
Trondheim
Norway

Email: harald.horn@corrocean.no

Chapter 10

L. Coudreuse
INDUSTEEL
BP368-Châteauneuf
F-42803 Rive de
Gier Cedex
France

Email: lionel.coudreuse@
industeel.arcelor.com

European Federation of Corrosion (EFC) publications: Series introduction

The EFC, incorporated in Belgium, was founded in 1955 with the purpose of promoting European co-operation in the fields of research into corrosion and corrosion prevention.

Membership of the EFC is based upon participation by corrosion societies and committees in technical Working Parties. Member societies appoint delegates to Working Parties, whose membership is expanded by personal corresponding membership.

The activities of the Working Parties cover corrosion topics associated with inhibition, education, reinforcement in concrete, microbial effects, hot gases and combustion products, environment-sensitive fracture, marine environments, refineries, surface science, physico-chemical methods of measurement, the nuclear industry, the automotive industry, computer-based information systems, coatings, tribo-corrosion and the oil and gas industry. Working Parties and Task Forces on other topics are established as required.

The Working Parties function in various ways, e.g. by preparing reports, organising symposia, conducting intensive courses and producing instructional material, including films. The activities of Working Parties are co-ordinated, through a Science and Technology Advisory Committee, by the Scientific Secretary. The administration of the EFC is handled by three Secretariats: DECHEMA e.V. in Germany, the Société de Chimie Industrielle in France, and The Institute of Materials, Minerals and Mining in the UK. These three Secretariats meet at the Board of Administrators of the EFC. There is an annual General Assembly at which delegates from all member societies meet to determine and approve EFC policy. News of EFC activities, forthcoming conferences, courses, etc., is published in a range of accredited corrosion and certain other journals throughout Europe. More detailed descriptions of activities are given in a Newsletter prepared by the Scientific Secretary.

The output of the EFC takes various forms. Papers on particular topics, for example, reviews or results of experimental work, may be published in scientific and technical journals in one or more countries in Europe. Conference proceedings are often published by the organisation responsible for the conference.

In 1987 the, then, Institute of Metals was appointed as the official EFC publisher. Although the arrangement is non-exclusive and other routes for publication are still available, it is expected that the Working Parties of the EFC will use The Institute of Materials, Minerals and Mining for publication of reports, proceedings, etc., wherever possible.

The name of The Institute of Metals was changed to The Institute of Materials on 1 January 1992 and to The Institute of Materials, Minerals and Mining with effect from 26 June 2002. The series is now published by Woodhead Publishing and Maney Publishing on behalf of The Institute of Materials, Minerals and Mining.

P. McIntyre
EFC Series Editor,
The Institute of Materials, Minerals and Mining, London, UK

EFC Secretariats are located at:

Dr B. A. Rickinson
European Federation of Corrosion, The Institute of Materials, Minerals and Mining, 1 Carlton House Terrace, London, SW1Y 5DB, UK

Dr J. P. Berge
Fédération Européenne de la Corrosion, Société de Chimie Industrielle, 28 rue Saint-Dominique, F-75007 Paris, FRANCE

Professor Dr G. Kreysa
Europäische Föderation Korrosion, DECHEMA e. V., Theodor-Heuss-Allee 25, D-60486, Frankfurt, GERMANY

Volumes in the EFC series

1 **Corrosion in the nuclear industry**
Prepared by the Working Party on Nuclear Corrosion

2 **Practical corrosion principles**
Prepared by the Working Party on Corrosion Education (Out of print)

3 **General guidelines for corrosion testing of materials for marine applications**
Prepared by the Working Party on Marine Corrosion

4 **Guidelines on electrochemical corrosion measurements**
Prepared by the Working Party on Physico-chemical Methods of Corrosion Testing

5 **Illustrated case histories of marine corrosion**
Prepared by the Working Party on Marine Corrosion

6 **Corrosion education manual**
Prepared by the Working Party on Corrosion Education

7 **Corrosion problems related to nuclear waste disposal**
Prepared by the Working Party on Nuclear Corrosion

8 **Microbial corrosion**
Prepared by the Working Party on Microbial Corrosion

9 **Microbiological degradation of materials – and methods of protection**
Prepared by the Working Party on Microbial Corrosion

10 **Marine corrosion of stainless steels: chlorination and microbial effects**
Prepared by the Working Party on Marine Corrosion

11 **Corrosion inhibitors**
Prepared by the Working Party on Inhibitors (Out of print)

12 **Modifications of passive films**
Prepared by the Working Party on Surface Science and Mechanisms of Corrosion and Protection

13 **Predicting CO_2 corrosion in the oil and gas industry**
Prepared by the Working Party on Corrosion in Oil and Gas Production (Out of print)

14 **Guidelines for methods of testing and research in high temperature corrosion**
Prepared by the Working Party on Corrosion by Hot Gases and Combustion Products

15 **Microbial corrosion (Proc. 3rd Int. EFC Workshop)**
Prepared by the Working Party on Microbial Corrosion

16 **Guidelines on materials requirements for carbon and low alloy steels for H_2S-containing environments in oil and gas production**
Prepared by the Working Party on Corrosion in Oil and Gas Production

17 **Corrosion resistant alloys for oil and gas production: guidance on general requirements and test methods for H_2S Service**
Prepared by the Working Party on Corrosion in Oil and Gas Production

18 **Stainless steel in concrete: State of the art report**
Prepared by the Working Party on Corrosion of Reinforcement in Concrete

19 **Sea water corrosion of stainless steels – mechanisms and experiences**
Prepared by the Working Parties on Marine Corrosion and Microbial Corrosion

20 **Organic and inorganic coatings for corrosion prevention – research and experiences**
Papers from EUROCORR '96

21 **Corrosion – deformation interactions**
CDI '96 in conjunction with EUROCORR '96

22 **Aspects on microbially induced corrosion**
Papers from EUROCORR '96 and the EFC Working Party on Microbial Corrosion

23 **CO_2 corrosion control in oil and gas production – design considerations**
Prepared by the Working Party on Corrosion in Oil and Gas

24 **Electrochemical rehabilitation methods for reinforced concrete structures – a state of the art report**
Prepared by the Working Party on Corrosion of Reinforced Concrete

25 **Corrosion of reinforcement in concrete – monitoring, prevention and rehabilitation**
Papers from EUROCORR '97

26 **Advances in corrosion control and materials in oil and gas production**
Papers from EUROCORR '97 and EUROCORR '98

27 **Cyclic oxidation of high temperature materials**
Proceedings of an EFC Workshop, Frankfurt/Main, 1999

28 **Electrochemical approach to selected corrosion and corrosion control**
Papers from 50th ISE Meeting, Pavia, 1999

29 **Microbial Corrosion (proceedings of the 4th international EFC workshop)**
Prepared by the Working Party on Microbial Corrosion

30 **Survey of literature on crevice corrosion (1979–1998): mechanisms, test methods and results, practical experience, protective measures and monitoring**
Prepared by F. P. Ijsseling and the Working Party on Marine Corrosion

31 **Corrosion of reinforcement in concrete: corrosion mechanisms and corrosion protection**
Papers from EUROCORR '99 and the Working Party on Corrosion of Reinforcement in Concrete

32 **Guidelines for the compilation of corrosion cost data and for the calculation of the life cycle cost of corrosion – a working party report**
Prepared by the Working Party on Corrosion in Oil and Gas Production

33 **Marine corrosion of stainless steels: testing, selection, experience, protection and monitoring**
Edited by D. Féron

34 **Lifetime modelling of high temperature corrosion processes**
Proceedings of an EFC Workshop 2001. Edited by M. Schütze, W. J. Quadakkers and J. R. Nicholls

35 **Corrosion inhibitors for steel in concrete**
Prepared by B. Elsener with support from a Task Group of Working Party 11 on Corrosion of Reinforcement in Concrete

36 **Prediction of long term corrosion behaviour in nuclear waste systems**
Edited by D. Féron and Digby D. Macdonald on behalf of Working Party 4 on Nuclear Corrosion

37 **Test methods for assessing the susceptibility of prestressing steels to hydrogen induced stress corrosion cracking**
Prepared by B. Isecke on behalf of Working Party 11 on Corrosion of Reinforcement in Concrete

38 **Corrosion of reinforcement in concrete: mechanisms, monitoring, inhibitors and rehabilitation techniques**
Edited by M. Raupach, B. Elsener, R. Polder and J. Mietz on behalf of Working Party 11 on Corrosion of Steel in Concrete

39 **The use of corrosion inhibitors in oil and gas production**
Edited by J. W. Palmer, W. Hedges and J. L. Dawson

40 **Control of corrosion in cooling waters**
Edited by J. D. Harston and F. Ropital

41 **Metal dusting, carburisation and nitridation**
Edited by H. Grabke and M. Schütze

42 **Corrosion in refineries**
Edited by J. D. Harston and F. Ropital

43 **The electrochemistry and characteristics of embeddable reference electrodes for concrete**
Prepared by R. Myrdal on behalf of Working Party 11 on Corrosion of Steel in Concrete

44 **The use of electrochemical scanning tunnelling microscopy (EC-STM) in corrosion analysis: reference material and procedural guidelines**
Prepared by R. Lindström, V. Maurice, L. Klein and P. Marcus on behalf of Working Party 6 on Surface Science

45 **Local probe techniques for corrosion research**
Edited by R. Oltra, V. Maurice, R. Akid and P. Marcus on behalf of Working Party 8 on Physico-Chemical Methods of Corrosion Testing

46 **Amine unit corrosion survey**
Edited by J. D. Harston and F. Ropital on behalf of Working Party 15 on Corrosion in the Refinery Industry

47 **Novel approaches to the improvement of high temperature corrosion resistance**
Edited by M. Schütze and W. Quadakkers on behalf of Working Party 3 on Corrosion in Hot Gases and Combustion Products

48 **Corrosion of metallic heritage artefacts: investigation, conservation and prediction of long-term behaviour**
Edited by P. Dillmann, G. Béranger, P. Piccardo and H. Matthiessen on behalf of Working Party 4 on Nuclear Corrosion

49 **Electrochemistry in light water reactors: reference electrodes, measurement, corrosion and tribocorrosion**
Edited by R.-W. Bosch, D. Féron and J.-P. Celis on behalf of Working Party 4 on Nuclear Corrosion

50 **Corrosion behaviour and protection of copper and aluminium alloys in seawater**
Edited by D. Féron on behalf of Working Party 9 on Marine Corrosion

51 **Corrosion issues in light water reactors: stress corrosion cracking**
Edited by D. Féron and J-M. Olive on behalf of Working Party 4 on Nuclear Corrosion

1

Carburisation and metal dusting of steels and high-temperature alloys by hydrocarbons

H. J. GRABKE, Max-Planck-Institut für Eisenforschung GmbH, Germany

1.1 Introduction: Thermodynamics

The two corrosion phenomena caused by carbonaceous gases, carburisation and metal dusting, are both a consequence of carbon transfer into the metal matrix of steels and alloys. In hydrocarbons, the carbon is transferred by the reaction

$$C_xH_y = y/2\ H_2 + xC \qquad [1.1]$$

The carbon may either be dissolved, form carbides or be deposited. Carbon deposition as graphite is possible at carbon activities $a_C > 1$. For hydrocarbon–hydrogen mixtures, the carbon activity can be calculated according to

$$a_C = \left(\frac{pC_xH_y}{K \cdot pH_2^{y/2}} \right) \qquad [1.2]$$

In the case of carburisation, the carbon dissolution in high-temperature alloys leads to internal carbide formation. The carbides $M_{23}C_6$ and M_7C_3 (M = Cr, Fe, Ni) are formed at low carbon activities between $10^{-3} < a_C < 10^{-2}$, starting with $M_{23}C_6$. With increasing a_C, $M_{23}C_6$ takes up more Fe and Ni and later converts to M_7C_3 [1–3].

Failure cases by carburisation occur mainly at high temperatures (>1000 °C), e.g. in the steam cracking of hydrocarbons for production of olefins (Fig. 1.1). Studies on carburisation have been conducted in CH_4/H_2 mixtures [2–6], where exact carbon activities can be established below $a_C = 1$, i.e. without carbon deposition. Some researchers have used other hydrocarbons, such as propylene, in their studies on carburisation [7, 8] which are very unstable and decompose on metal surfaces under carbon deposition. In these studies, it is assumed that $a_C = 1$ on the metal surface.

Metal dusting is to be expected if metallic materials are exposed to carbonaceous atmospheres at $a_C > 1$, i.e. subject to possible graphite formation. One may define metal dusting as a graphite growth in or into metals or alloys

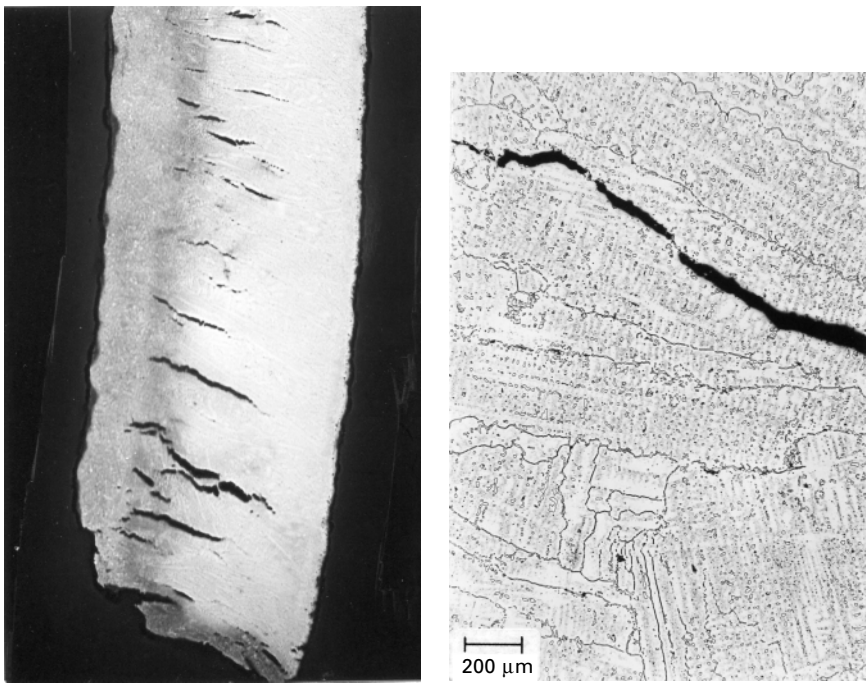

1.1 Carburisation of a tube from a cracking furnace, (a) cross-section of the tube wall showing internal cracks caused by the volume increase due to internal carbide formation progressing from the inner wall, (b) optical micrograph of the carburised microstructure with internal crack, coarse internal carbides formed at about 1100 °C.

leading to material destruction [9–15]. Failure cases caused by metal dusting have often been observed in gases containing CO and H_2, from the conversion of methane, used for synthesis of methanol, ammonia etc. or for direct reduction of iron ores. For these gas mixtures, a_C increases with decreasing temperatures so that metal dusting is imminent even at rather low temperatures (<600 °C). Failure cases caused by hydrocarbons (Fig. 1.2) have been reported only rarely [16, 17], which is surprising since many processes with hydrocarbons in the chemical and petrochemical industries are carried out at $a_C > 1$. Possible reasons for this fortunate situation are tackled in this paper.

1.2 Carburisation

Carburisation is observed in industrial processes where Fe–Ni–Cr alloys are used in carbonaceous atmospheres at high temperature, especially in the steam cracking of hydrocarbons for ethylene production. Carbon is transferred from the atmosphere into the metal matrix, diffuses inward and causes

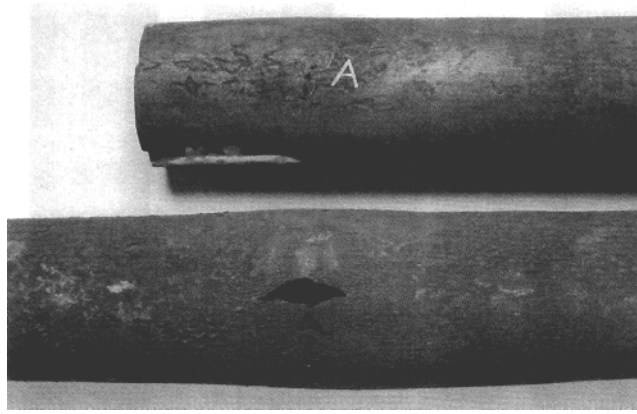

(a)

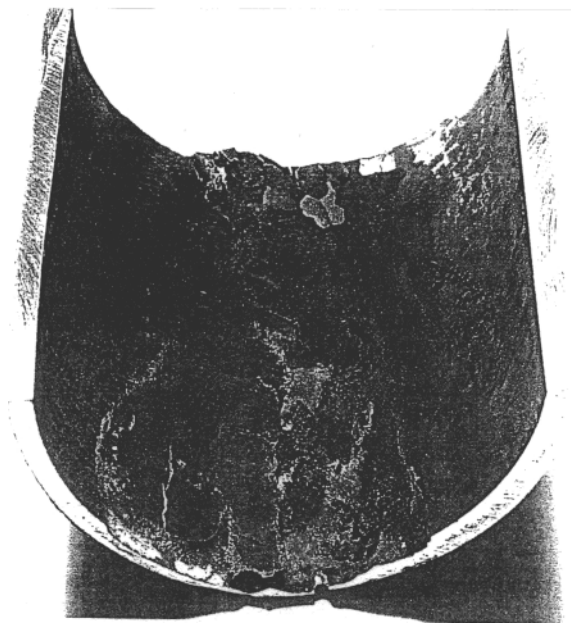

(b)

1.2 Failure case of a gas heater tube in a CCR platformer unit [17]. The newly installed 9%Cr-tube failed after 4 months by metal dusting. (a) The wall, cracked and even melted due to overheating as indicated by red scale, (b) coke deposits in the interior caused decreased heat transfer and overheating. The coke deposits stemmed from metal dusting as seen from the metallographic cross-sections: (c) showing coke on the surface and the carburised zone, and (d) a partially molten segment.

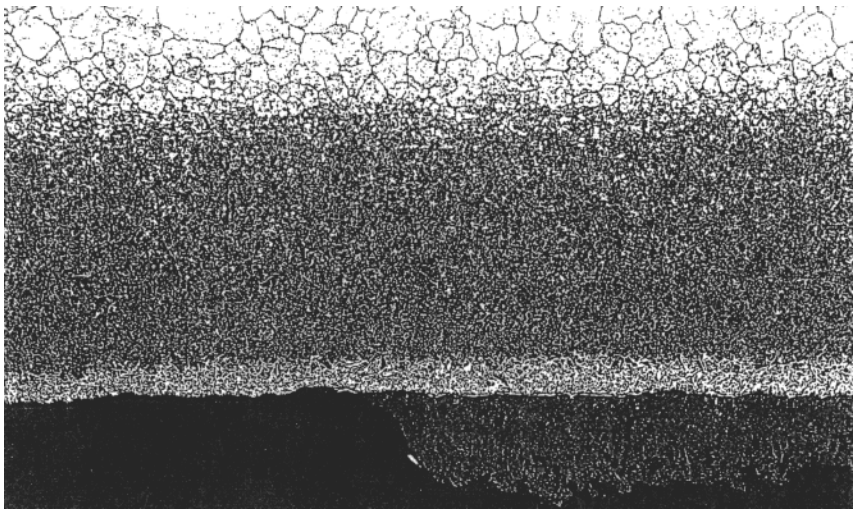

(c)

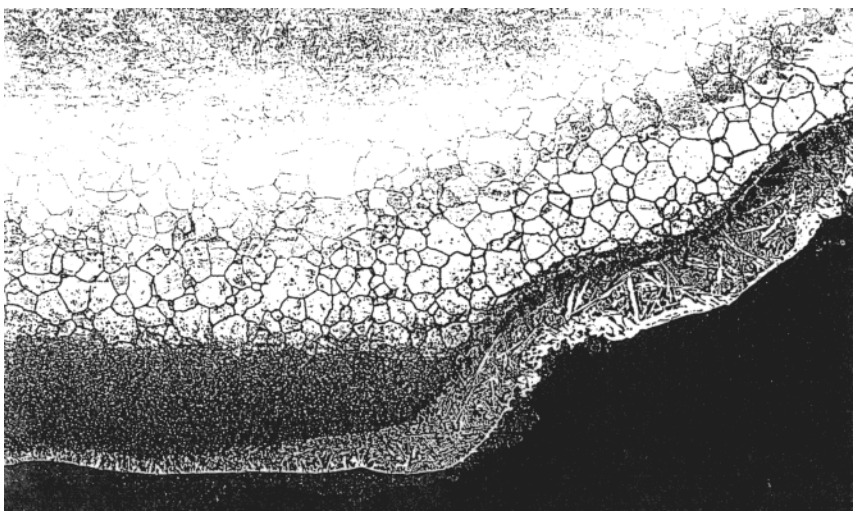

(d)

1.2 Continued

precipitation of the carbides $M_{23}C_6$ and M_7C_3 (M = Cr, Fe, Ni). At lower carbon concentration, at first the carbide $M_{23}C_6$ is formed, which is later on converted to M_7C_3 so that two zones with different precipitates are moving inward (see Fig. 1.3) [1–3]. The carburisation deteriorates the ductility and toughness of the materials, especially the low-temperature properties; additionally stresses are generated due to the volume increase by carbide formation [18]. Accordingly, failures occur, mainly when the components

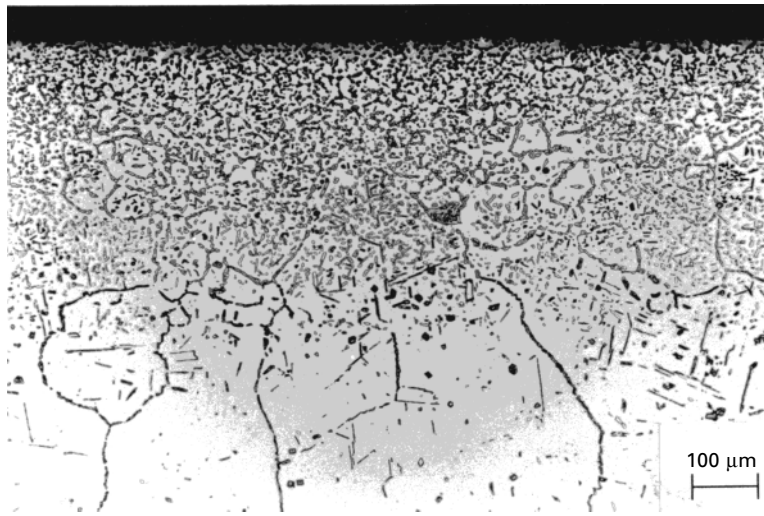

1.3 Internal carbide formation: metallographic cross-section of a sample of Alloy 800, carburised in H_2/1% CH_4 (a_C = 1) at 1000 °C; two zones with M_7C_3 and $M_{23}C_6$, and preceding $M_{23}C_6$ formation at the grain boundaries.

are cooling down during shutdown of a reactor. Generally, the effects on the high-temperature properties are less dangerous – the tensile and creep strength are improved and the ductility does not decrease markedly [18–21]. Under most conditions, the atmosphere is sufficiently oxidizing so that the alloys are protected against carburisation by an oxide layer which serves as a barrier against carbon ingress [22].

Carburisation is a corrosion problem mainly for cracking tubes in ethylene production, but also for components of industrial furnaces for steel heat treatments and sometimes for reformer tubes in steam-reforming of natural gas. The usual cast or wrought materials, HK 40, HP 40, Alloy 800 and 802 etc., with 20–45% Ni and 20–25% Cr at high temperatures form an outer spinel layer (Fe, Mn)Cr_2O_4 and an inner Cr_2O_3 layer [23]. The solubility of C in such oxides is virtually nil, as has been shown by exposures of bulk oxides in atmospheres tagged with ^{14}C [24]. The carbon permeation through grown Cr_2O_3 layers is extremely slow, only a few ppmC reaching the metal phase after many weeks exposure [25–28]. The permeation occurs by diffusion of carbon-bearing molecules through pores, channels or cracks of the oxide layer; thus carburisation is negligible in the temperature range 800–1000 °C, if an adherent, tight oxide scale has formed on the alloy. Cracking tubes can be used for many years if these conditions apply [22].

However, there are some possibilities of oxide scale failure, most frequent and momentous being the conversion of the chromium oxide in carbides [29–31]. This conversion will occur at the inner wall of cracking tubes when

they are covered with carbon deposit and heated to temperatures >1050 °C. The atmosphere in the porous carbon deposit at the oxide surface will have the carbon activity $a_C = 1$ (equilibrium with graphite) and its oxygen activity will decrease with increasing T [29]. At >1050 °C, the oxygen activity is so low that the equilibria of Cr_2O_3 and Cr_7C_3 or Cr_3C_2 are shifted to the stability of the carbides (Fig. 1.4) and the conversion will start. The rate of the reaction is slow in CO/CO_2 mixtures [30] but fast in the presence of carbon deposits.

Cracking tubes are endangered, especially during decoking, by the exothermic burning of the carbon layer with H_2O/air mixtures. Temperature control during the cracking operation or decoking to <1050 °C is the best remedy against failure of the protective scale. On alloys with sufficient Si content (>1.5% Si) a sublayer of SiO_2 may be formed beneath the Cr_2O_3 layer which gives protection even after conversion of the Cr_2O_3 [29, 32].

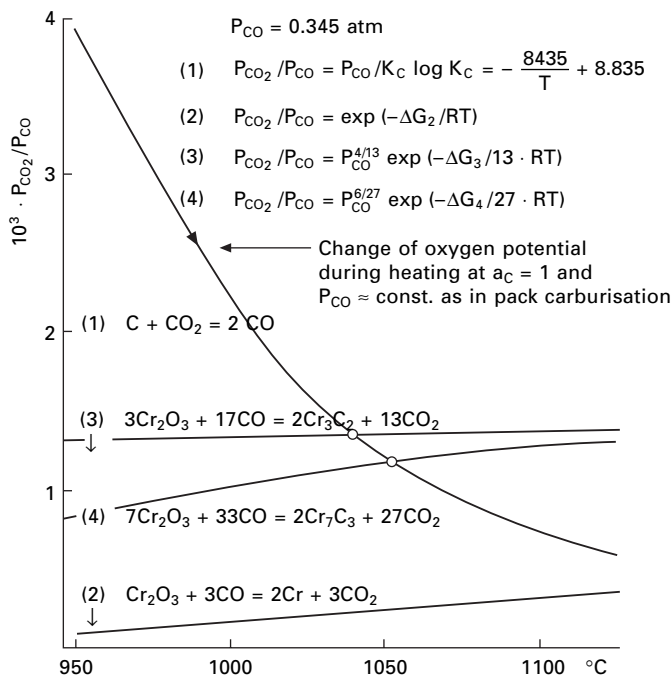

1.4 Thermodynamics of the reactions at high temperatures and $a_C = 1$ (equilibrium with graphite, resp. coke deposits) in the system Cr–O–C. With increasing temperature, the oxygen activity (~pCO_2/pCO) beneath the coke decreases (according to the Boudouard reaction) and at temperatures >1050 °C protective Cr_2O_3-scales are converted to unprotective carbides (pCO = 0.345 bar corresponds to the condition in the pack carburisation test [29]).

For steels with less Si, the carburisation at high temperatures >1050 °C is not hindered by any oxide layer and its rate is just determined by the inward diffusion of carbon. This process was studied by carburisation in CH_4/H_2 mixtures which avoids oxidation [2, 3]. The progress of internal carbide formation can be described by an equation which corresponds to the equation for internal oxidation

$$x^2 = 2 \cdot \frac{\varepsilon \cdot D_C \cdot c_C}{\nu \cdot c_M} \cdot t \qquad [1.3]$$

where D_C is the diffusivity and c_C the solubility of carbon in the metal matrix, ε is the labyrinth factor, ν the stoichiometric factor for the carbide MC_ν and c_M is the concentration of the metals involved in carbide formation. Carbon diffusivity and solubility depend on the composition of the metal matrix after Cr-carbide precipitation, i.e. in an Fe–Ni alloy. The product $D_C \cdot c_C$ shows a minimum at Ni/Fe = 4/1 [29, 33]. Correspondingly, the carburisation in a carbon pack at 1100 °C of alloys with different Ni/Fe ratios shows a minimum at 4/1 (Fig. 1.5). A similar effect of the nickel content is to be expected in practice, e.g. for cracking tubes.

Carburisation in the absence of a protective oxide layer can also be retarded by adsorbed sulfur, which blocks metal surfaces for the transfer of carbon [34]. The sulfur can be provided by appropriatly low additions of H_2S [35–37] or other sulfur-bearing molecules to the atmosphere, establishing an adsorption equilibrium $H_2S = H_2 + S(ads)$. With decreasing temperature, less H_2S is necessary for saturation and surface blocking (Fig. 1.6). The sulfur is effective when the oxide layer fails locally, due to creep, fatigue or thermal cycling, by cracking or spalling. Such scale defects can be sealed by adsorbed sulfur until the oxide scale heals again. From the curves in Fig. 1.6 it can be seen that there is an optimum H_2S/H_2 ratio at which suppression of carburisation is greatest; for higher values, the mass gain increases due to sulfidation under formation of CrS and additional carburisation. The optimum values correspond to the data shown later (Fig. 1.8) for the H_2S/H_2 ratio necessary to suppress metal dusting.

The failure of oxide scales by creep has been demonstrated by creep experiments in carburising and oxidizing $CO/H_2/H_2O$ mixtures [2, 3]. At low strain rates (about 10^{-9} s^{-1}) some carburisation occurred along the grain boundaries, followed by oxidation and then by opening of cracks at the surface. The carburisation is enhanced with increasing creep rate; small additions of Nb and Ce decrease the carbon uptake at equal elongation [38]. After exposure at higher creep rates (10^{-7} s^{-1}), carbides were formed, not only at grain boundaries but also in the bulk [2, 3]. Voids and cavities appeared at the interfaces of the carbide particles and the specimens failed by brittle fracture. There is a critical strain rate [39] between the values given, above which the scale does not heal and extensive carburisation occurs.

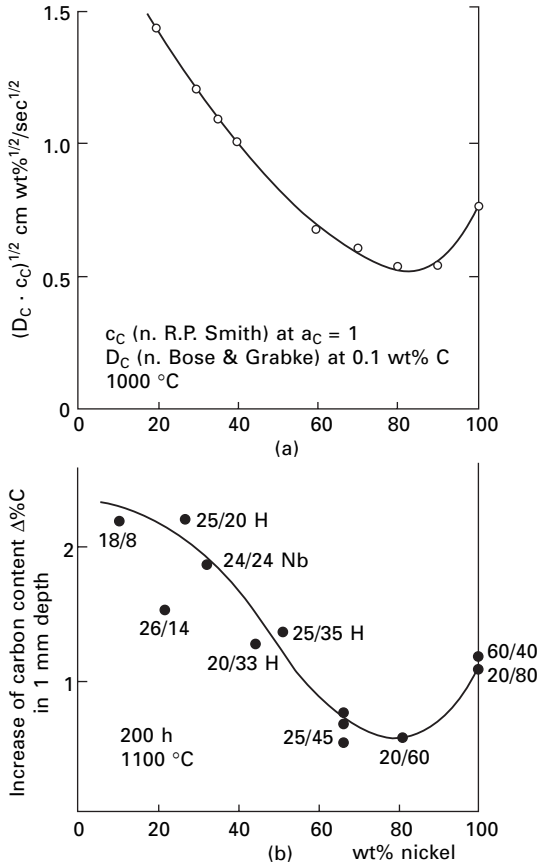

1.5 Dependence of carburisation kinetics on the Ni-content of alloys. (a) Term $(D_C \cdot c_C)^{1/2}$ which is decisive for internal carbide formation rate, in absence of a protective scale and after precipitation of the chromium carbides, for the system Fe–Ni–C at 1000 °C, compared to (b) results of pack carburisation tests [29] on various alloys (denoted by their Cr/Ni ratio) at 1100 °C where the Cr_2O_3 scale is converted to carbides and C-diffusion determines the progress of internal carbide formation.

However, in industrial practice such creep rates should not occur, and the enhancing effect of creep on carburisation is minor. The oxide scale also may be destroyed by growth of graphite beneath or within the scale [40]. In pores at the metal/oxide interface, the oxygen activity is low and $a_C > 1$, and graphite nucleates on the metal surface, generally not on oxides. Especially rough or porous materials are endangered by the graphite growth in pores leading to disruption of oxide and metal particles. Nowadays, the microporous zone at the inner walls of centrifugically cast tubes is removed by machining so that this kind of failure has become rare. Machining, or any other surface

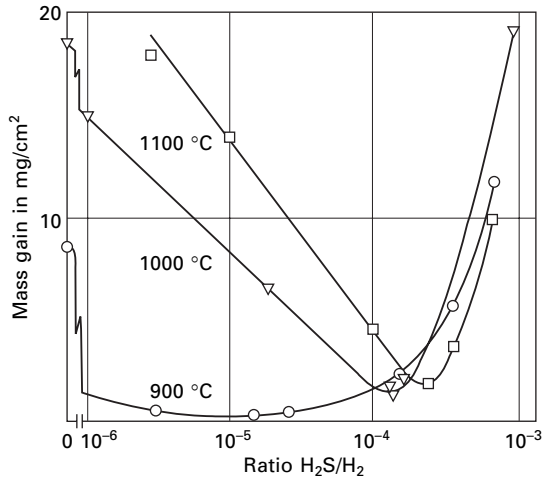

1.6 Effect of sulfur on carburisation: mass gain of Alloy 800 in $CH_4/H_2/H_2S$ atmospheres at 900, 1000 and 1100 °C plotted versus ratio H_2S/H_2, and decrease of mass gain by carburisation with increasing H_2S/H_2 ratio up to an optimum value, above which sulfidation occurs [35].

deformation (grinding, sand-blasting, shot-peening, honing) additionally favours the formation of a protective Cr-rich scale [41–43] which is important especially for temperatures below 800 °C (see next section, 'Metal dusting').

1.3 Metal dusting

1.3.1 Mechanisms of metal dusting

As noted before, metal dusting is to be expected if metallic materials are carburised at carbon activities $a_C > 1$, i.e. under a strong driving force for graphite formation. The carbon from the gas molecules should react to graphite (and, in fact, that is the overall reaction which occurs in metal dusting) and destroy the materials. As yet, two different reaction paths have been observed. For iron and Fe-based alloys, the reaction sequence is as follows (see Fig. 1.7):

(i) Transfer of C into the metal phase and oversaturation of the metal, i.e. $a_C > 1$ in the metal phase.
(ii) Formation of cementite M_3C (M = Fe, Ni) at the surface, which acts as a barrier for further carbon ingress. This causes:
(iii) Graphite precipitation, decreasing the carbon activity on the cementite to $a_C = 1$, whereby the M_3C becomes unstable and decomposes according to $M_3C \rightarrow C + 3M$.

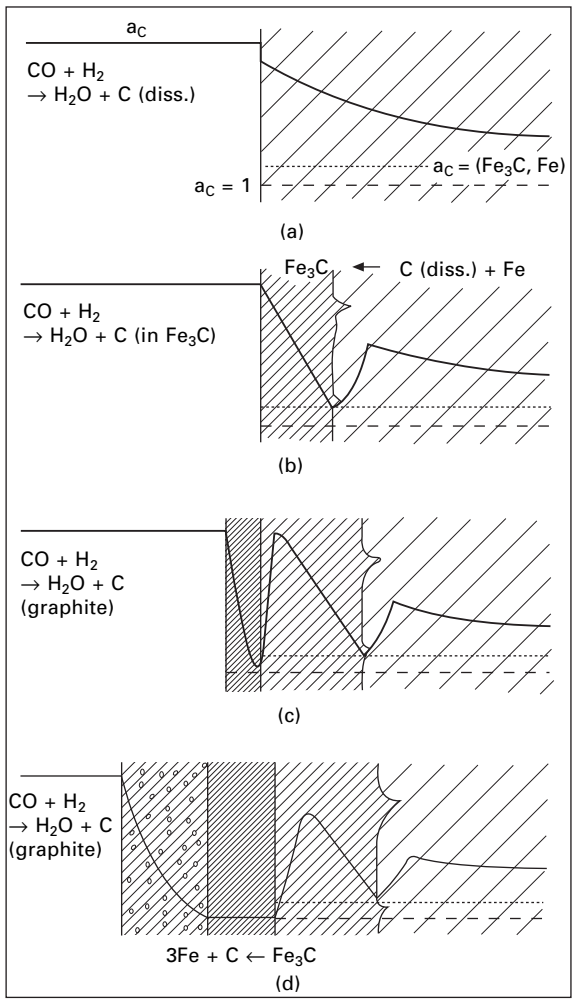

1.7 Mechanism of metal dusting on iron and low-alloy steels [9–15]. (a) Carbon transfer into the metal phase and oversaturation ($a_C > 1$), (b) formation of cementite M_3C (M = Fe, Ni) at the surface, (c) graphite deposition on the surface, $a_C \rightarrow 1$, M_3C unstable, and (d) cementite decomposition to graphite and metal particles acting as catalysts for carbon deposition, i.e. coke growth. In the case of high alloy steels, local failure of the scale is a preceding step, leading to pitting attack.

(iv) The carbon atoms from this decomposition are attached to the basal planes of graphite which grow into the cementite [15]. The metal atoms diffuse through the graphite and agglomerate to small particles (about 20 nm diameter).

(v) These particles act as catalysts for further carbon deposition and vast coke growth results.

Adsorbed sulfur effectively hinders step (iii), the nucleation of graphite, and in this way interferes with the mechanism. The adsorbed sulfur stabilizes the cementite and one can grow thick layers of cementite on iron and steels [14]. The continuous presence of only a few ppm H_2S in the atmosphere is an effective remedy against metal dusting of steels [14] (see Fig. 1.8). The data on the effect of sulfur on metal dusting can be readily combined with the data on its effect on carburisation [35–37].

For nickel, Ni-based materials and steels with Ni/Fe > 2/3 another simpler reaction sequence applies, not involving the unstable intermediate M_3C [10, 44]. After oversaturation of the metal phase, direct graphite growth into the metal phase follows, C-atoms from the super-saturated solid solution attaching to graphite basal planes [44]. Destruction of the metal results from the growth of graphite oriented more or less vertical to the metal surface, whereas graphite with basal planes parallel to the metal surface is harmless. Thus, the metal dusting attack on Ni is strongly dependent on the surface orientation and the direction of epitaxial deposition of graphite. Both these mechanisms, for Fe- and Ni-based materials, reflect the unstable situation at carbon activities $a_C > 1$, of metals which dissolve carbon.

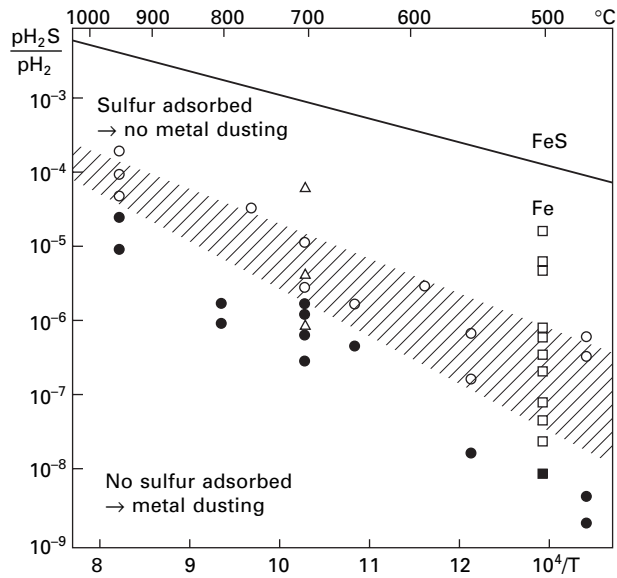

1.8 Effect of sulfur on metal dusting [14]: regions in the thermodynamic plot of sulfur activity ~pH_2S/pH_2 versus $1/T$, where no sulfur is adsorbed and metal dusting occurs; where a monolayer of sulfur is adsorbed and metal dusting is suppressed; and where the sulfur coverage approaches saturation and suppression is limited (hatched area): uppermost region is the stability range of FeS.

In the temperature range 500–700 °C, most critical for occurrence of metal dusting, generally ferritic 1–17% Cr-steels or austenitic 17–20% CrNi-steels are used. The low alloy 1–11% Cr-steels have no great chance to form a protective oxide scale under usual operation conditions. They are subject to an immediate start of metal dusting if not protected by sulfur. The appearance of metal dusting is characterized then by preceding internal carbide formation; the carbides are very fine so that, in the etched metallographic cross-section, a dark zone appears with no discrete particles (see Fig. 1.2). After precipitation of the stable Cr-carbides, the remaining metal matrix is dusting as described under formation of the coke layer, composed of metal and carbide particles and graphitic carbon (see Fig. 1.2). On ferritic steels with >11% Cr or austenitic steels with >17% Cr, a protective scale can be formed, and metal dusting generally occurs locally by pitting, starting from defects in the scale.

Besides prevention of metal dusting by sulfur, the protection by oxide scales is most important. In the temperature range in question, generally chromia layers act as protective scales or at least Cr-rich scales: (Fe, Mn) Cr_2O_4/Cr_2O_3. However, at relatively low temperatures (<700 °C) it is not certain that even steels with sufficient Cr form a Cr_2O_3 layer. Chromia formation can be favoured by a fine grain size and/or surface near deformation, since grain boundaries and dislocations act as fast-diffusion paths for the supply of Cr to the surface. The effect of grain size and surface working has clearly been shown, comparing ground specimens and chemically etched specimens [45, 46]. Probably also alloying additions of Si, Al and Mn help in the formation of a protective scale [47]. High Ni-contents retard the ingress of carbon, since diffusivity and solubility of C decreases with increasing Ni-contents [33]. Thus, alloys with high Cr- and high Ni-content are most resistant to metal dusting [49, 50].

1.3.2 Failure cases in platformer units

A case of severe attack has been reported [16] on the inner walls of charge heater tubes in a Continuous Catalyst Regeneration (CCR) platformer unit. The 6 mm thick tubes of $2^1/_4$ Cr–1 Mo steel had been in operation for ten years but then showed, locally, losses of wall thickness up to 4 mm by pitting. On the external surface of the tubes, relatively thick red scales were observed in the areas of pitting, which indicates overheating of the tube walls. Coke deposits were found in the reactors during shutdown. The metallographic cross-section showed a carburised layer at the inner wall of the attacked steel sheets. The latter two observations are evidence for the occurrence of metal dusting.

Metal dusting occurs in strongly carburising atmospheres at carbon activities $a_C > 1$, which condition certainly was present in the furnace feed consisting of hydrocarbons and a few percent of hydrogen. The sulfur content of the

feed was very low and scarcely sufficient to provide protection by formation of a protective monolayer of adsorbed sulfur [14]. Also, the water vapour content was far too low to obtain a protective oxide layer on the low-alloy steel.

A chloriding agent was injected intermittently which decomposed, forming HCl (g) so that adsorption of chlorine and also formation of volatile metal chlorides was possible.

In the earlier years, the furnace was operated at temperatures up to about 625 °C. It was concluded that a higher furnace loading in a period before the failure resulted in an increase of the skin temperature to about 645 °C, which was supposed to be one of the reasons for occurrence of metal dusting.

A second failure case in a CCR unit has been reported recently [17]. It happened in a plant where the furnace had been operated without failure for 24 years. Some changes had preceded the failure:

(i) there was a change of pipes; instead of 5%Cr steel tubes, new tubes made of a 9%Cr steel (P9) had been installed,
(ii) the amount of sulfur in the feedstock had been reduced due to the introduction of a new catalyst and
(iii) the operation temperature was raised, most probably up to about 675 °C.

The features of this failure case were similar to the previous case: materials loss was observed, coke was detected and the internal wall showed a carburised zone in the metallographic cross-section. The outer surface was partially covered with the 'red scale' and one tube had even cracked locally. Near the crack there were deposits in the tube and the microstructure of the steel indicated strong overheating. The new 9%Cr tube obviously failed due to metal dusting, coke formation inhibiting the heat transfer and locally increased temperatures.

By analyses of intact tubes from the same CCR unit, hints were found to explain why pipes installed earlier did not fail. The metallographic cross-section showed an internally carburised zone and a somewhat scarred surface, even pits with coke (see Figures 1.9a,b), i.e. indications of metal dusting. Auger-spectra taken on that surface showed graphitic deposits or metallic areas covered with adsorbed sulfur (see Figures 9c,d). Obviously, this material had been largely protected by adsorbed sulfur and only very slow metal dusting had taken place, retarded by the presence of either the graphitic carbon layer and/or adsorbed sulfur. In contrast, the new tubes had no chance to obtain such a protective coating, due to the lack of sulfur in the atmosphere and maybe, in addition, enhanced skin temperature.

The study reported below (Section 1.3.3) was intended to clarify the effects of temperature and also of the oxidizing (H_2O), sulfidizing (H_2S) and chloridizing (HCl) gas components on the occurrence of metal dusting in a hydrocarbon environment.

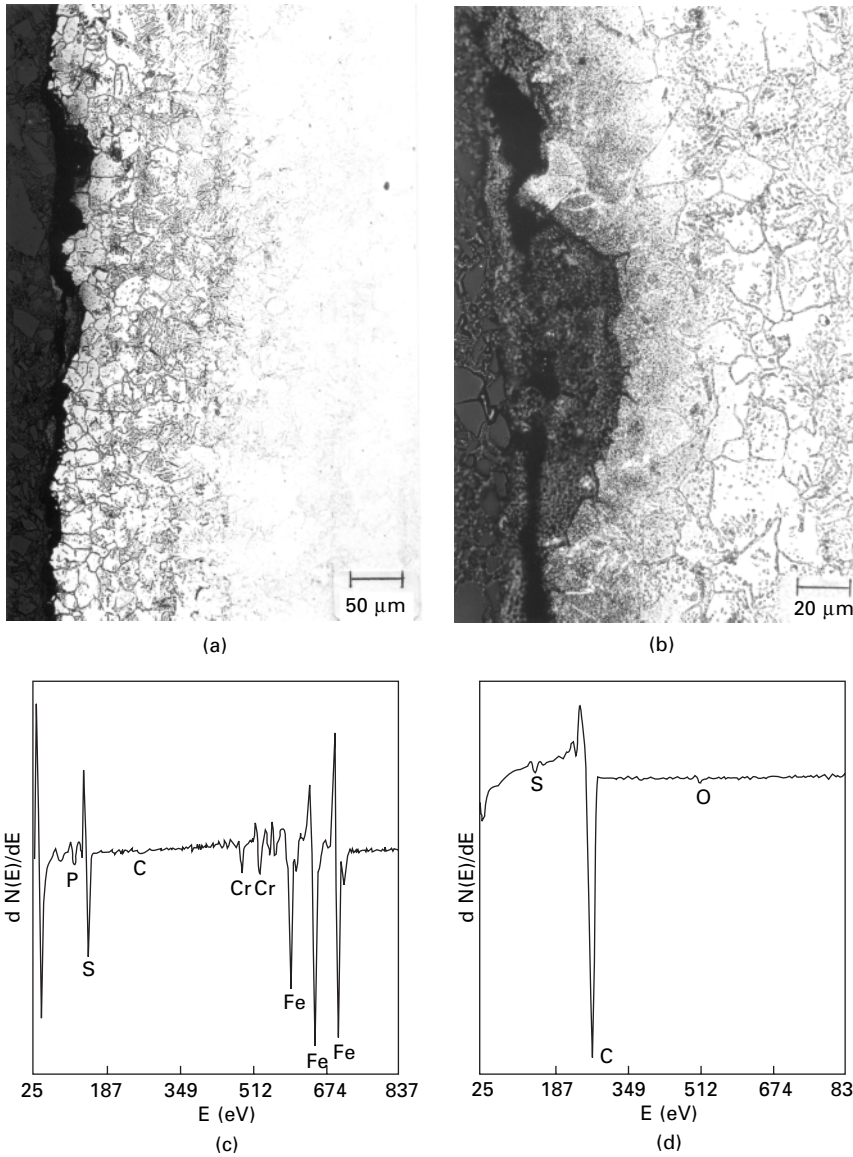

1.9 Study of the inner wall surface of a furnace tube from a CCR platformer unit made of 5%Cr-steel, nearly uncorroded after 24 years service: (a) and (b) metallographic cross-section showing about 150 μm carburised zone and pits with coke, i.e. clear indications of metal dusting, which was probably very slow, being retarded by sulfur adsorption and a layer of carbon. This is shown by Auger electron spectra, taken on the inside surface of the tube: (c) spot with metallic surface adsorbed sulfur and segregated phosphorus, (d) surface covered with graphitic carbon, containing some sulfur.

1.3.3 Laboratory simulation of metal dusting in CCR platformer units

The metal dusting in catalytic reforming furnace tubes [16] was simulated using butane: hydrogen (1:2) mixtures on two ferritic 2.25Cr–1Mo- and 9Cr–1Mo-steels and two austenitic steels, AISI 321 and Alloy 800 [51, 52]. Metal dusting, i.e. formation of coke containing metal from the steels, was observed only in the relatively small temperature range between 600–700 °C (see Fig. 1.10a). The metal wastage rates are clearly lower than in CO/H_2 mixtures. The 9%Cr-steel was most resistant. Metal dusting resistance is

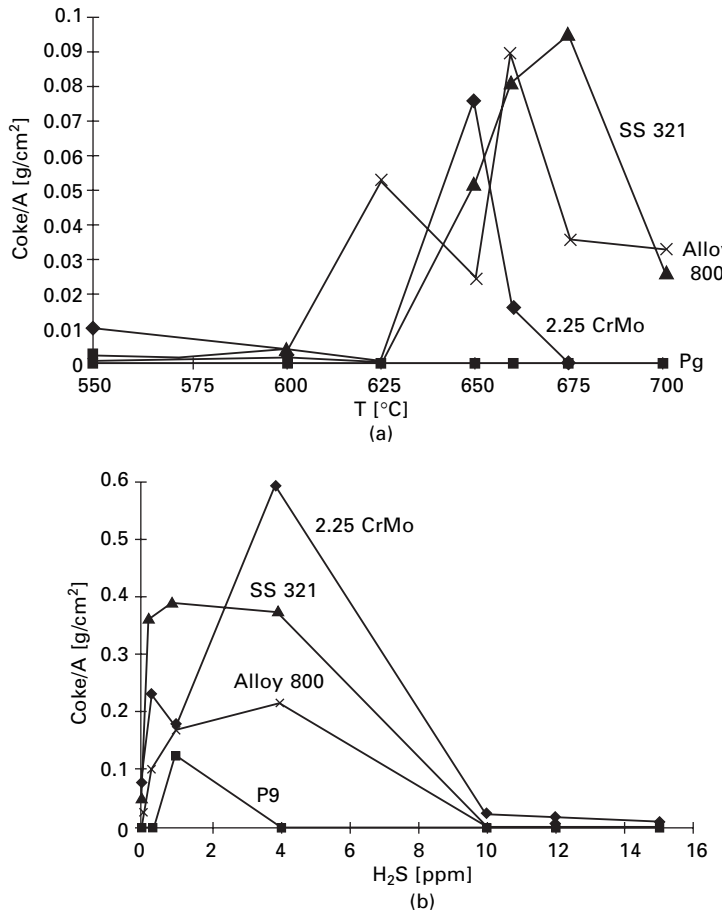

1.10 Results of a laboratory study on the metal dusting of four steels in butane–hydrogen. The coke formation within two days' exposure was taken as a measure of metal dusting attack. (a) Temperature dependence of attack, (b) effect of H_2S additions on metal dusting at 650 °C.

caused by the presence of a protective oxide layer, and its formation is favoured at higher temperatures; this explains the observed maximum of attack depending on temperature.

An attempt to protect the steels by preoxidation, i.e. heating up in H_2/0.6%H_2O had no clear effect; only for the steel AISI 321 was the metal dusting resistance clearly improved.

The well-known effect of H_2S-additions in suppressing metal dusting [14] was confirmed (see Fig. 1.10b). At 600 °C, contents of >1 vppm H_2S were sufficient; at 650 °C, additions of about 10 vppm would be necessary, which would not be tolerable for the catalytic process under discussion. Consequently, the operation has to be restricted to 625 °C or lower.

The process also requires additions of chloriding agents now and then; their effect was investigated using trichlorethylene (TCE). The presence of TCE enhances the metal dusting attack markedly, most probably due to destruction of protective oxide scales. Upon sufficient H_2S addition, this effect can be eliminated, but again the additions of H_2S would have to be too high at temperatures >620 °C.

Summarising, one may say that the heating of hydrocarbons in the temperature range 600–650 °C, as conducted in a Continuous Catalyst Regeneration (CCR) unit, needs very careful control concerning temperature and the additions of sulfur as well as chloriding agents, otherwise metal dusting may occur and cause severe failures. It is most surprising that, as yet, no more failure cases have been reported from refineries, since obviously many units operate under rather critical conditions.

1.4 References

1. H.E. Bühler, A. Rahmel, H.J. Schüller: *Arch. Eisenhüttenwes*. 38 (1967) 223
2. A. Schnaas, H.J. Grabke: *Oxid. Metals* 12 (1978) 387
3. H.J. Grabke, A. Schnaas: in W. Betteridge *et al*. (eds.) *Alloy 800*, North-Holland, Amsterdam, 1978, pp. 195–211
4. J. Harrison, J.F. Norton, R.T. Derricot, J.B. Marriott: *Werkst. u. Korr*. 30 (1979) 785
5. S. Forseth, P. Kofstad: *Werkst. Korros*. 46 (1995) 201
6. S. Forseth, P. Kofstad: *Mat. & Corr*. 49 (1998) 266
7. D.R.G. Mitchell, D.J. Young, W. Kleemann: *Mat. & Corr*. 49 (1998)
8. D.J. Young: *Mat. & Corr*. 50 (1999) 675
9. J.C. Nava Paz, H.J. Grabke: *Oxidation of Metals* 39 (1993) 437
10. H.J. Grabke, R. Krajak, J.C. Nava Paz: *Corr. Sci*. 35 (1993) 1141
11. H.J. Grabke, R. Krajak, E.M. Müller-Lorenz: *Werkst. Korros*. 44 (1993)
12. H.J. Grabke, C.B. Bracho-Troconis, E.M. Müller-Lorenz: *Werkst. Korr*. 45 (1994) 215
13. H.J. Grabke: *Corrosion NACE* 51 (1995) 711
14. H.J. Grabke, E.M. Müller-Lorenz: *Steel Res*. 66 (1995) 254
15. E. Pippel, H.J. Grabke, S. Strauss, J. Woltersdorf, *Steel Res*. 66 (1995) 217

16. M.H. Ravestein: *Corrosion 97*, Paper No. 496, NACE Int. Houston, Texas 1997
17. D. Blendin-Fulz: Working Party 'Refinery Corrosion' Meeting at *EUROCORR '99*, 1. Sept. 1999
18. A. Schnaas, H.J. Grabke: *Werkst. Korros*. 29 (1978) 635
19. D.F. Lupton, P.J. Ennis: *Res. Mech*. 1 (1981) 245–252
20. T.A. Ramanarayanan, R. Petkovic-Luton: in R.A. Rapp (ed.), *Proc. 6th Conf. on High Temperature Corrosion*, San Diego, 1981, NACE, Houston, 1983, pp. 430
21. J. Hemptenmacher, G. Sauthoff, H.J. Grabke: *Werkst. Korros*. 35 (1984) 247–253
22. S. Ling, T.A. Ramanarayanan: *Oxid. Metals* 40 (1993) 179
23. K. Ledjeff, A. Rahmel, M. Schorr: *Werkst. Korros*. 30 (1979) 11
24. I. Wolf, H.J. Grabke: *Solid State Commun*. 54 (1985) 5–10
25. H.J. Grabke, K. Ohla, J. Peters, I. Wolf: *Werkst. Korros*. 34 (1983) 495
26. I. Wolf, H.J. Grabke: *Proc. 8th Eur. Congr. on Corrosion*, Nice, November 1985, Centre Francais de la Corrosion, Paris, Vol. 1, p. 48
27. H.J. Grabke, I. Wolf: *Mater. Sci. Engg*. 87 (1987) 22
28. I. Wolf, H.J. Grabke, H.P. Schmidt: *Oxidation of Metals* 29 (1988) 289
29. H.J. Grabke, U. Gravenhorst, W. Steinkusch: *Werkst. Korros*. 27 (1976) 291
30. W.F. Chu, A. Rahmel: *Oxidation of Metals* 15 (1981) 331
31. J.A. Colwell, R.A. Rapp: *Metallurg. Trans*. 17A (1986) 1065
32. W. Steinkusch: *Werkst. Korros*. 30 (1979) 837
33. S.K. Bose, H.J. Grabke: *Z. Metallkde*. 69 (1978) 8
34. H.J. Grabke, E.M. Petersen, S.R. Srinivasan: *Surface Sci*. 67 (1977) 501
35. H.J. Grabke, R. Möller, A. Schnaas: *Werkst. Korros*. 30 (1979) 794
36. H.J. Grabke, R. Möller, A. Schnaas: in *Behaviour of High Temperature Alloys in Aggressive Environments*, (Ed. J. Kirman *et al*.) The Metal Society, London 1980, p. 759
37. J. Barnes, J. Corish, J.F. Norton: *Oxidation of Metals* 26 (1986) 333
38. J. Hemptenmacher, H.J. Grabke: *Werkst. Korros*. 34 (1983) 333
39. M. Schütze: *Oxidation of Metals* 25 (1986) 409
40. K. Ledjeff, A. Rahmel, M. Schorr: *Werkst. Korros*. 31 (1980) 2
41. S. Leistikow: *Mater. Chem*. 1 (1976) 189
42. H.J. Grabke, J. Hemptenmacher, A. Munker: *Werkst. Korros*. 35 (1984) 543
43. I. Wolf, S. Leistikow, H.J. Grabke: *Werkst. Korros*. 38 (1987) 556
44. R. Schneider, E. Pippel, J. Woltersdorf, S. Strauss, H.J. Grabke: *Steel Research* 68 (1997) 326
45. H.J. Grabke, E.M. Müller-Lorenz, B. Eltester, M. Lucas, D. Monceau: Steel Research 68 (1997) 179
46. H.J. Grabke, E.M. Müller-Lorenz, S. Strauss, E. Pippel, J. Woltersdorf: *Oxid. Metals* 50 (1998) 321
47. S. Strauss, H.J. Grabke: *Mat. & Corr*. 49 (1998) 321
48. H.J. Grabke: *Härterei-Techn. Mitt*. 45 (1990) 2
49. H.J. Grabke, R. Krajak, E.M. Müller-Lorenz, S. Strauss: *Werkst. Korr*. 47 (1996) 495
50. J. Klöwer, H.J. Grabke, E.M. Müller-Lorenz, D.C. Agarwal: *Materials Performance (NACE), Corrosion 97*, Paper 139
51. C. Gerk: *Diplom thesis*, Univ. Dortmund 1996
52. H.J. Grabke, C. Gerk: 'Effects of Temperature and of Hydrogen Sulfide and Trichlorethylene Additions on the Metal Dusting by Hydrocarbons', paper on *EUROCORR '99* Aachen, Sept. 1999

2

Integrity and life assessment of catalytic reformer units

J. M. BREAR, Stress Engineering Services (Europe) Limited, UK and J. WILLIAMSON, Consultant, UK

2.1 Introduction

This chapter outlines the technical approaches that can be made to address the integrity, failure risk and remaining safe serviceable life of plant used for the catalytic reforming of naphtha feedstock. In dealing with Catalytic Reformer Units (CRUs) the chapter will consider the major components, comprising fired heaters, reactors, transfer pipework and combined feed heat exchangers, in the overall context of an integrated, risk-based framework for integrity assessment.

The objective of the chapter is to provide an overview of the plant assessment technology tools that are available to aid decision making in the Inspection, Maintenance and Operations areas. The assessment approaches to each of the major component groups will be divided into actions that can be implemented in two separate timeframes. Firstly, those that can be expedited during a production period, while the plant is on-line, thus enabling guidance to be provided for the taking and planning of Inspection, Maintenance, or Operations decisions. Secondly, those actions that need the opportunity of a shutdown period, when direct qualitative and quantitative condition assessment techniques can be deployed. It should be noted that, in some cases, the same assessment models may be used in each of the two timeframes (Fig. 2.1). Generally, the use of the same model in the production and shutdown periods enables refinement, in terms of accuracy, of the results obtained prior to the shutdown. However, some of the models can be deployed only in the shutdown period, as this is the sole chance to access the necessary condition assessment data.

To summarise, therefore, this chapter is structured on a major component basis and the differential timeframe assessment approaches that can be made to these in the various types of CRU.

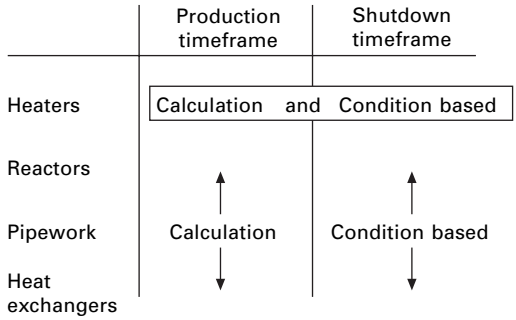

2.1 Model types for timeframes and major components. Condition is as determined by inspection.

2.2 Background

Plant, particularly that for use in high-temperature or high-pressure service, has generally been code designed on the basis of an allowable stress and a corrosion allowance for a specific design life. Refining industry experience clearly indicates that this design life is often conservative. However, it also indicates that in operation, where time-dependent degradation conditions prevail (corrosion, erosion, fatigue, creep, thermal degradation, embrittlement, etc.), life is nevertheless still finite and that, with time, absolute integrity status decreases and likelihood of failure increases. Thus, to optimise the complex interaction between profitable return on capital, production capability, and safety and environmental considerations, cost-beneficial inspection, maintenance, refurbishment and replacement guidance is necessary.

Confirmation of current integrity status and definition of the probability and consequence of failure are essential plant management requirements. The following sections of this chapter deal with the approaches that can be made, both during the production period and at shutdown by utilising plant assessment technology to provide this information. Previous reviews (Brear, 1997; Brear and Townsend, 1997) have detailed the individual assessment techniques and the overall phased approach to component life assessment.

The detail in this chapter relates specifically to Catalytic Reformer Units (CRUs), including Platforming, Ultraforming, Rheniforming, Powerforming and IFP reforming, of both the semi-regenerative and continuous catalyst regeneration (CCR) types. However, the philosophy adopted means that the principles for specific component types will be applicable to similar items on other production units.

2.3 Risk assessment

2.3.1 Principles of risk assessment

The objective of a risk-based assessment is to reduce operating costs by focusing the timing and scope of inspection (and other) activities, without incurring unacceptable risks. Naturally, cost reduction can only be achieved if the existing inspection programmes are over-conservative; it must be recognised that a formal study may in some cases lead to the conclusion that more money needs to be spent, rather than less, to achieve a given risk exposure. However, any rigorous analysis will ensure that the spend is optimised against the risk and will highlight the sensitivity of the result to variations in the timing and coverage of the inspection plan. Thus, the minimum spend for a defined risk, or the lowest risk for a set budget, are equally achievable goals. The integration of risk-based approaches into an overall plant life management programme has been addressed by the present authors (Brear and Williamson, 1998; Brear, 2003).

Within the refining industry, the risk-based inspection procedure put forward by the American Petroleum Institute in its Recommended Practices RP-580 (2000) and RP-581 (2000) has been generally adopted and its three levels can be summarised as follows:

Level 1 – Qualitative analysis of a process unit

Qualitative analysis of a process unit is the starting point for any plant- or unit-wide risk based inspection study. It can be carried out while the equipment is in operation and comprises four main steps. To ensure uniformity of treatment and coverage of all aspects, a formal workbook or appropriate software is used to identify, record and analyse the necessary data.

As with all methods, it commences with a plant review, in which familiarity with the situation is gained and data are gathered. The next steps are to determine the likelihood and the consequences of failure. Likelihood is categorised using a formula based on: design and construction quality, plant age, operating and inspection history, repair or modification history, future usage, general experience, and the identified or expected degradation mechanisms. The consequences of failure are similarly ranked using a formula based on: on-site and off-site human impact (fire, explosion, toxicity), environmental damage, capital equipment damage (repair, refurbishment, replacement, consequential damage), production loss and the potential for damage limitation. Though this appears involved, a formalised approach makes it simple, reliable and efficient in practice. Once the likelihood and consequence of each potential hazard have been identified, the risk exposure is determined, using a matrix as shown in Table 2.1.

The final step is to use this information in determining the necessity and

Table 2.1 Level 1 qualitative risk-assessment matrix

Risk level

Consequence category						
	Very high	High	High	Very high **1**	Very high	Very high
	High	Medium	Medium 1	High **1**	High **1**	Very high
	Medium	Medium	Medium 3	Medium 2	High **3**	High
	Low	Low	Low 26	Low	Medium	High
	Very low	Very low	Very low 8	Low	Medium	High
		Very low	Low	Medium	High	Very high

Likelihood category

scope for Levels 2 and 3 of the assessment. It is considered that items which fall in the low risk category in a Level 1 assessment do not require further assessment or detailed inspection. Current practice is reviewed and revised if appropriate, taking note of any statutory or regulatory requirements.

Level 2 – Semi-quantitative analysis of individual equipment items

Level 2 is a streamlined version of Level 3, intended to be less resource intensive, and suitable for inspector, rather than expert, use. It uses estimated likelihoods of failure obtained from generic databases, and of consequences based on estimated inventories – essentially a first order quantification of the factors addressed in Level 1 on a cost or square-metre-affected basis. The risk classes of Table 2.1 can now be replaced with order-of-magnitude numerical ranges. Since it is commonly observed that around 20% of the components carry 80% of the risk, it is often appropriate to restrict Level 3 analysis to the most critical items, use a Level 2 approach for the intermediate, and not proceed beyond Level 1 for the remainder.

The asymmetry of the matrix in terms of the relationship between risk level and the likelihood and consequence classes has been explored by Brear, Jarvis and Middleton (2002). It is noted that the higher weighting of consequence inherent in the qualitative Level 1 approach has a sound basis, and can be formalised, but care should be taken when moving to a Level 2 assessment as this asymmetry can distort the reassignment of risk levels.

Level 3 – Quantitative analysis of individual equipment items

Quantitative analysis of individual equipment items is the most detailed level of assessment and is directed at the highest risk items. It is fully quantitative and usually requires multidisciplinary expert input. The probability of failure

and consequences of failure are numerically quantified, using generic and specific data. Proprietary formulae are used to obtain the requisite modification factors for both probability and consequence calculations. Alternatively, hazard-specific predictive models can be applied, as exemplified in the later sections of this chapter.

Decision on actions

Whichever level of assessment is used, the risk level associated with each item can be determined and compared with other items within the same plant or with similar items elsewhere. The risk drivers can be identified, in broad terms of probability or consequence and in greater detail by consideration of the individual factors that contribute to each. Since the details of the inspection programme form an explicit input to the likelihood or probability calculation, it is easy to explore the effect on risk of changes in the inspection plan and thus perform the desired optimisation. Risk reduction can be achieved by shifting or focusing inspection resources, by improving inspection programmes or by consequence mitigation.

2.3.2 Example of a refinery-wide Level-1 risk assessment

The refinery under consideration was first built in the late 1940s. Almost every decade since has seen renewal, modification or expansion, with the result that major components had service lives between 50 000 and 250 000 hours. Given that current production was running at 115% of design, the operating company was desirous of establishing the potential for further life extension, with the support of an optimised inspection and maintenance programme. The existing inspection strategy was based on frequent observation and reaction to actual or potential problems coupled with such inspections and tests as required by the local regulatory authority. Major turnarounds were every four years, with intermediate shutdowns for cleaning.

Examination of the plant inventory, discussions with refinery personnel and general experience identified a large number of plant items as needing study; for the Catalytic Reformer Unit alone, forty-six items were selected. It should be noted that some ‘items’ represent a group of similar components, or a subsystem, where each member of the group can be considered as comparable at this first level of assessment. An API RP-581 (2000) workbook approach to the qualitative Level 1 risk assessment was followed and the results of the analysis are given in Tables 2.2 (and 2.1). Table 2.2 shows the assessed failure likelihood and consequence class for each item within the CRU, with the resulting risk class as determined using the API RP-580 (2000) matrix shown in Table 2.1, which also gives the number of items that

Table 2.2 Level 1 risk-based analysis of plant items in a typical catalytic reformer unit

Plant item	Likelihood	Consequence	Risk
Catalyst regeneration line	Medium	Medium	Medium
Charge heater	**High**	**Medium**	**High**
Debutaniser	Medium	Medium	Medium
Debutaniser feed-bottoms exchanger	Low	Low	Low
Debutaniser overhead trim cooler	Low	Low	Low
Debutaniser reboiler	**High**	**Medium**	**High**
Debutaniser receiver	Low	Low	Low
Debutaniser trim cooler	Low	Low	Low
Feed/effluent exchanger	**Medium**	**High**	**High**
Interheaters	**High**	**Medium**	**High**
Net compressor interstage drum	Low	Low	Low
Net gas compressor	Low	Medium	Medium
Products separator	Low	Medium	Medium
Reactor 1 outlet pipework	Low	High	Medium
Reactor inlet/outlet pipework	**High**	**High**	**High**
Reactor vessels	**Medium**	**Very high**	**Very high**
Recontact drum	Low	Low	Low
Recontact drum cooler	Low	Low	Low
Recycle gas compressor	Low	Medium	Medium
Regeneration tower	Low	Low	Low
18 other items	Low	Low	Low
8 other items	Low	Very low	Very low

fell into each category. In this particular case, one item (the reactor vessels) was assessed as 'very high risk' and a further 5 were classed as 'high risk'. Similar distributions of risk level were determined for the other units considered within the refinery (Brear and Williamson, 1998).

It was considered that those items classed as 'high risk' or above required further study, that those classed as 'medium risk' could be adequately covered by detailed routine inspection, and that the statutory level of inspection would suffice for the balance. The following sections exemplify the combined analyses used to refine the risk calculation and to predict the remaining life of typical high risk items.

2.4 Fired heaters

2.4.1 Factors controlling the integrity and life of fired heaters

The life of radiant tubes in fired heater service is governed by the combination of several possible time-dependent degradation mechanisms and by the tube

wall temperatures and loadings. The main degradation mechanisms in CRU service are fireside oxidation, thermal microstructural degradation and creep. However it must be noted that in certain plant types in this service the authors have found significant life limitations due to carburisation or metal dusting.

Typically, low alloy Cr–Mo steels enter service in the normalised and tempered condition, with a microstructure of transformation product (pearlite or bainite depending upon normalisation heat treatment) and ferrite grains (Fig. 2.2). With service exposure, spheroidisation slowly leads to degeneration of the original microstructure and after significant service, the microstructure will be completely degenerated, consisting of ferrite grains with intra and intergranular carbides. The material's tensile and creep strengths reduce during this process.

Tube materials in CRU fired heaters are usually of $2^1/_4$Cr1Mo specification, although ferritic tubes with higher chromium content, 5Cr1Mo and 9Cr1Mo are encountered, the last mainly in CCR service. Tube dimension design and corrosion allowance generally follow API RP-530 (various dates).

2.4.2 Assessment procedures for fired heaters prior to shutdown

Assessment procedures capable of giving an estimate of condition, probability of failure and serviceable lifetime while the plant is operating are based on calculation (Fig. 2.1). An inverse design (e.g. API RP-530) deterministic approach can be adopted, but this invariably produces conservative results. Thus, in line with the current trend for risk-based information, the more accurate approach is to deploy probabilistic techniques and a more rigorous

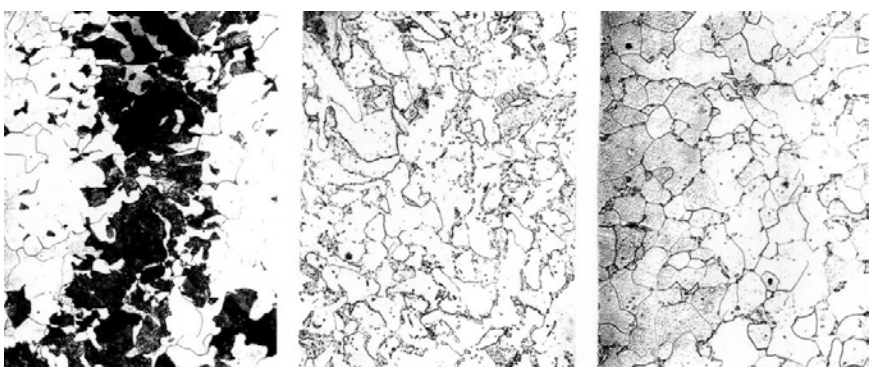

2.2 Typical thermal microstructural degradation in low alloy CrMo radiant tubes with increasing service.

tube life model for processing the available data. It is recommended that the use of simple deterministic calculations be restricted to the relative ranking of heaters that can then be subject, on a risk criterion, to the more rigorous probabilistic approach.

Prior to access at a shutdown, the available data will generally consist of:

- Tube metal temperature from installed thermocouples.
- Process temperature and pressure.
- Historic inspection tube thickness data.
- Materials specification and standard property data.
- Furnace design data.
- Service hours to date.

If tube metal temperature data are not available, they can be calculated from process information and verified by correlation with the historic metal loss rates. This procedure is obviously one of second choice; nevertheless, it has been adopted successfully many times. Alternatively, when the desired thermocouple tube metal temperature and tube wall thickness inspection data are available, one of the standard QA data procedures is to check that they are physically compatible. The authors have come across cases where either the thermocouple wall temperature data or the reported wall thickness data must be in error, as it was physically and thermodynamically impossible for them to co-exist. In such cases, the procedure is to compare the tube wall thinning history in question with an in-house database for all such similar alloys and compare the reported thermocouple data with calculated data from process information. It is generally clear which of the data sets is in major error.

Historic tube wall thickness data, from previous shutdown inspections, can be extrapolated to the current operating hours using the known relationships governing oxide formation and growth kinetics. However, care must be taken in processing these data to eliminate the effects that incomplete oxide removal has on inspection thickness readings. The upper part of Fig. 2.3 shows the historic raw UT inspection data. A clear change in measurement practice is evident following the early part of service when the oxide was removed prior to measurement and the true wall-thinning trend is seen. Subsequently, measurements were made through the oxide and the rising trend reflects total thickness of metal plus oxide. The lower part of Fig. 2.3 shows the data corrected to true thinning rate and extrapolated forward. It is common to find that reported tube wall thickness is apparently increasing, whereas in reality the opposite must be the case. Knowledge of oxidation behaviour allows the necessary correction to be made.

A probabilistic assessment prior to shutdown will give Inspection and Maintenance the best possible information at this stage upon which to base decisions defining future actions. The results will be subject to some of the

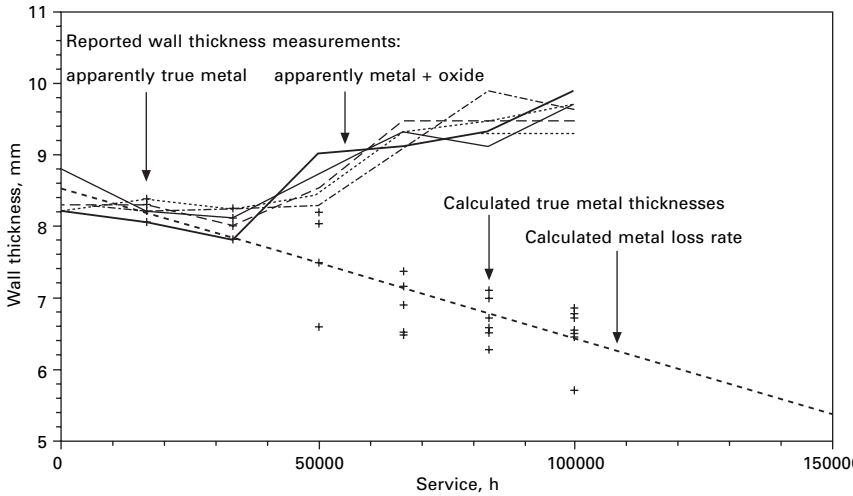

2.3 Corrections to inspection UT data to obtain true wall thinning rates.

uncertainties in the input data which, depending upon the answers, may be deemed acceptable without recourse to further refinement.

Materials properties are one such area and, depending on upon the actual position of the subject tubes in the materials properties scatter-band, can have a significant effect on the failure probability versus time results. Prior to shutdown, the probabilistic approach deals with this by assuming a normal distribution centred on mean published standard materials properties. Whilst it is possible that actual tube materials properties are below the mean value, it should be borne in mind that all standard materials data have been derived from laboratory tests conducted in an air atmosphere. The test data, and hence the derived stress allowables, are thus intrinsically conservative with respect to true creep behaviour, particularly when the design procedure makes additional allowance for service oxidation and corrosion.

A key advantage of this approach is that the tube life model developed to assess the radiant tubes in a specific heater in the production period will form the basic foundation for refinement when additional data on actual condition become available from justified shutdown actions.

2.4.3 Assessment procedures for fired heaters at shutdown

A shutdown obviously provides the opportunity to acquire the most up-to-date data on component condition. In particular, wall thickness and diametral strain data can be acquired, using conventional non-destructive methods. The opportunity also arises to address the question of component-specific

materials properties. The ideal is to sample worst-case tubes, based on inspection and operations history, and carry out post-exposure creep rupture testing, in vacuum, to determine materials capability. It also enables through-wall metallography to be performed and the wall thickness to be confirmed. However, such sampling involves weld repair. To avoid this disadvantage, and to enable wider coverage of the tube set, a hardness-based technique is available for estimating creep life from relative strength (Brear and Townsend, 1997). This has been validated on a number of materials.

Some inspectors favour the use of acetate replication to provide metallurgical tube condition information. Whilst this may be justified for fired heater tubes to ascertain evidence of local overheating, or to give comfort that little change is evident from new tube microstructures, generally speaking it does not provide useful quantifiable data. It is a common fallacy to use this technique on fired tubes to look for creep cavitation damage. Creep cavitation does not occur in ferritic tubes in this service until extremely late in life, close to imminent failure. A condition of significant distress will generally be clear from visual evidence of excessive fireside oxidation and localised bulging of parent tubes in the type of plant being discussed. The replication technique can provide useful information on weldment condition, particularly in the case of designs that have internal manifolds. (The foregoing comments are not generic to the replica technique, which can provide powerful interrogative benefits when applied to appropriate situations.)

A further advantage of tube sampling, particularly for 9Cr tubes in CCR service, is that the extent of any inner-wall degradation mechanisms can be established and quantified by metallography. Recent experience has produced several cases of inner-wall carburisation, (Fig. 2.4). This phenomenon initially

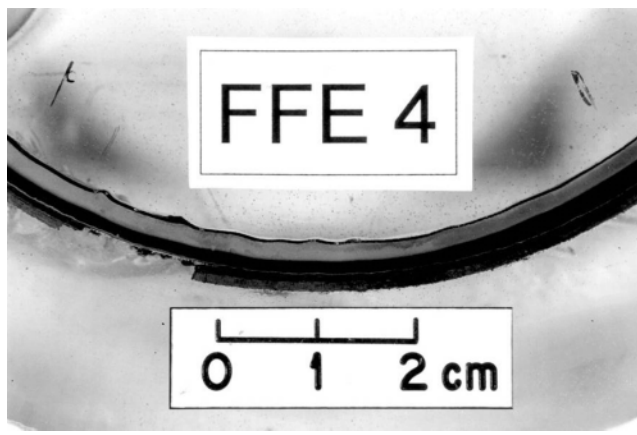

2.4 Fireside oxidation and inner wall carburisation in a 9Cr1Mo tube with metal temperatures peaking towards 700 °C.

strengthens the tube wall, but ultimately leads to crack initiation and through-wall crack propagation, and thus enhances rates of life consumption. In the early stages of propagation, crack arrest occurs at the interface between the carburised layer and the remaining unaffected wall (Fig. 2.5). The properties of the latter and the remaining net-section stress do not permit further crack growth. However, as the remaining non-carburised ligament decreases, the increasing net-section stress allows propagation to failure through the non-carburised material, (Fig. 2.6). The quantified metallographic data can be

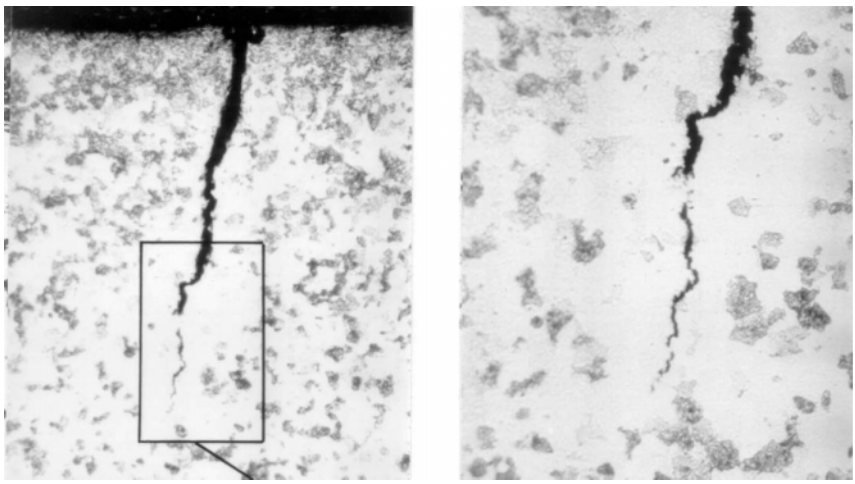

2.5 Multi-stage through-wall cracking in carburised layer in 9Cr1Mo tube.

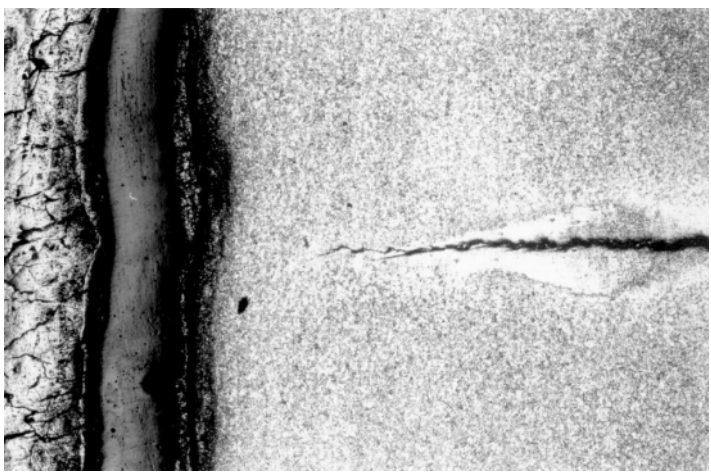

2.6 Near through-wall cracking in carburised layer in 9Cr1Mo tube.

incorporated into the pre-shutdown established life model, even if cracking has not yet initiated.

A promising NDE technique using TOFD for the detection of carburisation is under development (Lilley, 2006), and metal dusting can be indicated through higher than expected wall thinning. Carburisation tends to be prevalent only in high heat-flux service, which is the reason it is often associated with 9Cr tubes. Whilst mechanistically these are somewhat less prone to the phenomenon than the lower chromium tubes, the significant factor is high heat flux and the resulting tube wall temperature.

Other experience has produced instances of metal dusting in ferritic radiant tubes of both low and high chromium compositions (Fig. 2.7). It would appear that this could be associated with modern desulfurisation practice lowering the inhibition to carbon pick-up that sulfur provides. In mild form, metal dusting results in discrete pitting but at an extreme it can effectively produce a rapid inner wall thinning mechanism. Some inner-wall areas in Fig. 2.7 show near original wall surface, whereas other areas can be seen to show the deleterious effect of compound pitting. Again, if quantified metallographic data are available, the tube life assessment model can deal with the effect.

During and following the shutdown, reassessment of immediate fitness for purpose and long-term service capability can be reviewed and more accurate quantification made of future risk of failure both for groups of tubes and for the furnace as a whole.

Where the assessment suffers from inaccurate or inadequate thermocouple tube-skin temperature data, then the opportunity can be taken to install a small indicating device – 'PETIT'. This diffusion couple provides an effective

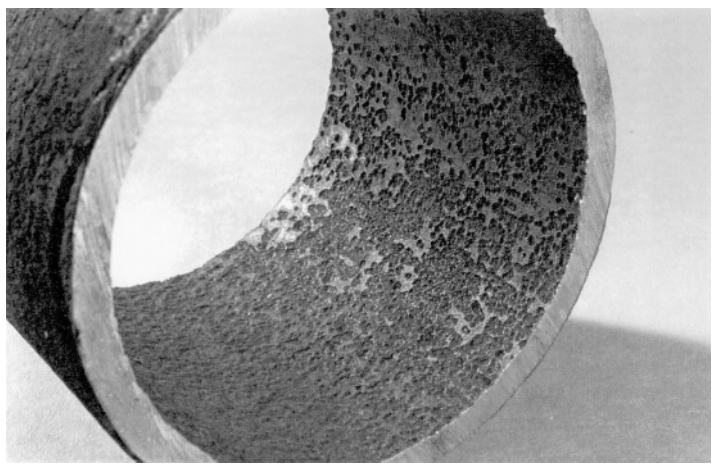

2.7 Example of metal dusting on inner tube wall.

temperature over the period between installation and removal, typically a few months to two years.

Adoption of the type of approach described above means Inspection and Maintenance can be better informed to make relevant decisions, hence both justifying and optimising the cost benefit of their actions and also guiding Operations regarding future plant capability (Fig. 2.8). The latter, in itself, can have significant cost benefits as any conservatism in the original design can sometimes be utilised in a controlled manner to allow enhanced production.

A paper giving a more detailed description of these procedures for fired tubes has been published (Brear and Williamson, 1992).

2.5 Reactor vessels

2.5.1 Factors controlling the integrity and life of reactor vessels

Reactor vessels in semi-regenerative CRU service are stand-alone items and can be either hot- or cold-shell depending upon design preference. In CCR service, the reactors are invariably of hot-shell design and are stacked to form a compartmented single vessel. In cold-shell service, carbon steel vessels are the norm, whereas hot-shell design necessitates the use of $1–1^1/_4$CrMo, or in some cases $2^1/_4$Cr1Mo, to meet the requirements for both high-temperature strength and resistance to hydrogen attack.

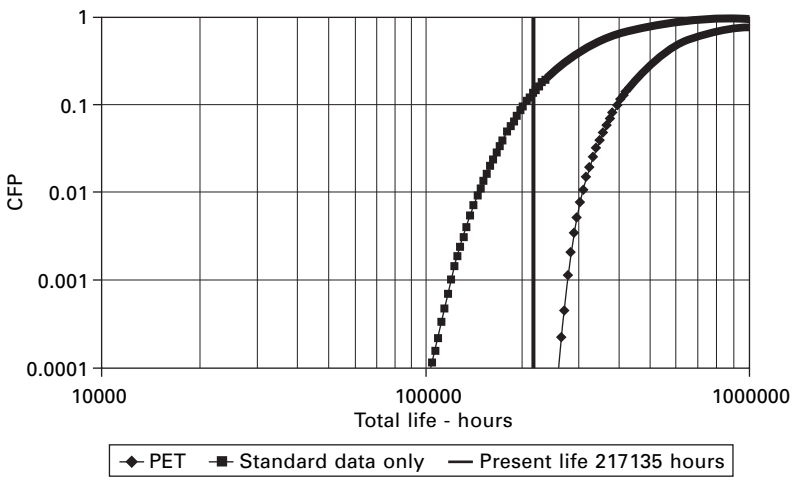

2.8 Predicted cumulative failure probability (CFP) showing initial production period results based on standard materials data, and refined results from component specific materials data obtained by post exposure testing (PET) of samples taken at shutdown.

The vessels are welded and in hot service it is the behaviour of the various weldments that generally dictates the vessel life. Weldment performance is dominated by the detailed design and subsequent fabrication of these features. The better designs ensure that the metallurgical discontinuity, i.e. weld metal and associated heat affected zones (HAZ), is not coincident with the geometric discontinuity that can often be associated with the joining of the two discrete parts. This factor has been addressed before, (Williamson, Bissell and Cane, 1988), as has the significance of this effect on inlet and outlet nozzle life (Fig. 2.9).

2.5.2 Assessment procedure for reactor vessels prior to shutdown

Plant integrity assessment technology can provide decision-making help on reactor integrity to Inspection and Maintenance in this period. The approach that can be adopted is the same as that for pipework and is therefore dealt with in detail under that section. Reactors can be much more readily inspected as an item than can the associated transfer pipework system on this type of plant. The latter is more costly to inspect effectively and therefore the necessity for guidance developed during the run period is higher. Thus for reactors, the emphasis is placed on inspection-based methods during shutdown, whilst for pipework more attention is given to pre-shutdown calculation.

Experience, however, can play a relevant part at this stage. Design review of the features associated with specific weldments can indicate if these are

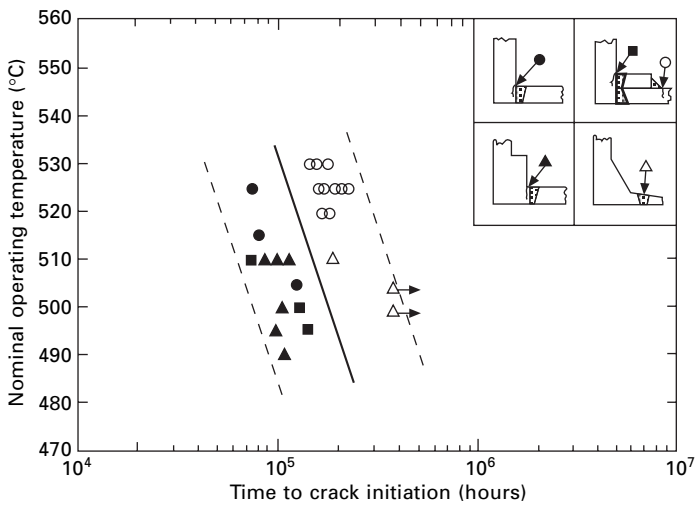

2.9 Effect of design and operating temperature on time to crack initiation in nozzle weldments.

more likely to accumulate damage at a given service time than best-practice designs. As mentioned above, the criterion of geometric and metallurgical notch coincidence is always important. In addition, if the pre-shutdown pipework analysis has been performed, then an indication of any likely excessive terminal-point loadings will be available. These can be a major influence on damage accumulation at set-in nozzle weldment locations. Current thinking indicates that thermal loadings in these regions must also play a part.

The involvement of the additional shell to reinforcing-ring weldment in designs following this philosophy brings an extra complication to the distribution and redistribution of damage propagating loadings in such areas. Experience indicates that the shell-side HAZ region of the re-pad weld will be most susceptible to enhanced creep damage accumulation (cavitation and cracking). Fortunately, experience also indicates that generally this damage propagates back under the re-pad in the same HAZ, as opposed to through the shell head (Fig. 2.10).

In summary, therefore, the production period approach to reactor assessment is a combination of simple inverse design calculations and connecting pipework analysis to identify high-stress regions, together with an experience-based assessment of likely high-damage accumulation features on the reactors.

2.5.3 Assessment procedure for reactor vessels at shutdown

Standard NDE procedures can be applied at shutdown to give information on current integrity status. Individual techniques can address surface integrity status, e.g. MPI, DPI, or internal wall and weldment integrity, e.g. UT and Radiography. However, a characteristic of these NDE approaches is that they provide information only on the current status and give no indication of the time for which this will persist at a safe serviceable level. For future planning and decision-making, techniques that provide information that is capable of predictive interpretation are required. Plant assessment technology can provide these. Metallurgical techniques applied through the non-destructive acetate replication route, and hardness determinations applied to the same high-quality prepared area, provide the basic data. In externally insulated vessels, creep damage leading to cracking initiates at the outer vessel surface since, after initial elastic stress redistribution, the principal tensile creep stresses are greatest at the outer surface.

Validated models for creep damage assessment are available and these can produce estimates of time to crack initiation. High-temperature crack growth models can then be used to predict both time to failure and the nature of that event.

Standard replication will provide additional, highly localised information on current surface, and with limited local excavation, on sub-surface condition.

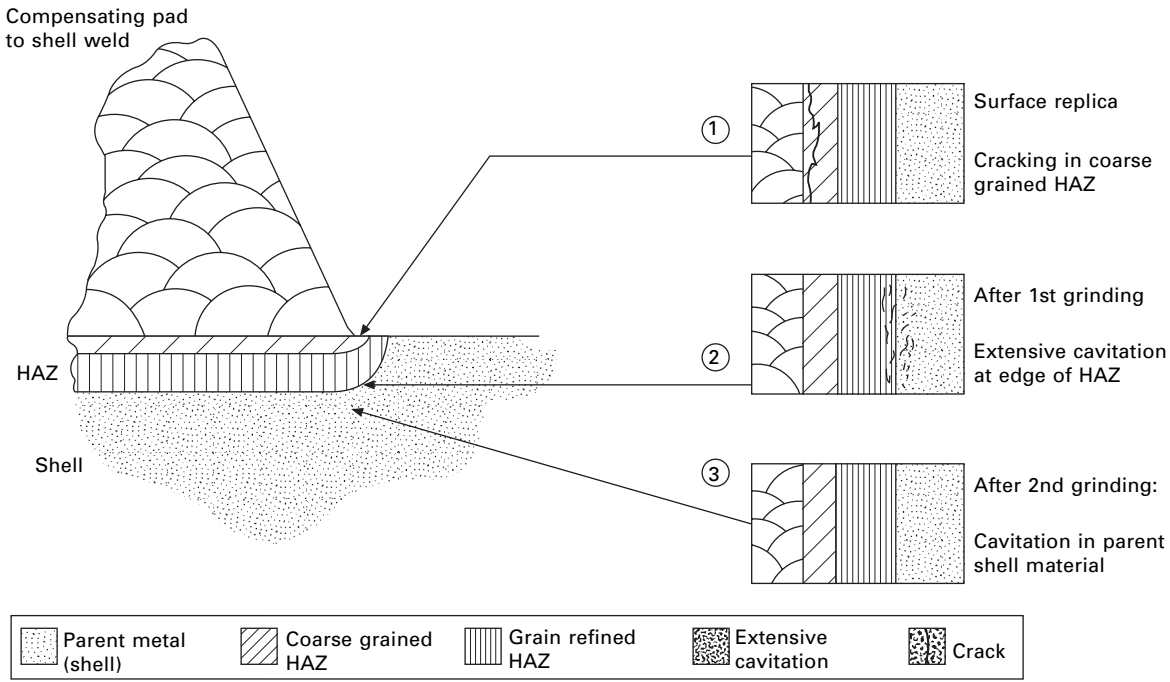

2.10 Damage development in re-pad nozzle designs.

If damage is evident in the form of cavitation or micro-cracking, 'A' Parameter or cavity density models can enable quantifiable results to be derived for future planning purposes (Cane and Townsend, 1983).

A cautionary note regarding the acetate replication technique is relevant. Like most NDE techniques, replication can be applied, albeit badly, with the minimum of training. However, to reproduce all the damage and relevant metallurgical features available from a replica site faithfully requires high degrees of practical skill. This requires operators to utilise best-practice metallographic laboratory techniques including multiple etch-polish procedures. Without such skill and care it is easy to mask or miss faithful reproduction of damage (Fig. 2.11). Finally, of course, the examination and interpretation of replicas is best performed by qualified, experienced metallurgists.

2.5.4 Specific experience on catalytic reformer plant

A client had a strategic requirement for an uninterrupted three-year run campaign on their No. 1 semi-regenerative CRU, while No. 2 CRU was being revamped. The nozzle design (Fig. 2.12) was not the optimum as the geometric change of section between the set-in nozzle and the reactor head was near a right angle and was coincident with the metallurgical changes associated with the weldment.

NDE inspection at a planned shutdown revealed significant nozzle cracking. A replica-based investigation and engineering analysis identified the nature, quantity and significance of the creep cracking and cavitation damage. Creep

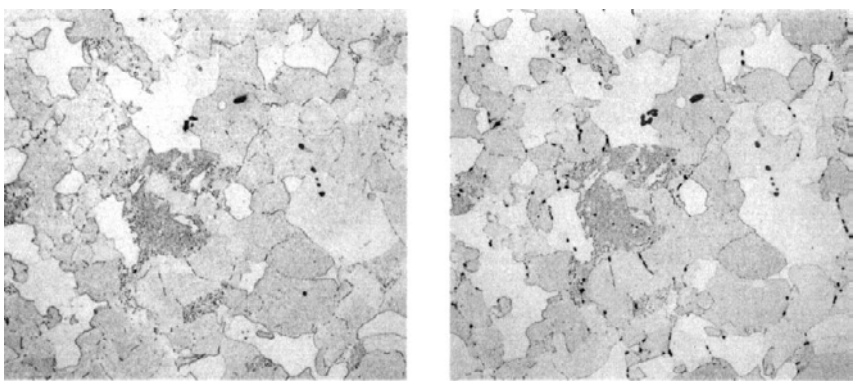

Inadequate preparation
Microstructure clearly resolved but no significant cavitation apparent

Correct application of procedure reveals extensive cavitation

2.11 Example of the results of incorrect (left-hand) and correct (right-hand) preparation procedures for acetate replication on the same sample.

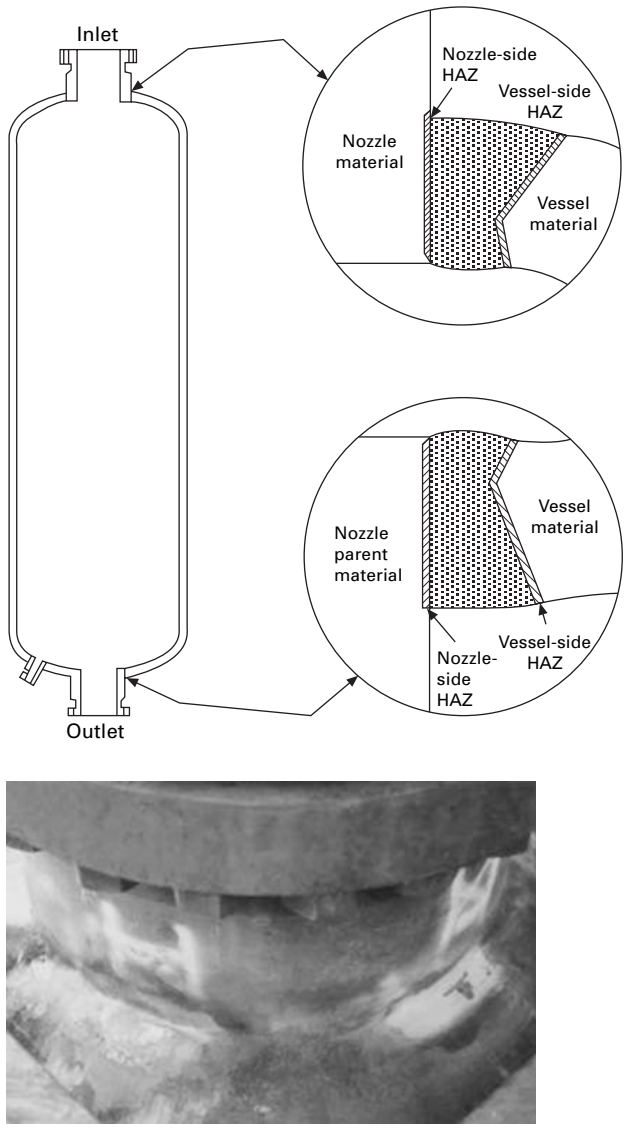

2.12 Reactor inlet nozzle and weldment geometry details.

crack growth analysis revealed that the existing cracks could grow to a critical size within the proposed three-year run period. Weld repair was thus a priority. An 'A' parameter creep cavitation damage depth profile was deployed to plan the extent of repair (Figures 2.13–2.15). A mechanical machining method was adopted to remove all cracking and cavitation from the weld metal and associated HAZ (Fig. 2.16) Replica checks at the bottom of the excavation were performed to confirm a damage-clear situation (Fig. 2.17).

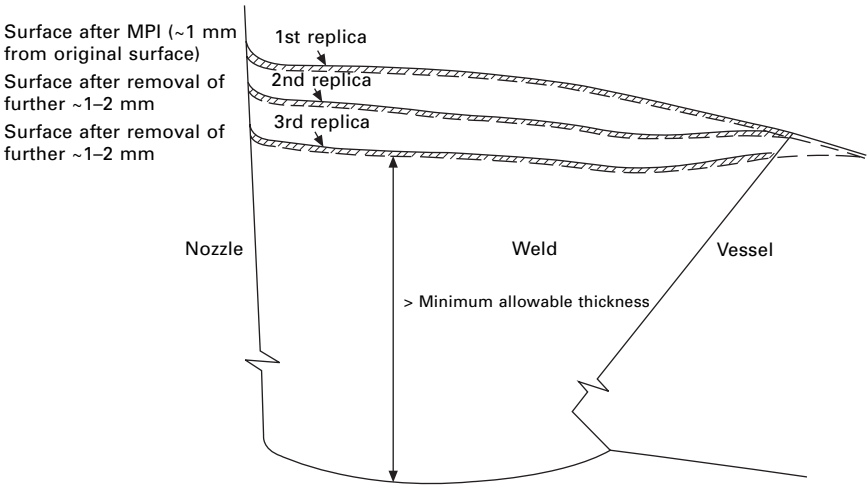

2.13 Replica locations taken at increasing excavated through-wall depth.

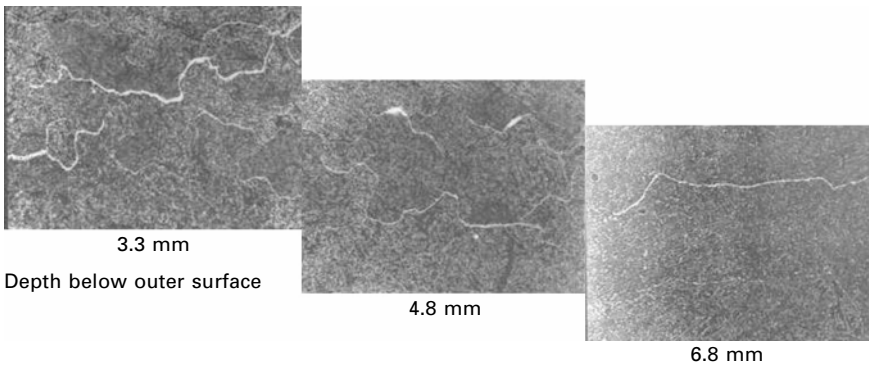

2.14 Creep damage decreasing through reactor wall.

Following repair and subsequent return to service, the required production campaign from No. 1 CRU was achieved.

2.6 Pipework

2.6.1 Factors controlling the integrity and life of pipework

Unlike reactor vessels where both hot- and cold-shell designs are extant, all CRU transfer pipework operates in hot service in a temperature range of approximately 400–530 °C. Parent material is generally of $1–1^{1}/_{4}Cr^{1}/_{2}Mo$

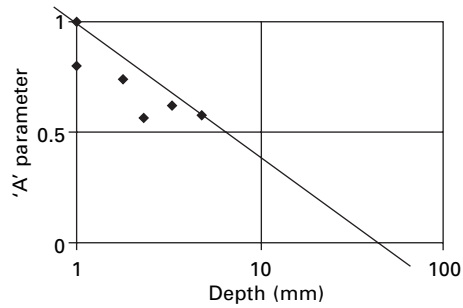

2.15 Quantification of creep damage variation through reactor wall (outer surface = 1 mm, inner surface = 100 mm).

(a)

(b)

2.16 Removing damaged weld metal and HAZ from inlet nozzle weldment.

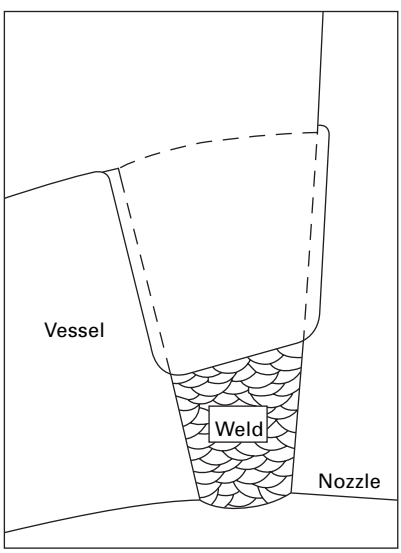

2.17 Nozzle weld profile after damage removal.

composition, with matching weld metal, and consequently it is operating in a regime where creep damage accumulation and the potential for hydrogen attack are major life-limiting factors. The integrity of high-temperature pipework systems is initially governed by the behaviour of the fabrication weldments under the various loadings characteristic of pipework systems. However, although more at risk to initial cracking and failure, welds are generally repairable and therefore do not absolutely limit the life of the component. The economic consequences of failure are generally more severe where failure occurs in the parent section of a component. However, this is not likely until several instances of severe weldment damage and leakage have been experienced and thus inherent prior warning is available.

The major high-temperature damage mechanisms on CRU transfer pipework are reheat cracking, and Type IV cracking (Fig. 2.18). The former results from residual stresses from welding that have not been adequately relieved during post-weld heat treatment (PWHT). Generally, if such damage is not found in the early stages of service it is unlikely to be initiated by the continually relaxing residual stresses. Of more concern is Type IV damage accumulation in the inter-critically annealed regions of the weldment HAZ. The loadings driving such damage are sustained and axial in nature and arise from pressure and externally applied system sources. Pressure stresses are generally adequately dealt with in design by the code procedure. However, it has been determined that the damaging loadings are those due to inadequate support of the installed pipework and insulation weight, to overweight pipework spools or to practical variations in design cold pull. System stresses are distributed within the pipework and are maximised at terminal weldments to heaters, reactors and heat exchangers where the dead weight imbalance loadings are reacted.

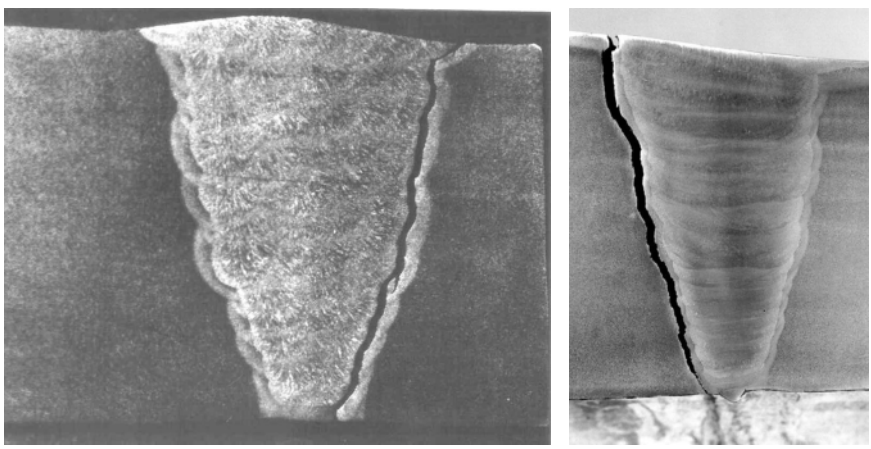

2.18 Examples of reheat cracking (left-hand) and Type IV cracking (right-hand) in butt welds.

A characteristic of Type IV damage, where it occurs, is the rapid rate of crack progression from approximately mid design life onwards. Experience of these rapid rates and subsequent leaks and failures emanates more from the power generation industry, where pipework runs are often longer than those on CRU plants, and the temperatures slightly higher. However, many examples of this type of damage have been found in CRU service, often necessitating removal by grinding, extensive weld repair or even near immediate replacement.

Particular attention must be given to transfer pipework where seam-welded pipe runs are used. In such cases, experience from the American power industry steam reheat line catastrophic failures should be borne in mind. The critical factors identified are weld geometry, weld metal and flux compositions and pipe ovality. Generally, older CRU units utilise seamless pipe in this service but some instances are known, particularly in larger capacity units, where seam-welded pipe is in service. Where necessary, this factor can be taken into account in the assessment procedure described below. Seam welds are subject to the full pressure hoop stress, as well as to many of the system loads. Failure of such a weld is likely to lead to a full-scale rupture, rather than a leak. Accordingly, they must be treated as critical items for assessment, and replacement, rather than repair, should be considered the ultimate outcome.

2.6.2 Assessment approaches for pipework prior to shutdown

Plant assessment technology can provide guidance at this stage by prioritising the high risk of failure areas on transfer pipework systems, thus enabling targeted inspection.

As stated earlier, the same approach can be applied to reactors. However, the assessment costs involved relative to inspection costs for reactors and pipework makes it much more cost beneficial in the case of the latter. The approach can thus be used for both component types, although the example given below is for CRU transfer pipework.

The information available prior to shutdown access will generally consist of:

- Pipework design details.
- Support and guide types and cold and hot settings.
- Materials specification for pipework.
- Process temperature and pressure data for each transfer line and their variation with time, particularly start and end of run on semi-regenerative units.

The production period assessment procedure is two-fold and involves stress analysis and probabilistic creep life calculation.

The stress analysis provides information on where high-risk areas are located within each run of the transfer pipework system, and the creep life analysis quantifies the probability of failure as a function of operating life for each location at which the stress has been calculated. The probabilistic treatment accounts only for creep life consumption through service life, as experience indicates that corrosion and other wastage processes are not a major factor in either reactors or transfer pipework. The assessment procedure is applied to each geometric element of each pipework run (Table 2.3). The table gives component/feature identification together with stresses calculated for start of run (SOR) and end of run (EOR) conditions. The present service hours reflect engineering changes that have been made to the pipework during service. The remaining life to 1% CFP is given, together with failure probability at the current service hours, and the associated risk ($ per year), again at the present time that reflects the varying consequences of failure associated with each of the pipework elements.

Due to some areas of uncertainty in the input data, the results, (Fig. 2.19) should be viewed on a relative, as opposed to an absolute, basis. Nevertheless, when the described combined approach is applied it provides an enhanced input to the inspection decision-making process (Barrien, 1998; Barrien, Jarvis and Townsend, 1997). The ability to inspect critical as opposed to all locations on the transfer pipework system has significant cost benefits.

2.6.3 Assessment approaches for pipework at shutdown

The procedure adopted is identical to that for reactors in the same situation. Targeted areas, as defined in Section 2.6.2, can be subject to standard NDE procedures and, if the pre-shutdown assessed risk is significant, also to *in-situ* metallographic investigation through the acetate replication technique with subsequent quantitative predictive interpretation. The results can be used directly in the shutdown period to recalibrate the relative probability of failure rankings and reduced or increased inspection instituted accordingly, depending upon results.

On a practical note, circumferential welds should always be replicated at the four quadrant positions as damage distribution can vary significantly due to the bending stresses often operating in pipework. Also, in view of the higher consequences of failure, 100% NDE coverage of seam welds is normally advised.

2.7 Heat exchangers

Combined feed heat exchangers can be assessed in the same way as reactor pressure vessels; therefore they need not be dealt with in detail here. The pre-shutdown approach that is adopted for pipework can be utilised but the

Table 2.3 Pipework components and results of two-stage analysis

	SOR	EOR				
Temperature, °C	450	500	Present	Remaining life	Present	Present risk,
Pressure, MPa	3	3.1	service, h	to 1% CFP, h	probability	$ / year
Position	Stress, MPa					
T-piece	59.35	66.24	249660	144138	2.41E-03	4.03E+02
Straight 1a	36.70	41.02	249660	1138227	8.17E-06	5.45E+00
Field weld 1b2a	36.70	41.02	249660	1138227	8.17E-06	5.45E+00
Straight 2b	35.10	38.98	249660	1315978	3.99E-06	2.66E+00
Bend 1	47.50	51.28	249660	501600	1.87E-04	1.25E+02
Straight 3a	33.60	36.66	249660	1537355	1.74E-06	1.16E+00
Straight 3b	32.90	34.90	249660	1702347	9.68E-07	6.46E-01
Bend 2	47.40	51.31	249660	503004	1.86E-04	1.24E+02
Straight 4a	31.20	34.44	249660	1860090	5.84E-07	3.90E-01
Straight 4b	38.30	42.16	249660	1023093	1.33E-05	8.85E+00
Bend 3	53.90	58.41	249660	284909	7.85E-04	5.24E+02
Straight 5a	37.20	40.38	249660	1146623	7.80E-06	5.20E+00
Field weld 5b6a	37.20	40.12	249660	1158710	7.40E-06	4.94E+00
SPL1	37.20	39.99	249660	1164795	7.21E-06	4.81E+00
Straight 6b	46.00	51.28	249660	531139	1.58E-04	1.06E+02
Bend 4	61.30	66.70	249660	124370	2.87E-03	1.91E+03
Straight 7a	47.30	52.62	249660	478307	2.17E-04	1.45E+02
SPL2	32.30	34.15	249660	1800602	6.96E-07	4.64E-01
Field weld 7b8a	33.20	36.50	249660	1572057	1.54E-06	1.03E+00
Straight 8b	39.80	44.10	249660	894435	2.38E-05	1.59E+01
Bend 5	53.90	58.54	249660	283214	7.95E-04	5.30E+02
Straight 9a	40.10	44.54	249660	868990	2.69E-05	1.79E+01
Straight 9b	32.80	35.57	249660	1661347	1.12E-06	7.49E-01
Bend 6	46.10	49.83	249660	561169	1.32E-04	8.81E+01
Straight 10a	30.60	32.52	249660	2071242	2.95E-07	1.97E-01

Table 2.3 Continued

	SOR	EOR				
Temperature, °C	450	500	Present	Remaining life	Present	Present risk,
Pressure, MPa	3	3.1	service, h	to 1% CFP, h	probability	$ / year
Position	Stress, MPa					
SPL3	30.60	32.01	249660	2118208	2.54E-07	1.70E-01
Field weld 10bB7	30.60	32.01	49932	2317936	1.84E-12	6.12E-06
Bend 7	37.10	41.57	49932	1296289	4.56E-10	1.52E-03
Straight 11a	29.30	30.41	249660	2400881	1.11E-07	7.40E-02
Straight 11b	29.30	30.41	249660	2400881	1.11E-07	7.40E-02
Reactor	49.30	55.59	249660	390410	3.80E-04	6.34E+01
		Circuit:	overall		7.84E-03	
			critical	124370	2.87E-03	1.91E+03

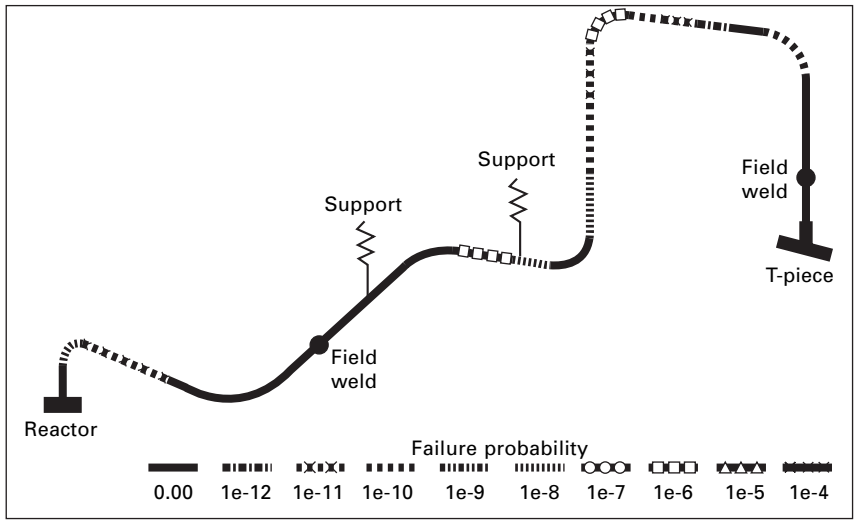

2.19 Results of pre-shutdown assessment showing calculated relative risk of failure of individual parts of pipework run.

cost benefit considerations that tend to preclude application to reactor vessels equally apply to heat exchangers. As with any fabricated vessel, critical locations are generally associated with weldments. Locations that constitute terminal reaction points, due to the connections with pipework, merit particular attention at the exchanger and pipework weldments.

A slight difference between nozzles on reactors and nozzles on heat exchangers is that whereas on the former the geometry is axisymmetric, on heat exchangers nozzle geometry effectively equates to a branch tee where the nozzle diameter is smaller than the body diameter. Hence, at the flank positions the loading is due to the full exchanger-body hoop stress whereas at the saddle position the loading across the nozzle/body weldment is only approximately half the hoop stress. The flank positions should therefore be given careful attention.

2.8 High-temperature hydrogen attack

2.8.1 Background to hydrogen attack

Mention was made earlier in this chapter of hydrogen attack being a potential life-limiting degradation mechanism. As experience indicates that this can manifest itself in reactors, pipework and heat exchangers, it is expedient to deal with the available assessment procedures in a common section.

Component susceptibility to hydrogen attack is a function of material chemical composition, microstructural response to fabrication heat treatments,

service temperature, hydrogen partial pressure and time. Attack can manifest as surface decarburisation or as in-depth void formation, blistering and cracking.

2.8.2 Assessment of hydrogen attack prior to shutdown

Predictive approaches that can be currently made in this period with respect to this particular damage mechanism are unfortunately restricted to comparison with the information available from the latest Nelson curves, API RP-941 (2004). Whilst this is an important source of information, it is increasingly found that the shortcomings inherent in this experience-based database can give cause for some concern. Currently there is no fundamental mechanistic basis for the positions or shapes of the various curves. There is also no inherent time dependency built into the majority of the Nelson curves, other than their general downward shift as increasing service experience on older plant data becomes available. Whilst the curves give some indication of the damage form to be expected (decarburisation, cavitation, micro-fissuring and major cracking), data on the development of the same with increasing service exposure is vital for realistic component management.

It is worthy of comment that there are initiatives in progress (within API, EFC and elsewhere) to address these shortcomings in what is otherwise the best assessment approach currently available. Brear and Church (1996) have demonstrated that the Nelson curves can be modelled in simple terms of carbon and hydrogen solubilities and diffusivities, and this work is currently being extended to address the kinetics of hydrogen attack. Work in Japan, particularly on $C^1/_2Mo$ steel (Kawano, 2004), has led to the development of kinetic formulae for hydrogen attack, which are now sufficiently well accepted to have found a place within the API RP580/581 (2000) procedure for risk-based inspection. However, further work remains to be done in this area.

2.8.3 Assessment of hydrogen attack at shutdown

The main viable approaches that can be made in the shutdown access period are visual examination for gross manifestation and advanced UT methods for inner-wall region damage, particularly when outside access is that which is most expedient (Kot, 2001). Areas for examination can currently only be targeted for likely susceptibility by consideration of temperature, hydrogen partial pressure (Nelson curves) and service time. *In-situ* metallography can be deployed for confirmation purposes where damage is near the surface or limited excavation is permissible and justified by the already known presence of the damage.

Assessment procedures are available for evaluating the effect of quantified levels of hydrogen attack on vessel integrity. These are mainly based on a remaining sound ligament approach and do not rigorously take account of

the accepted synergistic effect of creep crack growth rates in hydrogen charged and damaged material. As a consequence, reliance must be placed on adopting conservative values for the relevant parameters and the use of additional safety margins in interpretation of the data, as advised in API RP-579 (2000).

2.9 Conclusions

This chapter has illustrated that plant assessment technology tools can provide results, quantified in most cases in probability of failure versus time terms, that give the Inspection, Maintenance and Operations functions a basis on which to optimise the cost benefit of their decisions and actions, both prior to and during shutdown of the plant and which can be deployed within an integrated framework for through-life plant management.

2.10 Acknowledgements

The first draft of this chapter was written whilst the authors were employed by ERA Technology Limited, UK. The authors would like to thank their colleagues at ERA, SES Europe, and at client companies, for their contributions to the development of the underlying risk and life assessment technology. They are also grateful to the many plant operators who have shared their experiences of plant asset management. This work is published with the permission of the Directors of ERA Technology Ltd and the Directors of Stress Engineering Services (Europe) Limited.

2.11 References

American Petroleum Institute, *Calculation of heater tube thickness in petroleum refineries*, API Recommended Practice 530, various editions and dates

American Petroleum Institute, *Fitness for service*, API Recommended Practice 579, First Edition, 2000

American Petroleum Institute, *Risk based inspection* API Recommended Practice 580, First Edition, 2000

American Petroleum Institute, *Risk based inspection – base resource document*, API Recommended Practice 581, First Edition, 2000

American Petroleum Institute, *Steels for hydrogen service at elevated temperatures and pressures in petroleum refineries and petrochemical plants*, American National Standard/ API Recommended Practice 941, Sixth Edition, 2004

Barrien, P., 'Optimising refinery dependability and turnaround costs by application of a risk based inspection programme', Paper 588, *Corrosion 98* NACE, 1998

Barrien, P., Jarvis, P., Townsend, R.D., 'Risk based inspection and maintenance optimisation of high temperature plant', Conf. *Operating Pressure Equipment*, Brisbane, Australia, 7–11 April 1997

Brear, J.M., 'An integrated approach to through-life risk and reliability management' ETD Int Conf *Maintenance and Overhaul Management in Power Generation*, IMechE, London, 1–2 Oct 2003

Brear, J.M., 'A practical route for the life assessment of boiler pressure parts' SMiRT 13 Post Conference Seminar *Intelligent Software Systems in Inspection and Life Management of Power and Process Plants*, Paris, 25–27 August 1997

Brear, J.M. and Townsend, R.D., 'Modern approaches to component life assessment – damage, degradation, defects', SMiRT 13 Post Conf Seminar *Application of Intelligent Software Systems in Power Plant, Process Plant and Structural Engineering*, Sao Paulo, August 1995, Published as *CEC Report EUR 17669 EN*, ed A.S. Jovanovic, A.C. Lucia, JRC Ispra, 1997

Brear, J.M. and Church, J.M., 'Technical basis for API Publication RP941 (Nelson Curves)', Third Int Conf *Engineering Structural Integrity Assessment,* Cambridge, September 1996

Brear, J.M., Jarvis, P. and Middleton, C.J., 'Managing the pay-off between risk, reliability and remaining life – weighting the consequences', ETD Int Seminar *Risk Based Management of Power Plant Equipment*, Inst. Matls. London, 21–23 Oct 2002

Brear, J.M. and Williamson, J., 'Life assessment of fired heater tubes in the refinery and petrochemical industries', NACE Int Conf *Corrosion Asia*, Singapore 1992

Brear, J.M. and Williamson, J., 'Managing the life of high temperature refinery plant – the interaction between risk based inspection and remaining life assessment', ERA Conf *Engineering Asset Management for Utilities, Industry and Commerce*. Paper 7.4, London, October 1998

Cane, B.J. and Townsend, R.D., 'Prediction of remaining life in low alloy steels' Proc. Seminar *Flow and Fracture at Elevated Temperatures*, ASM Philadelphia, 1983, pp 279–316

Kawano, K., *Recent activities on high-temperature hydrogen attack*, Idemitsu Engineering Company Ltd., Chiba, Japan (available via the internet), published 2004

Kot, R., 'Hydrogen attack, detection, assessment and evaluation', *10th Asia-Pacific Conf. on Non-Destructive Testing*, Brisbane, Sep 2001

Lilley, J. and Ruiz Camarena, H., 'The detection and assessment of carburisation damage in visbreaker heater tubes', *9th European Conference on NDT*, 25–29 September 2006, Berlin, DGZfP (German Society for Non-Destructive Testing) Proceedings BB 103–CD.

Williamson, J., Bissell, A.M. and Cane, B.J., 'Non-destructive condition assessment and remanent life prediction of reactor vessels in petrochemical plant', Int Conf *Life Extension and Assessment*, The Hague, 1988

3

The use of spot hydrogen flux measurements in assessing corrosion and crack risk in refinery applications

F. D E A N, Ion Science Ltd, UK

3.1 Introduction

The movement of mobile atomic hydrogen through steel, known as hydrogen permeation, is a pre-requisite for most types of hydrogen damage, including hydrogen induced cracking (HIC), stress oriented hydrogen induced cracking (SOHIC) and disbonding. Hydrogen emanating from the external or exit face of a pipe or vessel is known as efflux. Efflux measurements provide information relating to cracking risk, and also to the cause of hydrogen permeation; namely certain reactions at the steel interior or entry face. The objective of this chapter is to define circumstances conducive to hydrogen permeation through steel, and provide a calculation which uses efflux, steel thickness and temperature to obtain an indicator of cracking risk, and corrosion rates at the entry face.

3.2 Scenarios leading to hydrogen permeation and detection

The progress of hydrogen to an efflux detector on the external pipe or vessel face involves three essential steps: hydrogen entry into the vessel wall, permeation through it, and exit from the external surface to some means of detection. Factors governing this progress are summarised in Table 3.1.

At low temperatures (less than 100 °C), hydrogen efflux observed from steel in refinery service is almost exclusively the consequence of hydrogen entry into steel due to corrosion by certain active corrosive agents known as hydrogen promoters. Of these, sour gas and hydrofluoric acid (HFA) are of most significance. At higher temperatures, hydrogen efflux has been observed in association with naphthenic acid corrosion [1] and acid salts [2] (it does not depend so crucially upon the presence of hydrogen promoters) and due to direct dissolution of hydrogen gas within the process stream into steel.

As can be seen from the right-hand column of Table 3.1, there are a number of factors facilitating the movement of hydrogen through steel at

Table 3.1 Summary of factors affecting hydrogen permeation through steel from entry to sensor detection

	Factor affecting hydrogen progress	Progress is retarded by...	Progress is facilitated by...
Hydrogen entry	Access of hydrogen gas or corrosive agent to entry surface	Corrosion product build up[a]	Product breakdown (cyanide, low pH, high flow velocities, HT, internal inspection)
		Corrosion-resistant coatings, e.g. metallisation	
	Hydrogen entry reactions at surface	Corrosion inhibitors	Inhibitor removal (high flow velocities, HT)
		High pH	Low pH
		–	LT: Sour gas and HFA HT: Reaction with any protic (acid) compounds and H_2 gas
	Hydrogen solubility in steel *c*	High steel Si content	Many steel alloying elements and their nitrides and carbides[b]
		LT	HT
Hydrogen permeation	Rate of diffusion through steel (diffusion coefficient *D*)	Many steel alloying elements and their nitrides and carbides	
		LT	HT
	Steel thickness	Thick steel walls	Thin steel walls
	Removal of mobile hydrogen into deep traps	Recently commissioned or heat-treated steel	Pre-corroded steel
	Extensive blistering or delamination	LT	HT
		LT	HT

Hydrogen exit	Hydrogen desorption	Very low permeation flux	Sensing technology which strips hydrogen from surface
	Hydrogen migration through coatings	Integral metal coatings, thick, aged coatings	Organics in coatings, e.g. in alkyd and epoxy coatings[c]
	Sensing interfaces	Various	Various

LT = low temperature, <100 °C. HT = high temperature, >100 °C.
Notes:
[a] The passivation of corrosion reactions is very closely dependent on the corrosive scale formed. For example, at ambient temperatures, wet H_2S corrosion is almost completely passivated by FeS formation, whereas fluoride product only partially passivates HF corrosion [8].
[b] Steel constituents which increase solubility c tend to retard its diffusion through the steel. Since permeability $P = D \cdot c$, steady state efflux is not strongly affected by composition.
[c] Fusion bonded epoxy (FBE) and epoxy resins have been reported [9] not to significantly affect hydrogen efflux from steel surfaces.

high temperatures ('HT', >100 °C), namely a decreasing effectiveness of barriers preventing access of hydrogen donors to the steel surface, a decreased kinetic barrier to hydrogen entry reactions, increasing solubility of hydrogen, increased rate of diffusion and decreased trapping of diffusible hydrogen within the steel at grain boundaries and within voids, including pre-existing blisters.

The effect of elevated temperature on facilitating hydrogen permeation through steel to a monitor on the external surface is to shorten the time of transience though the steel and to increase the flux of hydrogen through the steel, and efflux from the exit face. The same may be said of thickness. For steel walls of greater than a few millimetres in thickness [3–6], a well defined corrosion activity at an entry face will generate a steady state flux through steel inversely proportional to its thickness. However, the time required for hydrogen to traverse steel increases as the square of thickness. For this reason thick steel is more subject to cracking than thin steel.

3.3 Measurement of hydrogen activity based on flux measurement

As indicated above, the hydrogen efflux emanating from steel is influenced by both temperature and thickness. Thus it is preferable to 'normalise' efflux measurements with respect to steel temperature and thickness, to obtain a more universally comparable parameter indicating HIC risk and corrosive action. It is desirable for this normalised parameter to have some physical meaning. In this chapter the parameter recommended is the minimum hydrogen activity at the hydrogen entry face, a_0, of, for example, a pipe or vessel subject to sour gas or HF corrosion.

a_0 is dimensionless, and is a direct indicator of steel propensity to crack and corrosion activity. The conversion presented in Table 3.2 is appropriate for steel temperatures below 150 °C (300 °F), obtained from a reliable efflux probe.

3.3.1 Confidence guidelines

The conversion of flux into activity is considered valid for all low alloy carbon steels in petrochemical service. Limitations of the conversion provided herein are implicit in the derivation provided in the next section.

The most important assumption that will be made in field use is that a measured efflux J corresponds to a steady state flux, J_{ss}. In many situations, corrosion activity will vary with time, and a spot flux measurement conversion should be viewed as yielding a minimum hydrogen activity at the entry face, irrespective of whether the flux is rising or falling. A high degree of confidence can obtained from low variance of efflux registered over time periods, as

Table 3.2 Manual calculation of hydrogen activity at inside of pipe from hydrogen flux measurement. To convert flux into an activity of hydrogen at the inside face of a vessel or pipe wall, the following are required:
– the pipe temperature in deg C to the nearest 5 deg
– the pipe or vessel wall thickness in mm
– the flux measured in pl/sqcm/s normalised to 20 °C (= Hydrosteel measurement)
Enter values in the table from left to right. Use a calculator to obtain a_0 in column H.

A	B	C	D	E	F	G	H
Enter site reference here	Enter test date here	Enter test time here	Enter temperature of steel in °C here	Obtain E value from D value using table below. Enter here	Enter thickness of steel in mm here	Enter flux in pl/sq cm/s here	Enter **E** × **F** × **G** = hydrogen activity a_0 here
Example	05/09/01	12:00	40	0.0352	9	1200	380

D value	E value	D value	E value	D value	E value
–20	0.6046	40	0.0266	100	0.0032
–15	0.4409	45	0.0216	105	0.0028
–10	0.3255	50	0.0177	110	0.0024
–5	0.2430	55	0.0146	115	0.0021
0	0.1833	60	0.0121	120	0.0018
5	0.1397	65	0.0101	125	0.0016
10	0.1075	70	0.0084	130	0.0014
15	0.0835	75	0.0071	135	0.0012
20	0.0654	80	0.0060	140	0.0011
25	0.0517	85	0.0051	145	0.0010
30	0.0411	90	0.0043	150	0.0009
35	0.0330	95	0.0037		

Table 3.3 Recommended time scales for ensuring confidence that invariant efflux measurement corresponds to J_{ss}, the steady state flux

Thickness	Temperature	Evaluation time
< 13 mm	< 50 °C	1 hr
	> 50 °C	15 min
13 to 26 mm	< 50 °C	4 hr
	> 50 °C	1 hr
26 to 39 mm	< 50 °C	12 hr
	> 50 °C	3 hr

shown in Table 3.3. For example, suppose efflux from a 9 mm pipe wall at 40 °C increases from 1100 to 1200 pl/sq cm/s over a 1 hr period. Variation is low, so that the upper value of 1200 can be used to yield $a_0 = 380$ from Table 3.2 with high confidence. Note, the maximum flux is always used in obtaining a_0 from a monitored flux transient.

Uncertainty may result from incorrect steel temperature. It can be seen from the manual conversion in Table 3.2 that hydrogen permeation is very sensitive to temperature, and an error of 10 °C introduces about 30% error in the conversion.

3.3.2 Meaning of activity a_0

a_0 is the hydrogen activity at a corroding face necessary to generate steady state flux registered at the hydrogen exit face (the outside of the pipe) of a specified thickness and temperature.

Strictly, a_0 is dimensionless, indicating the concentration of hydrogen in steel relative to the concentration when steel is equilibrated with 1 bar of hydrogen gas. Thus, if $a_0 = 10$, then the steel at the corroding face contains $10 \times$ the hydrogen content of that steel exposed to 1 bar hydrogen gas.

Two distinct advantages of using hydrogen activity a_0 over concentration c_0 (e.g. ppm) as a criterion of hydrogen damage risk and corrosion are that:

(i) Much less error is obtained in determining a_0 from permeation data than c_0 from diffusion data, as diffusion parameters vary much more with steel composition and process route.

(ii) Interpretation of c_0 requires recourse to the prevailing steel temperature, whereas a_0 is directly related to a mechano–chemical parameter: the equivalent H_2 gas pressure that would be in equilibrium with steel of activity a_0 is equal to $(a_0)^2$ bar.

Cracking susceptibility

Because the concentration of hydrogen in steel varies as the square root of hydrogen gas pressure in equilibrium with it, a value of $a_0 = 10$ corresponds to an equivalent hydrogen pressure of 100 bar. Values of $a_0 = 1000$ are commonly generated in sour environments, from which the susceptibility of hydrogen to associate in steel and form hydrogen gas can be readily appreciated. However, the activity at which steel cracks is very dependent on the quality of the steel and whilst poor steels have been found to crack at $a_0 < 130$, high quality sour service steels can readily withstand $a_0 = 1000$ without discernible hydrogen damage. If activities are used as a risk based inspection criterion Table 3.4 can be used for guidance. Even though a_0 is independent of steel temperature and thickness, due to the long transience time for hydrogen in thick, cold steel, corresponding a_0 values are attributed additional risk.

Corrosion rates

Correlation of corrosion rates with hydrogen activity is expected to be close. At present we consider a value of $a_0 = 100$ to correspond to a corrosion rate of approximately 0.2 mm per year. At the time of writing, it can be stated that H_2S saturated NACE solution (pH 3) typically generates a flux corresponding to $a_0 = 1000$. This is a subject of active investigation. (Corrosion rate/flux correlation is actively under evaluation in a Joint Industrial Project between Ion Science and Bodycote Materials Testing. Further details are posted on www.ionscience.com.)

3.3.3 Derivation of activity conversion

Hydrogen permeates steel in very much the same way as heat through any solid. Thus the flow of hydrogen through steel can be likened to heat transfer through a solid, the hydrogen concentration gradient to a temperature gradient,

Table 3.4 Hydrogen damage risk. 0 = zero, 3 = high

Carbon steel quality	Is steel more than 16 mm thick AND at less than 50 °C?	Activity a_0		
		10 to 99	100 to 999	1000+
Poor, or near an average weld	No	1	2	3
	Yes	2	3	3
Average, or near a quality weld	No	0	1	2
	Yes	1	2	3
Sour service	No	0	0	1
	Yes	1	1	2

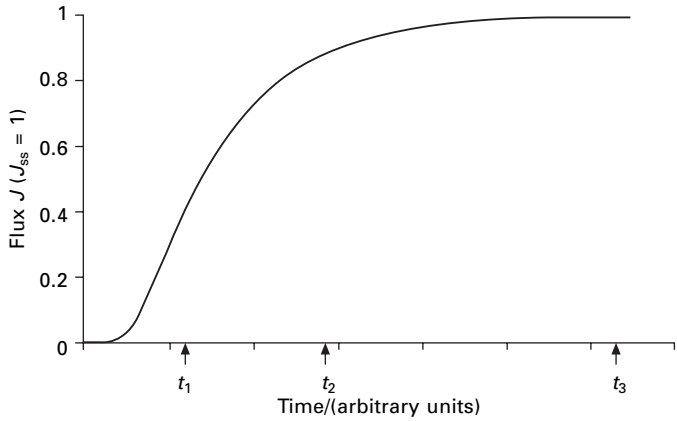

3.1 Flux transient at hydrogen exit face of steel following step increase in hydrogen entry at entry face.

and the solubility of hydrogen in steel to a heat capacity of a solid. The analogy is close because both hydrogen permeation through steel and heat transfer through solids are diffusive processes, whereby flow per unit area, or flux*, J (/ $Ncm^3 \cdot cm^{-2} \cdot s^{-1}$), is proportional to a concentration gradient. For steel,

$$J = -D \cdot dc/dx \qquad [3.1]$$

where D (/ $cm^2 \cdot s^{-1}$) is the hydrogen in steel diffusion coefficient, c (/ $Ncm^3 \cdot cm^{-3}$) the hydrogen concentration**, and x the distance from the hydrogen entry face. The time dependent form of Fick's 1st Law of diffusion, equation [3.1], can be used to derive flux transients through steel as a consequence to a step increase in c at the entry face, designated c_0, at a certain time t_0. The flux emanating from the exit face (e.g. the pipe external surface) in Fig. 3.1, and corresponding concentration distribution after progressive times, t_1, t_2 and t_3 are shown in Fig. 3.2. Note that the surface flux at any time is equal to the concentration gradient at the surface, and after time t_2 the concentration gradient through the steel is almost uniform, the flux reaches a steady state, J_{ss}, which can be used to evaluate c_0 through a thickness of steel w(/ cm). From equation [3.1]:

$$c_0 = J_{ss} \cdot (w/D) \qquad [3.2]$$

---

* For ready conversion of parameters, hydrogen quantities are quoted throughout in Ncm^3. 1 Ncm^3 = 1 cm^3 H_2 gas at 1 bar and 0 °C. Hydrosteel fluxes are converted accordingly. Units are cited immediately after each parameter is defined.

** 1 $Ncm^3 \cdot cm^{-3}$ = 11.36 ppm hydrogen in steel. Note this refers to *diffusible* hydrogen.

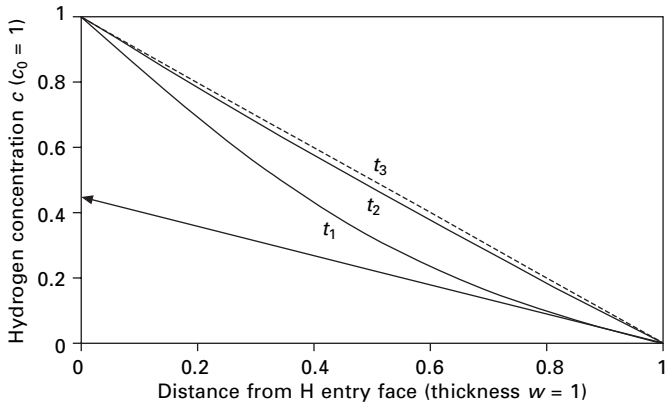

3.2 Corresponding hydrogen concentration profile through the steel at times t_1, t_2 and t_3. Note that applying eqn. [3.2] to the flux obtained at time t_1 yields an underestimated concentration at the entry face, whereas after t_2 the concentration gradient is sufficiently uniform for the equation to apply.

The chemical activity of hydrogen liable to cause damage or signify a degree of corrosive action is defined by the chemical activity, a:

$$a = c \,/\, c^0 \qquad [3.3]$$

where c^0 (/ $Nm^3 \cdot cm^{-3} \cdot bar^{-1/2}$) is the solubility of hydrogen in steel in equilibrium with H_2 gas at 1 bar. Solubility varies with H_2 pressure p according to:

$$c = c^0 \cdot p^{1/2} \qquad [3.4]$$

Thus the hydrogen activity a corresponds to an equivalent equilibrium H_2 gas pressure of a^2 bar. Permeability P (/ $Ncm^3 \cdot cm^{-1} \cdot bar^{-1/2} \cdot s^{-1}$) is defined by

$$P = D \cdot c^0 \qquad [3.5]$$

Combining and re-arranging equations [3.2] to [3.5] we obtain an entry surface activity a_0:

$$a_0 = p^{1/2} = J_{ss} \cdot (w/P) \qquad [3.6]$$

Finally we introduce the variance of P with temperature T (/ K). Both D and c^0 vary with T as $A \cdot \exp(-B/T)$, so their product, P, is of the same form. The evaluation of P at low temperatures for a comprehensive series of steels and steel treatments is given by Grabke and Riecke [7]. We use a value for a typical low alloy steel to determine P from steel temperature:

$$P = 0.00187 \exp(-4126/T) \qquad [3.7]$$

A remarkable feature of permeability is that it is not affected significantly by typical variations in composition or process treatment. Particularly at low temperatures, many alloying elements and their nitrides and carbides increase hydrogen uptake in 'flat' or reversible traps, decreasing D, but correspondingly increasing c^0. In accordance with equation [3.5], P is scarcely affected. Silicon appears exceptional in decreasing c^0 significantly at concentrations >1%, which are seldom encountered. Equation [3.7], is considered accurate to within 10% for most carbon steels in petrochemical service.

3.4 References

1. F.W.H. Dean, *Corrosion 2002*, NACE, paper 0234, NACE, Houston April 2002.
2. F.W.H. Dean, D.J. Fray, T.M. Smeeton, *J. Material Sci. and Technol.*, **18** (2002), 851.
3. M.R. Bonis, J-L. Crolet, *Corrosion 2001*, Paper 1067.
4. M.R. Bonis, J-L. Crolet, *Corrosion 2001*, Paper 1072.
5. M.R. Bonis, J-L. Crolet, *Corrosion 2002*, Paper 2036.
6. F.W.H. Dean, J. Material Sci. and Technol., **21(3)** (2005), 347–351.
7. H.J. Grabke, E. Riecke, *Materiali in Tehnol.*, **34(6)** (2000), 331–342.
8. F.W.H. Dean, P.A. Nutty, M. Carroll, *Corrosion 2001*, NACE, Paper 01636.
9. R.D. Tems, A.L. Lewis, A. Abdulhadi, *Corrosion 2002*, Paper 0345.

4

Degradation of carbon steel under the influence of sulfur in a refinery furnace – remaining life prediction

J. HUCIŃSKA, Gdańsk University of Technology, Poland

4.1 Introduction

Several furnaces are found in a number of oil refinery units. They are mainly used for preheating the feed to a reaction temperature before the feed enters a reactor or a distillation column. Furnace tubes are usually designed for a limited service life of 10 years [1]. However, some damage to the tubes is unavoidable during this time, regardless of proper material selection and the correct operation conditions.

In general, the damage to elevated-temperature equipment can be examined during shutdowns using many non-destructive testing methods. Material discontinuities can be revealed by means of ultrasonic, radiographic, liquid penetrant and magnetic current techniques, and the thickness of elements can be checked by ultrasonic measurements. It is also possible to assess the remaining life of a component by taking some replicas from the components' surface, analysing the replicas using an electron microscope and then comparing the data with standard microphotographs of a similar material whose remaining life is known [2, 3].

This chapter presents some studies carried out to extend the life-time of refinery furnace tubes beyond their classically defined design life. The material and the service conditions are given and the results of some in-service non-destructive examinations of one of the tubes are reported. Some results of destructive after-service examinations of the tube are also presented and elevated temperature damage is evaluated. An assessment of presumable further damage to the steel has been performed and the remaining life of the tubes is predicted.

4.2 Material and service conditions

The material used for the studies was a commercial carbon steel. The steel was in the form of tubes of 168 mm diameter, and 7 mm thickness. The tubes were in furnace service in the Refinery of Gdańsk for 11 years. The

Table 4.1 Characteristics of the carbon steel tested and the service conditions

Characteristics	Description
Composition of steel in wt. %	C–0.17, Mn–0.69, Si–0.22, P–0.035, S–0.035, Cr–0.11, Ni–0.10, Cu–0.17
Heat treatment of steel	Normalising
Equipment	Furnace in desulfurising unit, radiant section, 48 vertical tubes around burners
Environment	Heavy naphtha after desulfurisation, about 0.3 ppm of sulfur. Temperature and pressure: 200–220 °C, 140 kP (first 9 years) and 130–160 °C, 60 kP (last 2 years)
Maximum metal skin temperature	About 380 °C (first 9 years) and about 220 °C (last 2 years)

characteristics of the steel and the service conditions are presented in Table 4.1. It is shown in the table that during the last two years of service the temperature in the furnace was distinctly lower.

4.3 In-service examinations

Ultrasonic testing method WIT [4, 5], based on ultrasonic wave attenuation measurements at 12 MHz, was used for in-service examinations of the tubes. It is well known that damage to the steel surface and/or degradation of the steel structure changes the attenuation of the waves. Though the WIT method does not show any relation between the attenuation and the mode of steel damage, it reveals deviations from the standard state of the steel.

The same six tubes of the highest metal skin temperatures were examined every time: on the fire-side of the furnace and 3.5 m above the furnace floor. Intensity attenuation coefficients A_{12}^{L} were measured and compared with coefficient $A_{12}^{L} <= 1$ in the as-received steel. Comparing the actual attenuation measurements and the Brinell hardness (HB) measurements with standard characteristics, presumable mechanical properties of the steel including ultimate tensile strength (UTS^{WIT}) and yield stress (YS^{WIT}) at 20 °C were assessed. Non-destructive characteristics of the tube of the highest attenuation coefficients are shown in Table 4.2. It can be seen that the furnace service resulted in a remarkable growth of the intensity attenuation coefficients in the tube. However, the wall thickness of the tube was about the same as in the as-received state and the presumable mechanical properties were within standard requirements [7]. After 11 years of service, the tube was disassembled and put on destructive testing.

Table 4.2 Non-destructive characteristics of the carbon steel tube by means of WIT method [6]

Characteristics	Time of service, years			
	4	6	9	11
Wall thickness, mm	7.0	7.0	6.5	6.5
A_{12}^{L}, dB/cm	1.75	>2	2.23	1.83
HB	132	144	145	152
UTS^{WIT}, MPa	430	455	475	475
YS^{WIT}, MPa	(255)	(285)	280	280

4.4 After-service examinations

Experimental

Full-section samples situated on the fire-side of the furnace, close to the ultrasonic measurements' position were collected from the tube for destructive examinations. They were compared with a sample taken from the as-received element.

Plane orthogonal sections of some samples were prepared metallographically and etched using a solution of 4% by volume nitric acid in ethanol. They were examined making use of a field emission Hitachi 4200 scanning electron microscope (SEM) linked to an X-ray energy dispersive spectrometer (EDS). A Jeol JXA-50A electron probe microanalyser (EPM) was used to assess the carbon content across the sections. Specimens for transmission electron microscopy (TEM) were prepared from the sections using the carbon extraction replica technique. The types of the extracted precipitates were identified in a Jeol JEM 100C TEM using the selective diffraction technique, and the composition of the precipitates by means of EDS was determined.

Some mechanical properties examinations were also performed. They included tensile tests carried out at 20 °C and 400 °C on full-section specimens by use of an Instron 1195 machine, and Charpy impact tests at 20 °C on half size V-notch specimens using a 300 J Izod machine.

Results

The SEM examinations revealed that the inside surface (IS) of the tube was covered with a thin and fragile scale consisting of iron and sulfur. In some areas of the samples, inclusions of internal scale in a subsurface metal layer were present, reaching a depth of about 200 μm. Disappearance of pearlite grains and some boundaries of ferrite grains in this layer were noted.

TEM examinations of the carbon extraction replicas provided basic information on in-service degradation mechanism of the steel. TEM micrographs of the replicas taken from the as-received specimen and from the after-service specimen were compared. In the received specimen sound

carbide/cementite lamellae within pearlite grains were present. The diffraction analyses confirmed that the carbides were of Fe_3C type. In the after service specimen, damage to lamellar microstructure of cementite and a partial disintegration of the pearlite grain was seen. The diffraction analyses revealed the heavily deformed quasi-crystalline structure of these particles.

EDS analyses proved that degradation of the cementite lamellae in the steel took place under the influence of sulfur. The results of the analyses shown in Table 4.3 indicate that large amounts of sulfur were present in the degraded particles situated beneath the IS of the tube, down to a depth of 3.5 mm. The greatest concentration of sulfur was found 0.2 mm beneath the surface and the concentration gradually decreased towards the middle-wall. The degraded particles were also enriched in trace elements: manganese, chromium and silicon.

The destruction of cementite under the influence of sulfur resulted in the release of carbon from the cementite lattice and the penetration of the carbon into the steel interior. Complete decarburisation of the metal layers situated close to the IS was noted and an increase of the carbon content up to about 0.3 wt. % in the middle-wall was recorded using the EPM technique.

The results obtained from the tensile testing are shown in Table 4.4 They indicate that in-service degradation of the steel structure resulted in a decrease in mechanical properties of the steel: ultimate tensile strength (*UTS*), elongation (*E*) and yield stress (*YS*) in particular. In some specimens, *UTS* and *YS* values below the minimum level required by the standard at 20 °C were noted.

The Charpy-V impact data are presented in Table 4.5. Energy to fracture (*EF*) and brittle fracture area (*BFA*) at 20 °C are mentioned. It can be seen that the steel was embrittled during service. Some after-service specimens showed 50% of brittle fracture area, indicating 20 °C to be the ductile–brittle transition temperature of the material.

4.5 Conclusions

Elevated temperature damage to refinery furnace tubes may consist of corrosion-dependent failures and temperature-related defects connected with degradation of the steel microstructure and creep damage. At high temperatures, a steel tube may fail due to deformation and creep fracture even at a stress level well below the yield stress, whereas at low temperatures corrosion and microstructure degradation processes prevail. These two ranges can be determined by yield strength and rupture stress *vs* temperature curves [8].

The extent of the probable damage and the remaining life time of the furnace tubes operating at the creep range may be assessed on the basis of material examinations, including replica techniques, and confirmed taking into account the service records and corrosion rates, according to Appendix E of the American Petroleum Institute's Recommended Practice [8].

Table 4.3 Chemical composition of cementite within pearlite grains in the steel determined by SEM, EDS

Specimen/distance from the IS in mm	Number of grains	Chemical composition in wt. % (variation range/ **average**)				
		Fe	Mn	Cr	Si	S
After service/0.2	21	53.52–92.98	0.00–16.39	0.00–11.37	0.00–9.49	1.42–26.97
		80.57	**2.78**	**3.76**	**2.81**	**10.07**
After service/0.8	18	71.76–96.92	0.00–9.59	0.00–9.50	0.00–7.45	0.44–12.17
		87.92	**1.71**	**2.51**	**2.33**	**5.53**
After service/1.5	16	84.38–97.82	0.00–2.94	0.00–3.02	0.00–8.57	1.01–5.97
		92.90	**1.18**	**0.95**	**2.66**	**2.31**
After service/2.5	25	93.90–99.73	0.00–3.48	0.00–1.84	0.00–0.48	0.10–3.03
		97.02	**1.28**	**0.44**	**0.07**	**1.19**
After service/3.5	12	91.96–98.57	0.72–1.63	0.25–2.00	0.04–2.33	0.00–3.16
		97.01	**1.17**	**0.69**	**0.48**	**0.65**
As received	10	96.75–97.94	1.16–1.61	0.00–0.53	0.23–0.40	0.31–0.83
		97.74	**1.41**	**0.17**	**0.32**	**0.36**

Table 4.4 Tensile properties of the as-received and the after-service specimens

Material	$UTS^{20°C}$ (MPa)	$YS^{20°C}$ (MPa)	$E^{20°C}$ (%)	$YS^{400°C}$ (MPa)
As-received	477	360	31	205
After-service	452, 440, 406, 418, 448, 445	256, 256, 205, 197, 238, 234	26, 24, 24, 28, 31, 30	127, 129, 145
Standard requirements	440–540	Min. 255	Min. 21	Min. 127

Table 4.5 Charpy-V impact data of the as-received and the after-service specimens at 20 °C

Material	*EF* (J)/ *BFA* (%)
As-received	66/ 0, 68/ 0, 65/0, 58/ 0
After-service	50/ 50, 51/ 50, 44/ 50, 50/ 50, 44/ 50, 42/ 50, 50/ <50, 51/ <50

In this chapter, damage to carbon steel operating in the refinery furnace below the creep range in a desulfurised naphtha environment has been presented. Because of low sulfur content in the naphtha (0.3 ppm) and low stream temperature (200 °C), it could be assumed before the service that the sulfide corrosion rates of the steel would be negligible. It could also be expected that at a metal skin temperature not exceeding 400 °C, no degradation processes of carbide phase/cementite in the steel would take place.

Low sulfide corrosion rates of the steel, classically defined by thinning of the furnace tube walls [9], were confirmed by in-service ultrasonic measurements of the tubes. No metal thinning up to 6 years of service was recorded, followed by a corrosion rate 0.16 mm/year during the next 3 years, and no metal thinning during the last two years. However, after 4 years of service, high attenuation coefficients of ultrasonic waves in the steel were recorded and a further increase in attenuation up to 9 years was noted. Because the degradation of the steel structure was not probable and the presumable mechanical properties assessed by the WIT method were within standard requirements, it was thought that some damage to the IS of the tubes occurred or that carbon-bearing deposits on the IS formed. This assumption seemed to be confirmed by the decrease in the attenuation coefficients during the last two years when the operation temperature and the metal skin temperature were distinctly lower.

Destructive examinations of the tube disassembled after 11 years of service revealed only a thin and fragile sulfide scale layer on the IS. It has been proved that sulfide corrosion of the steel was manifested by the thinning of the tube wall only to a small degree. However, under the influence of sulphur, a broad internal degradation of the chemistry and structure of the steel took

place. The sulfur entered the steel and displaced inward, reaching the middle-wall of the tube. The sulfur penetrated the steel along grain boundaries of pearlite and ferrite, and along interfacial ferrite/ cementite boundaries in pearlite grains. Cementite particles were transformed by the sulfur into quasi-crystalline precipitates, rich in sulfur and trace elements: manganese, chromium and silicon. The precipitates gradually disappeared with the increasing sulfur content that resulted in the formation of a cementite-free decarburised layer beneath the surface. In this layer, inclusions of internal iron sulfide scale formed.

Such unexpected degradation of steel under the influence of sulfur was responsible for the increase in the attenuation coefficients during the first 9 years of service. The decrease in attenuation noted after the next 2 years proved that at lower temperatures the process of the internal damage of the steel was suppressed.

The mechanical testing results of the ex-service tube exhibited some embrittlement of the steel. However, the yield strength of the steel, which was the most important indicator of safe service, fulfilled the standard requirements at 400 °C.

Because of the low service temperature and no expected further damage to the steel, it was decided to put the furnace tubes into operation for another two years, until the nearest shutdown inspection season.

4.6 References

1. R.A. White and E.F. Ehmke, *Materials Selection for Refineries and Associated Facilities*. NACE, Houston (1993), p. 131.
2. R.D. Townsend, in *Microstructure and Mechanical Properties of Aging Materials*. The Minerals, Metals and Materials Society, Warrendale, Pennsylvania (1993), p. 1.
3. H. Watanabe, Y. Ohkita, S. Kawakami and A. Kanaya, in *Microstructure and Mechanical Properties of Aging Materials.* The Minerals, Metals and Materials Society, Warrendale, Pennsylvania (1993), p. 243.
4. J. Stefanowicz, Z. Konieczny, A. Ratajczak, Z. Żuraszek, *Przegląd Mechaniczny*, XLIV, No. 6, (1985), p. 10.
5. J. Stefanowicz, Z. Konieczny, A. Ratajczak, Z. Żuraszek, *Przegląd Mechaniczny*, XLIV, No. 7, (1985), p. 8.
6. *Material Testing Reports No.: W-692-042 (1992), W-0692-0120 (1994), W-0697-0120 (1997), W-0699-0120* (1999) in Refinery of Gdańsk, Poland. WITEX S.A. Poznań, Poland.
7. *Steels for Elevated Temperature Service*. Polish Standard PN-75/H-84024.
8. *API Recommended Practice 530*, American Petroleum Institute, Washington, D. C. (1988).
9. *Corrosion in the Petrochemical Industry*. ASM International, Materials Park, Ohio (1995), p. 330.

5

Troubleshooting corrosion problems in HF alkylation units

M. ROCHE, Total S.A., Exploration & Production, France,
C. GRENET, Total France, Raffinerie des Flandres, France and
M. RICHEZ, Total France, Centre Européen
de Recherche et de Technique, France*

5.1 Introduction

Elf Antar France operates two alkylation units using hydrofluoric acid as catalyst, one at Donges refinery, which has been in service since 1982, the other at Grandpuits refinery, which has been in service since 1979. These units use the UOP process. Other HF alklylation units are in operation in the Elf Group or associated company refineries abroad: one at Milford Haven (Wales) using the Phillips process, another at CEPSA Algeciras refinery in Spain, using the UOP process. The purpose of these units is to convert the butenes produced by crackers to alkylate on the basis of the simplified reaction: $iC_4 + C_4 \rightarrow C_8$. This reaction requires the presence of a concentrated acid as catalyst; HF or H_2SO_4. Because of the great toxicity and highly aggressive nature of HF, this type of alkylation requires many precautions, and systematic operation and maintenance. Basic information is provided in the literature [1–4]. The purpose of this chapter is to provide an overview of Elf's experience, essentially in France, and of their efforts to try to increase the service life of the most critical items of equipment.

5.2 Corrosion problems in HF alkylation units

5.2.1 Surface corrosion

As a result of the formation of a protective layer of iron fluorides, carbon steel is resistant to HF as long as its water content does not exceed 3% and the temperature 70 °C. Most equipment is built of this material. However, if the velocity of the fluids at the surface of the metal is more than 1 m/s, the protective layer can be removed by erosion. Thus, when process conditions are too aggressive, the use of nickel-based alloys becomes essential: Alloy

*This chapter was written when the authors were employed by Elf Antar France and it has not been updated.

400 is widely used as a lining in vessels, for mechanical parts (pumps, valve components, etc.), gaskets, exchanger tubes and thermometric wells, and even as solid material for the HF regeneration column. Alloys B2 and C276 are also used for some pump impellers and internals of valves.

The very large quantity of iron fluorides formed in new equipment or when units are restarted after chemical cleaning or mechanical descaling, can give rise to major fouling causing operating conditions to worsen progressively (excessive pressure drop at low points in the pipework, clogging of column plates, obstruction of exchanger tubes, blocking of valves, etc.). It may be useful to choose a nickel-based alloy to extend the duration of a run for some tube bundles which are very sensitive to clogging.

Careful drying of the unit before start-up and monitoring of the circulating acid water content are obviously essential in order to limit the production of iron fluorides and to protect equipment from corrosion. A maximum water content of 20 ppm in the feed is generally specified at start-up. Regular HF regeneration is essential, partly to eliminate the polymers which become dissolved in the acid and partly to keep the water content as low as possible.

5.2.2 Hydrogen embrittlement

HF, like H_2S, promotes penetration in the material of atomic hydrogen created by acid corrosion at the surface. Hydrogen embrittlement can then lead to the formation of cracks or blisters. A number of precautions are therefore taken when manufacturing the equipment:

- Clean steel plates with low level of inclusions (S < 30 ppm).
- Hardness limited to <200 HB and monitored.
- Equivalent carbon limited to 0.40%.
- Stress relieving treatment on welds, cold-hardened areas, exchanger tube bends, etc. When heat treatment is applied, the requirement V + Nb < 0.1% is recommended. Relaxation treatment for Alloy 400 components (welds, formed sheets, exchanger tube bends) is also recommended. This treatment cannot always be effectively applied to heterogeneous welds with Alloy 400 used for repairs, which crack frequently. Experience at Donges shows that compliance with a maximum equivalent carbon of 0.33% can avoid heat treatment. High strength materials are sensitive to stress cracking, e.g. threaded rods should preferably be to ASTM A193 B7M, i.e. B7 which has undergone heat treatment for 201 to 235 HB hardness with a yield strength (Re) > 552 MPa.

5.2.3 Experience at Donges and Grandpuits refineries

The corrosion problems experienced at Donges and Grandpuits are described below, subdividing the unit into eight sections:

(i) *Prefractionating section:* The products separated are of commercial quality and no corrosion risk exists.

(ii) *Drying section:* The isobutane cut from prefractioning and the olefins cut are dried in dryers containing alumina. The dryers are regenerated when the water content of the effluent exceeds 10 ppm. Drying limits the amount of water introduced into the reaction area. No particular deterioration of the equipment has been observed, except on the water side of cooling bundles.

(iii) *Reaction section*: The feed contacts the concentrated acid in the shell of two cooling exchangers. The reaction is exothermic. The water flow is adjusted so that the reaction temperature remains below 40 °C. The only incidents encountered in these items of equipment involve defects at expanded tube to plate connections in exchangers. Where this is the case, concentrated acid passes into the cooling circuit and causes vigorous corrosion of the tube plate. To limit this hazard, the tubes are expanded and welded and not just expanded. In new bundles, tube expansion is inspected for tightness after fitting, if possible with helium. If there are any leaks, the presence of HF is immediately detected by analyzers (fluorides and pH) in the cooling water circuit. A shutdown is then planned before serious deterioration occurs.

(iv) *Acid storage and regeneration section:* This section can be subdivided into two parts:

- The HF storage area, at ambient temperature, where no significant corrosion is observed.
- The regeneration area (column and polymer recovery tanks). The regeneration column receives acid containing polymers from the settling drums in the reaction area. The acid is stripped by butane at 170 °C. The regenerated acid is recovered at the top of the column; water and polymers are removed from the bottom. Water is removed in the form of the azeotrope HF/H_2O (40/60%), which is highly corrosive. This column is therefore of solid Alloy 400. It can corrode in the central part of the shell, and on the internals. At Donges, a section of shell was replaced after 14 years service and the trays are replaced at every shutdown. The polymers recovery drum, which has a lower operating temperature (120 °C), is of Alloy 400 clad carbon steel and shows no significant corrosion. Only the potash neutralization tank at Donges shows corrosion pitting at the top, doubtless due to deposits.

(v) *Isostripper fractionating section:* The effluent from the reaction section and the regenerated acid are fractionated in the isostripper into:

- At the top, a cut rich in HF, which is returned to the reaction area.
- A cut rich in iC_4 which is recycled to the reaction section.
- A butane cut which is sent to the reaction section.

- An alkylate cut at the bottom of the column.

This section can be subdivided into two subsections:

- The top of the column and its associated equipment: this equipment is in contact with HF and may be affected by significant corrosion. At the Donges refinery, for example, the isostripper top was replaced in 1994 following corrosion which occurred at the inlet point of regenerated acid. This section of shell and the upper cone were then lined with Alloy 400. Since then, they have performed satisfactorily. The top part of the column is of carbon steel with a reinforced corrosion allowance, and the thickness is measured annually. The exchangers and the top drum are also affected by corrosion and fouling: it has been found necessary to use Alloy 400 cladding and tube bundles (electroless nickel coating is being tried on one of the bundles at Grandpuits).
- The bottom of the column and its associated equipment: this equipment is in contact with alkylate containing residues of HF. Corrosion risks are nevertheless small.

(vi) *HF stripper fractionating section:* The HF-rich cut leaving the top of the isostripper is separated in a settling drum. The HF liquid phase is returned to the reaction section, while the butane-rich hydrocarbons phase is processed in a stripper. Residues of hydrofluoric acid leave from the top, while a butane cut, which is treated in defluorinators or passed to the acid regeneration column, is obtained from the bottom. All this section is likely to be affected by corrosion. The top of the column and the column feed settling drum, where HF concentrates, are particularly exposed (already replaced and/or protected by Alloy 400 cladding).

(vii) *LPG processing section:* The various LPG cuts coming from the reaction section, which still contain residues of HF, are neutralised before being sent to storage or to other units. Treatment is by passing over alumina at 220 °C to decompose combined fluorine, followed by neutralisation with potash. The equipment in this section is in good condition and shows little corrosion. The most sensitive items of equipment are the tube bundles, where corrosion develops on the water side (poor circulation), and on the product side when deposits form at the surface. In fact defluorination of LPG produces acid and water as a result of reaction with alumina. Thus, in the exchangers located between the defluorinators and the potash neutralization column, fluorides in the presence of water can give rise to corrosion beneath deposits, if condensation occurs (as happened at Grandpuits). The frequency with which the alumina bed is replaced should be adjusted to maintain a residual fluoride content low enough at the outlet of the defluorinators.

(viii) *Neutralization section:* It is in a potash neutralisation column that the flare gases are neutralized. This section operates at low pressure (0.5 bar). There is a high corrosion risk if there is any malfunction. This is the situation at the Grandpuits site, where the top line from the column is replaced every three years (electroless nickel lining of the line is to be carried out together with a modification of the internals).

5.2.4 Role of residual elements in steel

In October 1992, an LPG leak containing 1.25% of residual HF occurred on the overhead line from the fractionator to the depropaniser at the Milford Haven unit; the line was made of ASTM A106 Grade B steel. This incident gave rise to a thorough investigation of the cause. Analysis showed that the leaking pipe, which had a residual thickness of 2 mm and was covered with 12 mm of fluorides, had an appreciably higher residual element content (Ni + Cr + Cu = 0.49%) than the adjacent, less corroded pipe (0.14%), which had a residual thickness of 5 mm and was covered with 2 mm of fluorides. This finding led the licensor (Phillips) to recommend a criterion for the choice of steels which should be used in contact with HF [5]:

$$Ni + Cr + Cu < 0.2\%$$

It should not be forgotten that the requirement in ASTM A106 Gr.B is:

$$Cr + Cu + Ni + Mo + V < 1\%$$

and $Cr < 0.40$, $Cu < 0.40\%$, $Ni < 0.40\%$.

This precaution, which is thought to reduce corrosion rate by a factor of 3 to 4, no doubt by improving the protection provided by fluorides, is included in the 1995 revision of NACE publication A171, which states that the adverse effect of residual elements increases with temperature [2]. NACE Technical Committee T8-20 (corrosion in HF alkylation units) has not, however, decided to adopt this recommendation because sufficient consistent information is lacking. In the short term, when operators find corrosion in their units they usually check the validity of this criterion. Thus, when this was found to be verified on a depropaniser feed line at Amuay's Lagoven refinery, where a flange with a high residual content became severely corroded, CAPCIS carried out electrochemical tests to explain it [6]. A joint research project to continue this work (effect of residual elements, microstructure and welds) is now being performed. In addition to figures from Milford Haven, Table 5.1 provides the results of a few analyses performed at Donges and Grandpuits. They show that no element has high residual levels in cases where there is little corrosion, but the opposite is not true. Compliance with the criterion does not always guarantee that a high level of corrosion will be absent. It would seem that there are exceptions, but in general the criterion tends to be correct

Table 5.1 Elf's experience on the effect of residual elements

		Ni + Cr + Cu (%)		
Unit	Location	Equipment	Corroded	Not corroded
Milford Haven	Fractionator to depropaniser	3″ pipe A 106 Gr.B	**0.49%**	0.14%
Donges	Head of isostripper	(inlet) pipe	**0.40%**	0.13%
		shell	0.09%	
		gusset		0.07%
		tray supports	0.06%	0.09%
Grandpuits	Head of isostripper	pipes		0.13%
		elbows	**0.31%**	

when the HF content is high; the opposite tends to occur when the HF concentration is low, because of a galvanic corrosion effect. A communication to Eurocorr '98 concluded that the criterion was not valid in excessively dilute medium (1% HF), it being thought that such a level of dilution was possible in areas of maximum corrosion [7]. It is nevertheless felt that corrosion tends to start in the presence of the HF/H_2O azeotrope, and that extreme dilutions are only likely during the start-up period. In the current discussion, Elf's position is to attempt to use steels that comply with the criterion when making repairs. Nevertheless, obtaining supplies of this type of steel on the French market has proved to be very difficult, because of the widespread manufacture of steels from recycled scrap in electric furnaces.

5.3 Leak prevention in an HF alkylation unit

5.3.1 Special measures

The high volatility and toxicity of HF mean that very special precautions have to be taken to ensure that circuits are completely tight at flanges and valves. The essential nature of the measures taken in the acid section of the unit can be listed as follows:

- Tightening of boltwork using a torque wrench is the rule.
- The condition of joint surfaces is of 'smooth finish' quality.
- All valves subject to inspection are tested with gas oil (testing of the body, tests upstream and downstream of the opening); in circuits containing acid, internals are of solid Alloy 400, bearing surfaces of PTFE, gland packing of graphite, threaded rods of B7M.
- An HF-sensitive paint (colour change) is applied to all flanges and stuffing boxes.

5.3.2 'Alkylation' type spiral gaskets

The type of gasket initially specified for the acid sections in the UOP alkylation units at Donges and Grandpuits was a spiral carbon steel gasket, cadmium-plated with Alloy 400 herringbones and PTFE linings. During the first runs, a corrosion problem resulted in leaks and meant that many of the joint faces had to be remachined during shut-downs (more than 250). The corrosion started from the inside of the flange and managed to extend beneath the gasket. This damage can be explained by the presence of a cold dead zone which encourages the retention of acid condensation water. The solution consisted of adding an internal barrier of PTFE supported on the centering ring. This modification was tested on several joints during a run and was finally adopted for both refineries. Extensive use of this new gasket has made it possible to reduce remachining considerably (less than 10), and also the retightening of flanges when in operation.

5.4 Protective coatings tests

5.4.1 Resistance of organic coatings

Of the non-metallic materials, PTFE is wholly resistant to HF and hydrocarbons, but its use as a coating for repairs made *in situ* is virtually impossible because its polymerisation requires heat treatment under conditions which are hardly compatible with the facilities normally available when working on plant. Epoxy coatings do not withstand HF, even when present in traces.

5.4.2 Potential of several coatings

A search of coatings which could significantly increase the service life of carbon steel in areas affected by corrosion has been undertaken by Elf since 1998. The coatings investigated were intended to:

- Solve the problems of local thinning appearing in certain items of equipment, by application *in situ* during shut-downs.
- Find a less expensive solution than Alloy 400, particularly for those exchanger tubes most threatened by corrosion and clogging.

A first series of 1 month autoclave tests in deaerated liquids consisting of HF + 5% or 10% of water heated to 70 °C at 6 bars yielded the results summarised below:

- Low corrosivity for bare carbon steel in the medium containing 5% water. Higher corrosivity when water was 10% (around 0.5 mm/year), but less than in the most corroded parts of the unit (approximately 1 mm/year, assuming permanent contact with the corrosive medium).

- Good resistance of Alloy 400 and of solid nickel 200 (with nevertheless a few micropits).
- Poor resistance of Alloy 400 coating applied by thermal arc spraying.
- Poor resistance of electrolytic silver-plating cold applied using a pad (disbonding, severe attack on the underlying steel).
- Good behaviour of factory-applied electroless nickel coating: adhesion maintained, a deliberate scratch did not give rise to any galvanic corrosion. Some micropits or microcracks were however observed on some metallographic sections. Thermodiffusion treatment of the coating (at 650 °C) is favourable for regularity of surface pattern. After a model test which demonstrated the excellent performance of the coating when tubes were pulled into baffle plates, it was decided to build an exchanger whose constituent parts would be coated with thermodiffused electroless nickel. This exchanger has just been put into service.

In addition to these, a second series of tests has just been completed with other coatings such as electrochemical nickel sulphamate applied by pad (very low porosity), Alloy 400 hypersonic sprayed, Alloy 625 plasma sprayed, and composite cold-applied coatings of the vinyl-ester type containing glass flakes or graphite. These tests were performed using HF/H_2O azeotrope under the same temperature and pressure conditions. They confirmed the extreme corrosivity of this medium: 15 mm/year in the case of steel, 0.6 mm/year in the case of nickel 200. Alloy 400 offered satisfactory resistance on its own, but the porosity was still sufficient to bring about corrosion of the underlying steel. Solid parts of the composite coatings resisted well in their mass, but they cracked. Other tests will be carried out under more realistic conditions.

5.5 Conclusions

- HF alkylation units require special operating experience because of the risks of corrosion to certain items of equipment and the safety aspect associated with the toxicity of HF.
- In France these units are still operated on the basis of three-year runs between scheduled inspections, but even these are difficult to achieve without shutdowns caused by operating problems in the acid sections.
- The relaxation of French regulations with a view to greater flexibility should nevertheless mean that items of equipment that are not affected by significant corrosion risks could only be inspected every six years; this applies more particularly to the ‘non-acid’ sections.
- Most of the problems have now been satisfactorily identified and the risks have been controlled by inspection, both when in operation and during shutdowns. Equipment is repaired and replaced before incidents having an effect on safety and the environment occur.

- The accumulation of experience has made it possible to solve some problems and reduce maintenance costs, for example through the development of suitable tight gaskets.
- The development of protective coatings, e.g. electroless nickel or some cold-applied composite coatings, is one way forward for the technical and economic optimisation of this type of unit.

5.6 References

1. API RP 751, *Safe Operation of Hydrofluoric Acid Alkylation Units*
2. NACE Publication 5A 171, *Materials for Receiving, Handling, and Storing Hydrofluoric Acid*
3. T8-20 Task Group NACE, A survey of plant practices and experience in HF alkylation units, *Corrosion '94* NACE, Paper N° 511
4. Nidi Publication N° 443, *Corrosion resistance of nickel-containing alloys in hydrofluoric acid, hydrogen fluoride and fluorine*
5. H.H. Hashim, W.L. Valerioti, Effect of residual copper, nickel, and chromium on the corrosion resistance of carbon steel in hydrofluoric acid alkylation service, *Corrosion'93* NACE, Paper N° 623
6. G. Chirinos, S. Turgoose, R. Newman, Effects of residual elements on the corrosion resistance of steels in HF, *Corrosion'97* NACE, Paper N° 513
7. M. Somervuori, M. Tavi, O. Forsén, Effect of residual elements on corrosion behaviour of carbon steel in dilute hydrofluoric acid, *Eurocorr '98*, Utrecht

6

Corrosion in the overhead system of a sour water stripper

O. FORSÉN and J. AROMAA, Helsinki University of Technology, Finland; T. HAKONEN and K. RINTAMÄKI, Neste Oy, Finland

6.1 Introduction

The purpose of a sour water unit is to pretreat refinery process waters by removing hydrogen sulfide, ammonia, and other gaseous impurities before the actual waste water treatment. This pretreatment step is essential to reach the target purity level of the waste water. Gaseous hydrogen sulfide and ammonia that have been removed from the process water are treated after the sour water unit because of atmospheric pollution control requirements. The sour water unit is an important tool, and it is essential for complying with atmospheric pollution regulations.

Condensation of gaseous compounds in the overhead system of the sour water unit causes corrosion problems. The heat exchanger and the following reflux water line are subject to corrosive water containing hydrogen sulfide and ammonia. To solve the corrosion problems, a spiral type heat exchanger was changed into a lamellar one and the material was changed from AISI 316L austenitic stainless steel to SAF 2205 duplex stainless steel. This did not solve the corrosion problems and the heat exchanger has been replaced by another one made from 904L. The reflux water line is made from carbon steel and some leaks have been repaired. This work is based on a Masters thesis which concentrated on the corrosion problems caused in the sour water unit overhead system and on the possible effects of process changes. The main goal was to verify the applicability of selected materials and, if necessary, to find a suitable construction material for the heat exchanger.

All crude oils contain sulfur and nitrogen. During refining, some of the sulfur converts to hydrogen sulfide and some of the nitrogen to ammonia. Both compounds are toxic and they will dissolve in steam and water used in the refining process. These waters are separated from the hydrocarbon stream in water separation stages of each unit process; they are called sour waters and must be treated accordingly in the sour water unit. Here, hydrogen sulfide is converted to elemental sulfur, and ammonia is decomposed into hydrogen and nitrogen. The Finnish term for sour water translates as ‘acid

water', which has meant that the main problem has sometimes been misunderstood. The pH of a sour water can vary between 1 and 9, and usually it is slightly alkaline with a pH of about 8–9.

The sour water unit at Porvoo Works is a part of the SuperClaus sulfur removal process licensed by Comprimo B.V. The cleaning of sour water is effected by a physical method. The cleaning is done in an evaporator column. The sour water is preheated and fed to the top of the column and it flows downwards. The stripping gas, steam, flue gas, air, etc. is fed from below. As the partial pressures of gaseous impurities decrease, their solubilities decrease and the gases go to the overhead system. The stripped process water goes to the waste water treatment. The overhead offgases containing hydrogen sulfide and ammonia are condensed and treated. This sour gas contains a large amount of water vapour. The purpose of condensation is to prevent transport of water to the sufur recovery. All sour waters are collected to a storage vessel, which has a retention time of 12 hours for oil separation. It has a capacity corresponding to 24 hours operation. The water is pumped to two stripping columns. The sour water has an average composition of 6000 mg/l H_2S and 4000 mg/l NH_3 with pH varying between 8 and 9. The treated water contains 0–5 mg/l H_2S and 0–50 mg/l NH_3.

The heat exchanger arrangements of the stripping columns are different. One of them has a two tube and shell heat exchanger with an overhead vessel. The gas design temperature is 120 °C before and 96 °C after the heat exchanger. The cooling water temperature after the heat exchanger is 40 °C. The other stripping column has a single lamellar heat exchanger with design gas temperatures of 115 °C before and 96 °C after, and the cooling water temperature after the heat exchanger is 45 °C. The condensates are corrosive, especially the first droplets that form. The stripper return-waters from the heat exchanger can contain 70 000 mg/l H_2S and 60 000 mg/l NH_3. These concentrations are more than ten times higher than their average concentrations in sour water. One attempt to reduce the corrosivity of the return water is to dilute them by additional spooling water feed. The use of spooling water increases the unit load and consumes energy.

The damage history of the overhead heat exchanger is rather short. The first heat exchanger was a spiral type made from AISI 316L stainless steel. The heat exchanger had been in operation since 1972 and during reconstruction of the sour water unit in 1993 no damages were noticed. In May 1994 a leak was detected and during the subsequent inspection it was decided that the heat exchanger was so corroded that repair was not worthwhile. An identical heat exchanger was installed but replaced in May 1995 with a duplex stainless steel SAF 2205 lamellar one. After three months of operation, corrosion damages were detected in the duplex stainless lamellar heat exchanger and so the second spiral heat exchanger was repaired and re-installed. In January 1996 a leak was detected and large areas of the lower part of the spiral were

badly corroded. In March 1996 a second lamellar type heat exchanger, this time made from austenitic 904L, was installed. In addition, the system for spooling water was installed. Leaks have been detected in the return line made from carbon steel. All corrosion damages have been classified as uniform corrosion.

As previously indicated, the main corrodent in sour water is hydrogen sulfide. The conditions are reducing. Ammonia will increase the pH of the solution. When the pH is high enough, the sulfide exists as HS^- ion. Dissolved cyanide, chloride and oxygen will also affect the corrosivity. Cyanides will destroy protective iron sulfide layers and chlorides will accelerate corrosion. High temperature, low pH and increase of oxygen concentration will increases the risk of stress corrosion cracking. Nascent hydrogen as a result of cathodic reaction can cause hydrogen damage. According to the cyanide analysis, the concentration of cyanide is less than the detection level (2 mg/l) and so it is not causing corrosion. The concentration of chloride ions is very low, but as with every real process, the risk of accidental chloride increase is possible. Therefore danger of pitting, and crevice corrosion and stress corrosion cracking of stainless steels cannot be excluded.

6.2 Experimental procedures

The test materials were heat exchanger and piping construction materials that had been used, i.e. austenitic stainless steels AISI 316L and 904L and carbon steel. Duplex stainless steel SAF 2205 was not tested in the field, but, in addition, titanium was tested. The materials selection study consisted of two tasks: the localised corrosion resistance of stainless steels was studied in the laboratory under simulated conditions and all materials were tested in the actual process using electric resistance probes and corrosion potential monitoring. Laboratory tests were made by using the so-called 'Avesta cell' [1]. Only the effect of chlorides was tested by using an ammonia solution with pH of 11–12 and a chloride concentration of 100 mg/l, without hydrogen sulfide. The sample surface temperature was 75 ± 2 °C. In the cyclic polarisation curves, the polarisation scan rate was 10 mV/min and the threshold current density 5 mA/cm^2.

Field experiments were made by using Metal Samples ER-probes and CorrOcean measuring devices and software. Corrosion probes were installed in stripper return water and sour gas lines, i.e. the water returning from the water and gas separation by condensation in the heat exchanger and the gas going to the sulfur treatment. Installation of probes in the heat exchanger itself was not possible. Each test material was monitored for a time period of about one month. The effect of spooling water feed to the heat exchanger was also studied by monitoring the corrosion of the probes.

6.3 Test results

The corrosion potential of AISI 316L was about –40 mV vs. SCE whereas the corrosion potentials of SAF 2205 and 904L were –210 to –220 mV. The polarisation curve of AISI 316L shows a clear hysteresis loop, but those of the others do not (Fig. 6.1). In visual inspection of the samples, the AISI 316L was pitted, but no corrosion was detected in SAF 2205 and 904L.

The ER probe results of carbon steel in return water showed clearly that uniform corrosion happens. At first the spooling water was on and the corrosion rate was 4.6 mm/year. When the water feed was stopped, the corrosion rate increased to 7.3 mm/year, but returning the water feed did not bring it down. When the same procedure was repeated, the corrosion rate increased further to 10.5 mm/year. The corrosion rate of carbon steel had a tendency to increase over time and the wire probe failed after 23 days. However, in the sour gas line, the water content of the gas is very low and no condensation happens. The corrosion rate of carbon steel in sour gas was virtually zero.

The corrosion of AISI 316L in return water proceeds in short intervals. The steel has some tendency to passivate, but the reaction product layer spalls off every time (Fig. 6.2). The shape of the curve resembles that of the semilinear scale growth seen in high temperature corrosion, i.e. short successive

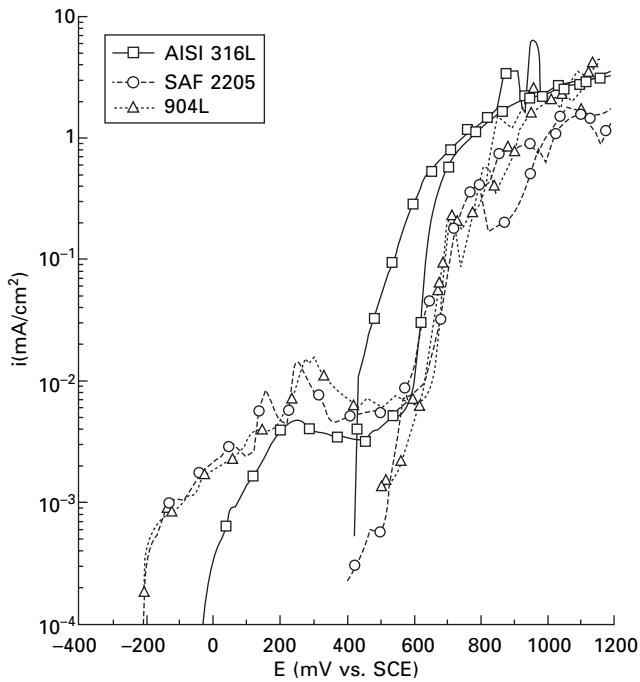

6.1 Cyclic polarisation curves in ammonia solution.

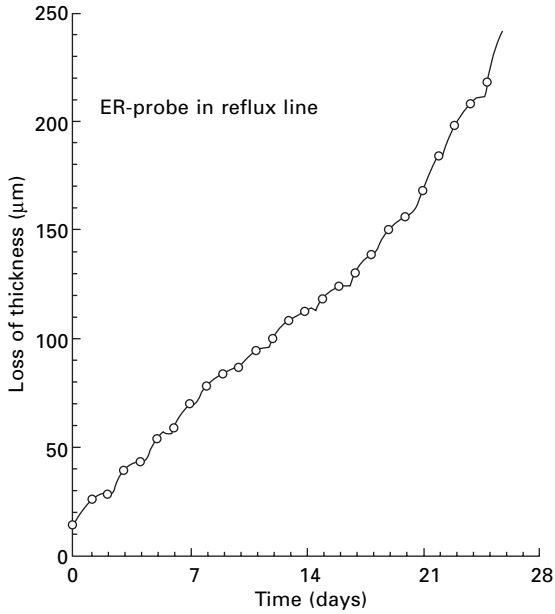

6.2 Loss of thickness of AISI 316L probe in return line.

periods of parabolic rate law. The corrosion rate at the normal operating temperature range was 2.2–2.6 mm/year, and it was not dependent on spooling water. Without spooling water and at higher temperatures, the corrosion rate was 5.5 mm/year.

The corrosion rates of 904L and titanium were low. The spooling water had no effect on the corrosion of 904L and its corrosion rate during 22 days test was virtually zero. Titanium corroded slightly at the beginning of the test. The calculated corrosion rate was about 0.05 mm/year.

Corrosion monitoring indicated that the redox potential was low (–440 mV and –610 mV vs. SCE in two separate periods). The concentration of reducing impurities was higher when the spooling water was off, and then the redox potential was lower. The corrosion potential of steel was –740 to –710 mV. It was not affected by spooling water. The corrosion potentials of austenitic stainless steels AISI 316L and 904L were –430 to –420 mV or about –400 mV, when the redox potential was lower. The corrosion potential of titanium was first –450 mV, but in the more reducing solution it decreased to –520 mV. It is assumed that titanium did not remain passive.

6.4 Discussion

The conditions in the sour water system are most severe when the redox potential is low and the pH is high. The main corrosion problem is general

corrosion caused by HS^- ions in combination with ammonia, resulting in pH > 10. ER-probe results show that carbon steel and AISI 316L are not suitable for heat exchanger or return water line use. The duplex stainless steel SAF 2205 was ruled out due to its poor behaviour in service. Austenitic stainless steel 904L did not corrode in ER-probe tests and it has given good service experience. Titanium could have been an alternative, but as the conditions are reducing, it was ruled out, though ER-probe tests did not indicate significant corrosion.

The corrosion potentials of stainless steels were compared with Pourbaix diagrams for Fe–S–H_2O, Cr–S–H_2O and Ni–S–H_2O systems [2]. The corrosion potential of carbon was in the stability area of FeS_2. As sulfide scales are seldom protective, corrosion of steel was rapid. The corrosion potentials of stainless steels were in the stability areas of Fe_2O_3 and Cr_2O_3, but the dominant nickel compound was soluble $HNiO_2^-$. This does not mean that nickel is selectively dissolved, but may explain the different behaviour of AISI 316L and 904L in ER-probe tests. A higher amount of alloying elements is required to maintain a stable reaction product layer. The stable form of titanium was TiO_2, but fear of incomplete passivation and hydrogen problems have excluded titanium.

The units operated without troubles for twenty years. Only after process changes did the corrosion problems begin. Existing systems could not handle the more corrosive conditions resulting in the need for heavier inspection and later in shutdown and repair. The large initial cost of the 904L heat exchanger has been justified by continuous trouble-free operation. The use of spooling water had no effect on the corrosion of 904L and so it could be discontinued and thereby save energy costs.

6.5 References

1. R. Qvarfort, New Electrochemical Cell for Pitting Corrosion Testing, *Corrosion Science* 28 (1988), pp. 135–140.
2. EPRI, *Computer-calculated potential–pH diagrams to 300 °C. Volume 2: Handbook of diagrams*. Project 1167–2 Final report 1983.

7

Corrosion of aboveground storage tanks for petroleum distillates and choice of coating systems for their protection from corrosion

A. GROYSMAN, Oil Refineries Ltd, Israel

7.1 Introduction

Crude oil is a mixture of various types of hydrocarbons. Crude oil may contain water, some salts (NaCl, $CaCl_2$, $MgCl_2$), hydrogen sulfide and microorganisms. Petroleum products include hydrocarbons which are not aggressive to alloys under ambient conditions. In spite of this, all petroleum products (especially gasoline, naphtha, kerosene, gasoil and fuel oil) give rise to the corrosion of tanks, pipes and pumps, made of mild steel. The objectives of the work described in this chapter are:

- A study of the corrosion of the aboveground storage tanks (AST) containing petroleum products and crude oil after 25–58 years of service.
- A study of the reasons for the corrosion and its mechanism in the AST.
- An examination of the resistance of industrial coating systems in the gasoline mixtures (with added aromatic solvent or oxygenate) and salt water under accelerated laboratory conditions.

7.2 Experimental procedures

(i) The thicknesses of various parts of the AST were measured by means of a thickness gauge (26DL of 'Panametrics'). The accuracy was ± 0.01 mm.

(ii) The corrosion form and rate of the mild steel coupons were determined in laboratory tests in mixtures of petroleum distillates and water. Petroleum distillates were gasoline (98 octane), naphtha and kerosene. The ratio of water to organic phases varied from 0.02 to 90% vol. The laboratory experiments lasted 7 days. Weight loss method was used.

(iii) The morphology and chemical content of rust was determined by means of a Scanning Electron Microscope and Energy Dispersive Spectroscopy (SEM & EDS).

(iv) The concentration of dissolved water in the petroleum products after 7 days corrosion tests was measured by means of the Karl-Fischer method.
(v) The resistance of coating systems was examined under laboratory accelerated conditions in three phase solution of the following content: aqueous (3% NaCl + 0.2% $NaBO_3$), organic (gasoline with 60% vol. of toluene or 15% vol. of MTBE – Methyl tert-butyl ether) and vapor phase.

7.3 Calculations

Corrosion rate of various parts of the AST was calculated according to the formula:

$$K = (D_o - D_i)/t \quad [7.1]$$

where: K = corrosion rate, mm/year; D_o = original thickness of plates, mm; D_i = measured thickness of plates after t years of service, mm; t = service period of AST, years.

The minimum acceptable shell plate thickness for tanks was calculated according to API Standard 653 [1].

7.4 Results and discussion

7.4.1 Gasoline aboveground storage tank

The thicknesses of the shell plates of the gasoline AST measured after 55 years service, the calculated minimum acceptable shell plate thickness, and the corrosion rates are presented in Figures 7.1 and 7.2 (the numbers of the

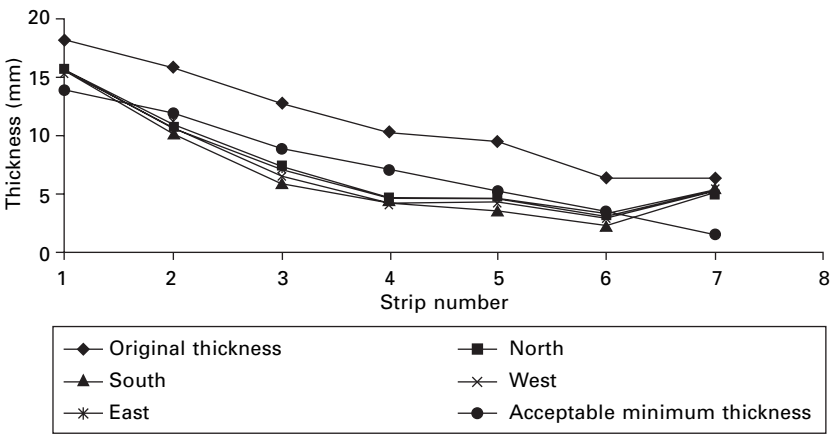

7.1 Thickness vs. Strip number, gasoline tank, 55 years.

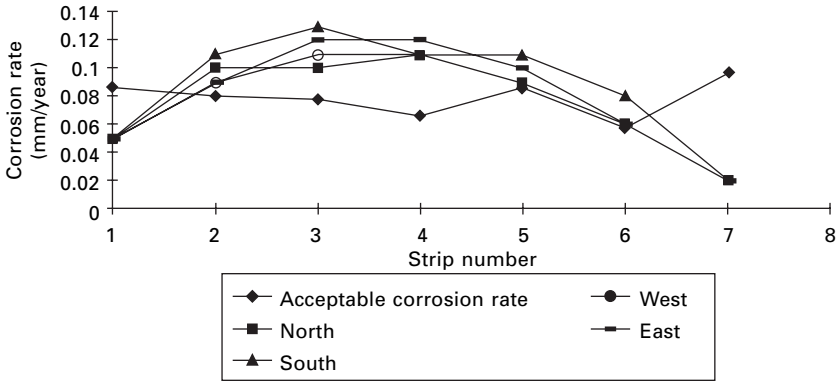

7.2 Corrosion rate vs. Strip number, gasoline tank, 55 years.

shell plates begin from the bottom – lower plate). The thicknesses of the shell plates Numbers 2–6 after 55 years of service were less than the minimum acceptable thickness calculated according to the standard [1]. The measured corrosion rate of the inner surface of the gasoline AST depends on the shell plate number and the direction (south, north, west and east). The average corrosion rates were 0.04–0.13 mm/year. Corrosion rate as a function of the shell plate (strip) number is described by means of curves, with maximum on the 3^{rd}–4^{th} strips (see Fig. 7.2). Maximum corrosion occurred on the southern part of AST, probably because of considerable fluctuations of temperature during the day – night cycle. As a result of direct exposure to sunlight, temperatures were higher on the southern part of the AST, and the solubility of water increased.

When the temperature decreased in the evening, the solubility of water in the gasoline diminished. Polar molecules of water separate from the gasoline – water mixture onto the steel surface, and an electrochemical mechanism takes place in the presence of dissolved oxygen. The inner side of the shell and the floating roof had suffered most from corrosion. Usually the floors were in good condition. Therefore, the corrosion mechanism is probably related to the temperature fluctuations, presence of dissolved water and oxygen in the gasoline, and periodical water separation on the steel shell surface of the tanks.

7.4.2 Study of mild steel corrosion in petroleum distillates

In order to define the reasons and mechanism of steel corrosion in petroleum products, experiments were done with mild steel coupons in mixtures of distillates and water, under laboratory conditions. After exposure of the coupons in the mixtures during 7 days of intensive agitation, corrosion rates and form were determined. The results show that the ‘critical’ concentration of water

in the petroleum product must be reached for the severe corrosion of steel to take place (Fig. 7.3).

There is a correlation between the corrosion rate of the steel and the water concentration in the gasoline. A similar phenomenon was found in mixtures of naphtha and kerosene with water. The 'critical' concentration of water in gasoline is 200 ppm, in naphtha it is 1000 ppm. The general corrosion rate in the pure (without water) gasoline, naphtha and kerosene is 0.002–0.004 mm/year. Injection of the 'critical' water content into gasoline, naphtha and kerosene results in a drastic increase of the general corrosion rate to 0.6–0.8 mm/year.

SEM & EDS analysis of corrosion products formed on the coupons during lab tests and on the inner side of AST plates show the presence of iron and oxygen in the rust. This fact confirms the electrochemical mechanism of mild steel corrosion in gasoline and in the other petroleum products that were investigated; that is, corrosion under water and oxygen attack in the presence of hydrocarbons. The corrosion mechanism is similar to the corrosion under a water film in the atmosphere during 'wetting – drying' cycles [2, 3] or splash zone corrosion [4].

Just as the atmosphere supplies water and oxygen to the steel surface during atmospheric corrosion, gasoline supplies water and oxygen to the steel surface in contact with gasoline. The solubility of oxygen in hydrocarbons is higher (60–70 ppm) than in water (8 ppm) [5]. Therefore, oxygen diffuses from the organic phase to the water phase according to the solubility in each phase and the concentration gradient up to oxygen saturation in the aqueous phase. The water drops saturated with oxygen separate from the organic phase on the steel surfaces because of the high polarity of water molecules, and the electrochemical corrosion of steel then takes place.

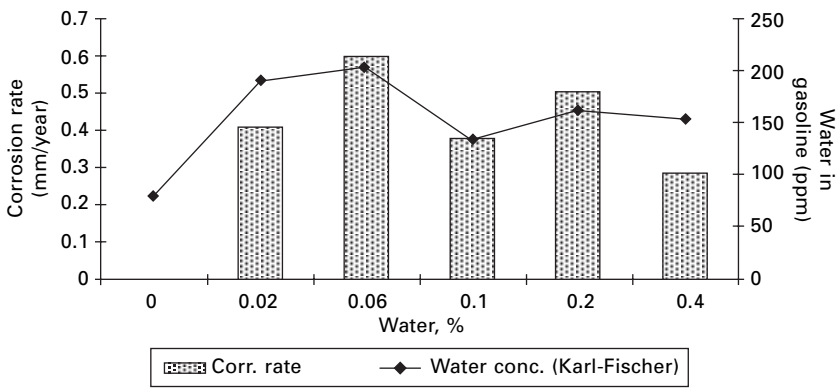

7.3 Corrosion rate of mild steel in mixtures of gasoline/water and water in gasoline vs added water.

7.4.3 Gasoil aboveground storage tanks

The inner side of the shell had not suffered from corrosion. The inner side of the roof was attacked by hydrogen sulfide which evolves from the gasoil. The content of sulfur in the corrosion products formed inside of the roof reached up to 50% by weight. Pitting corrosion occurred at a rate of about 1 mm/year.

The floors were attacked by microorganisms. Shallow pits were formed on the floor after 25 years of service. Localized corrosion rates reached up to 0.5 mm/year. Heterotrophic bacteria and sulfate-reducing bacteria (SRB) were found in the sludge.

7.4.4 Heavy fuel oil storage tanks

The inner side of the shell has hardly suffered from corrosion. The corrosion rate varied from 0.006 to 0.014 mm/year. There was no influence of geographic direction. The main corrosion problem in these tanks occurred on the inner side of the roofs and to a lesser extent on the floors. Usually the roofs were changed every 10–15 years because of severe corrosion, and even holes had formed [6]. The average corrosion rate of the roof was 0.5 mm/year. Corrosion products formed on the inner side of the roof consisted mainly of iron sulfides. This means that hydrogen sulfide was responsible for the severe corrosion of the roof. The second region suffering from corrosion in the heavy fuel oil tanks was the floor. Sludge was formed during storage of the fuel oil. Large quantities of heterotrophic microorganisms and SRB were found in the sludge. These microorganisms were responsible for the localised attack in the floors. The analogous microbiologically induced corrosion was determined in the floors of the crude oil tanks after 25 years of service.

7.5 Examination and choice of coating systems for the protection of the AST from corrosion

The API RP 652 standard [7] recommends the use of coating systems based on two generic types, epoxy and polyester. This standard does not deal with the following items:

- The standard does not relate to the coating systems based on zinc-rich, silicone-epoxy, polysiloxane and polyurethane materials.
- The standard does not relate to the petroleum products containing oxygenates (for example, MTBE – Methyl tert-butyl ether) or aromatic solvents (toluene, benzene and xylene), added to increase the octane number. It was recommended to re-examine the resistance of the polyester coatings in the fuels containing oxygenates [8].

- The standard only concerns the protection of bottoms, and does not relate to the protection of inner side of roofs and shells.

In order to make up these deficiencies, 45 industrial paint and coating systems from 28 manufacturers were examined under laboratory conditions in a three phase medium: 3% NaCl + 0.2% $NaBO_3$ aqueous solution, gasoline with 60% vol. toluene or 15% vol. MTBE added (the organic phase), and the vapor phase. The panels with the coatings were placed in the beakers containing the aggressive solution in such manner to enable examination of the resistance of the coatings in each of the three phases: aqueous, organic and vapor. Visual examination was made every 7–10 days according to the standards [9, 10]. The experiments lasted 3 months. The solutions were refreshed every month.

The results showed that in most cases defects on the coatings appeared during the first month of exposure in the aggressive three phase medium. Twenty four coating systems failed because of various type of deterioration (mainly blisters) in the liquid (aqueous or organic), the vapour phase, or both phases. Only 21 of the 45 investigated industrial coating systems were resistant to the gasoline (with aromatic solvent and MTBE added) and salt aqueous solution. They were (thickness in microns in parentheses): inorganic zinc silicate (150), epoxy (200–1500), silicone-epoxy (250), epoxy-phenolic (300), polysiloxane (300), coal tar epoxy (400), polyurethane (500), epoxy reinforced with glass and mineral flakes (500), glass filled epoxy with rust convertor, inhibitor and passivator (600), vinyl ester with acrylic copolymer (1250), epoxy vinyl ester (1500) and vinyl ester (1500). These systems were included in the new Paint Specification of the oil refinery. Some of them, based on the epoxy systems, were introduced into practice for the protection of the inner floor surfaces of ASTs which are currently in service.

7.6 Conclusions and recommendations

(i) A corrosion survey of the inside surfaces of ASTs containing various petroleum products and crude oil was made after 25–58 years of service and showed the following:
   - Gasoline and naphtha ASTs: the shell plates and floating roofs suffer from severe electrochemical corrosion in the presence of dissolved water and oxygen.
   - Gasoil, kerosene, fuel oil and crude oil ASTs: the floors and the roofs suffer severely from corrosion. Hydrogen sulfide is the main cause of the severe corrosion of the roofs.

   Microbiologically induced corrosion is the cause of the severe localised corrosion of the inside of the floors in these ASTs.

(ii) Laboratory investigation of mild steel corrosion in the mixed ‘petroleum

distillate – water' (with various ratios) showed the existence of 'critical' concentrations of water in the petroleum distillate above which corrosion drastically increased.

(iii) Twenty-one (of 45 investigated) coating systems are included in a new Paint Specification of the oil refinery for the protection of the insides of ASTs containing petroleum distillates with oxygenates and aromatic solvents.

7.7 References

1. API Standard 653, *Tank Inspection, Repair, Alteration, and Reconstruction*, 1991.
2. Tomashov N.D., Development of the Electrochemical Theory of Metallic Corrosion, *Corrosion*, 1964, Vol. 20, No. 1, P. 7t–14t.
3. T. Tsuru, A. Nishikata and J. Wang, Electrochemical studies on corrosion under a water film, *Materials Science and Engineering*, 1995, Vol. A198, P. 161–168.
4. *Metals Handbook, Corrosion*, Ninth Edition, ASM International, 1987, Vol. 13, P. 893.
5. *Solubility data series. Oxygen and ozone*. Vol. 7, Ed. Battino R., Pergamon Press, Oxford, 1981, 519 p.
6. A. Groysman, Corrosion in Equipment for Storage and Transportation of Petroleum Products, *Chemistry & Chemical Engineering*, No. 32, March 1998, p. 13–23 (Hebrew).
7. API Recommended Practice 652, *Lining of Aboveground Petroleum Storage Tank Bottoms*, 1991, 10 p.
8. API 1132, *Effects of Oxygenated Fuels and Reformulated Diesel Fuels on Elastomers and Polymers in Pipeline Terminal Components*, 1994, 36 p.
9. ASTM D714 – 87. *Standard Test Method for Evaluating Degree of Blistering of Paints*.
10. ASTM D610 – 89. *Standard Test Method for Evaluating Degree of Rusting on Painted Steel Surfaces*.

8

The use of coatings to prevent corrosion in process vessels operating at elevated temperatures and pressures

A. D. GASKIN, Belzona Inc., USA

8.1 Conventional materials of construction and their limitations

Process equipment within the oil, gas and petrochemical industry is constructed of base materials selected to resist the operating conditions known to exist during its predicted service life.

The basic materials of construction used for process equipment are generally:

- *Carbon steel:* Used for most applications where corrosion is limited and operating conditions are not too demanding. In most cases, corrosion allowances are built into the original design to give an acceptable service life. Coatings can be used to give additional protection to immersed areas provided the operating temperatures are within the capability of the coating material, generally around 100 °C maximum.
- *Overlaid carbon steel:* The most common means of upgrading carbon steel to give additional corrosion capabilities is to overlay with stainless steel. This process is often more cost effective than utilising stainless steel and the overlaid surface gives excellent corrosion protection but can still be affected by other mechanisms of corrosion such as chemical attack, stress corrosion and bacterial corrosion. Additional problems can arise if the overlaid surface is locally damaged, resulting in the occurrence of severe galvanic corrosion.
- *Austenitic stainless steel:* While giving better performance than overlaid materials, can still suffer the problems associated with stress corrosion and bacterial attack. Cost and manufacturing difficulties are also deciding factors when adopting this approach to corrosion resistance.
- *Duplex stainless steel:* Utilised in the oil, gas and petrochemical industry for critical equipment construction where erosion and corrosion resistance is required. However, it can be susceptible to galvanic and crevice corrosion effects. Manufacturing difficulties and repair capability, combined with high cost, limit the use of this material for large constructions.

Design engineers are continually faced with a dilemma when selecting materials of construction, particularly as they are always faced with getting an acceptable material based on the 'predicted' operating conditions and at the lowest acceptable cost. The cost limitations of new construction often result in Maintenance Engineers having to solve the resultant problems in much more difficult environments and within the pressures of limited resources, difficult accessibility and limited time constraints.

The use of cold-curing protective coatings has been an alternative approach to upgrading the corrosion resistance of base materials such as carbon steel. However, the limitations of these materials until now have restricted their use to less aggressive applications. Often, the selection of a coating is not restricted by the operating conditions but by other factors such as decontamination processes, where to gain access to vessels for inspection or maintenance purposes, steam at temperatures up to 200° C or chemical washing is used. The temperatures and pressures associated with these processes exceed the capability of most coatings and this almost always results in coating failure and re-application following a shutdown. These limitations are also considered at the design stages and often discount coatings as a means of protection.

8.2 Characteristics and limitations of traditional coating systems

8.2.1 Thermo-setting unsaturated polyesters

Characteristics

- Low cost, readily available materials.
- Good application characteristics.

Limitations

- Shrinkage results in brittleness.
- Incomplete backbone functionality reaction during polymerisation resulting in open/permeable structures.
- Sensitive to oxygen during cure, resulting in incomplete reactions and reduced performance.
- Limited heat resistance under immersion conditions, as the ester linkages are attacked by hydrolysis.
- Health and safety limitations due to styrene (co-reactant and diluent) flammability.
- Poor storage stability.

8.2.2 Formulated glass flake unsaturated polyesters and vinyl esters

Formulated glass flake unsaturated polyesters and vinyl esters are in general use as corrosion protection systems, with good chemical resistance, and immersion temperature resistance up to 100 °C. Some reinforced systems are claimed to perform up to 125 °C, although experience has shown severe permeation at elevated temperatures, leading to blistering and rapid failure.

Characteristics

- The inclusion of graded flake glass properly orientated and applied reduces the inherent permeability of the resin system to create good barrier protection and corrosion resistance.

Limitations

- The high film build nature of the system creates difficulty in manual application.
- Application using airless spray requires additional diluent, which does not fully react in the matrix, thus leading to permeation and blistering when immersed.
- The brittle nature of the system makes it susceptible to impact damage and it has inherently poor cavitation resistance.
- Unsuitable for applications where chemical compositions are constantly changing:
  - Low cross-link density systems susceptible to swelling in solvents.
  - Ester linkages hydrolyse under acid conditions.
  - Glass flake filler attacked by strong alkalis.

8.2.3 Thermosetting polyurethane resin systems

Material types such as thermosetting polyurethane resin systems are designed to have inherent flexibility, tear strength and impact resistance, which in many cases are required by the coatings.

Characteristics

- Fast curing system.
- Cross-link densities variable by design to give rigid, semi-rigid or flexible coatings.
- Good cavitation resistance.
- Good abrasion resistance.

Limitations

- Limited heat resistance.
- Immersion resistance limited, particularly in aqueous solutions, as the urethane linkages are attacked by hydrolysis due to coating permeability
- Sensitive to moisture before, during and after cure (foaming).
- Require primers for acceptable levels of adhesion.
- Limited storage stability.

8.2.4 Traditional epoxy resin systems

Epoxy resin systems can be formulated in many ways, depending upon the ultimate properties, application characteristics and in-service conditions.

The most commonly available systems are:

(i) Solvent/water based epoxy resin systems: These systems are normally formulated with ease of application in mind or, in the case of water based epoxies, the overriding factor is one of health and safety or environmental factors.

These systems are normally low film build as they rely upon the evaporation of the carrier (solvent or water) to effect the cure of the system. These systems are normally used for non-immersion applications due to their high permeation rates and are more commonly referred to as 'paints' rather than coatings.

Limitations

- Low film build.
- Considerable shrinkage during cure.
- Extended cure times.
- Susceptible to blistering in immersion conditions due to solvent entrapment.
- Limited immersion temperature resistance.

(ii) Solvent free epoxy resin systems: These materials are designed to have high mechanical strength and have negligible shrinkage. Pigments and fillers are also used in these types of resin systems to perform specific functions, as well as provide a barrier to liquid ingress. Fillers include spherical, lamellar and mixed particle shapes to increase corrosion resistance, abrasion resistance and erosion resistance.

Limitations

- Low reactivity at low temperatures.

- High viscosity and poor application characteristics.
- Limited immersion temperature resistance.

8.3 Development of high-temperature resistant coatings

With the ever increasing demands of the industry, the limitations of cold curing polymeric coating systems have restricted the use of such materials to basic corrosion protection applications. However, the inherent properties and formulating capabilities of epoxies, coupled with the obvious cost benefits, could provide engineers with viable alternatives to traditional materials of construction for protection of vessels and fluid flow equipment. Developing technology including the availability of new resin systems and catalysts which can be formulated by specialist chemists to design such materials is now becoming available. After considerable Research and Development investment, coupled with extensive in-house and independent testing, such systems are now available.

Development work was carried out in two phases:

Phase 1: Utilising modified phenol epoxy novolac technology to design a product to withstand immersion temperatures in aqueous/hydrocarbon fluids up to 130 °C. This was completed in 1994.
Phase 2: Increasing the immersion temperature resistance up to 185 °C by further developments using enhanced resins and chemically bonded fillers.

Two years of extensive in-house and independent testing have now been completed with substantial projects undertaken. The system has also undergone extensive independent testing by Shell Expro and found to be the only coating system tested which will withstand a combination of immersed temperatures of 130 °C at 30 bar pressure.

8.3.1 Phase 1 – Modified phenol epoxy novolac coating experience

Modified phenol epoxy novolac coating technology has been available commercially since 1994. This system provides a viable alternative to traditional materials of construction, and experience to-date has shown that the system is capable of performing in the most arduous of conditions within process equipment in the Oil and Gas Industry.

Case history

Equipment – Oil and gas test separators
Material of construction – Carbon steel

Coating system – Epoxy novolac
Application date – 1995 and on-going
Specification – Grit blast to SA 2.5 with a minimum 75 μ profile. Apply phenol epoxy novolac system at a total thickness of 1000 μ. Ambient cure period of 36 hr at 25 °C, followed by in-service post-curing.

Testing

Independent testing carried out by Statoil for hydrocarbon service application service in North Sea environment.

Test temperature – 80 °C
Test pressure – 100 bar.
Test procedure – Detailed in Statoil report – Includes cold and hot rapid decompressions.
Results – No failure of *Belzona 1391* phenol epoxy novolac. Further testing being carried out at temperatures up to 120 °C.

Installation list

Statoil, BP, Shell, Mobil, DPC, Amerada Hess, Oryx, Chevron, Phillips, Conoco, Total, PT Badak, Exxon, Amoco, Schlumberger, Halliburton.

8.3.2 Phase 2 – Modified high-temperature system

The modified high-temperature system has been developed over recent years from the modified phenol epoxy novolac system which, though successful at temperatures up to 120–130 °C, begins to break down as the immersion temperature approaches the heat distortion temperature (143 °C), the mode of failure being blistering due to water permeation.

In order to dramatically increase this immersion temperature resistance, it was necessary to further increase the heat resistance of the polymeric binder, and chemically bind the fillers within the material, thus producing a composite system with a highly cross-linked matrix. A variety of methods were attempted. However, a major unconventional breakthrough came midway through the project which permitted upgrading the phenol epoxy novolac system's heat resistance, at the same time as providing chemical bonding sites for heat resistant fillers, dramatically increasing the heat distortion temperature (figures in excess of 280 °C have been recorded), as well as reducing the permeability of the system. The development of this system is now complete and field testing has given excellent results. This finely balanced formulation has undergone further refinements to enhance the application characteristics and increase erosion and chemical resistance.

Testing conditions

In-house testing was carried out using pressure cells similar to those utilised in the Statoil tests. The design parameters of these cells were:

- Maximum cell fluid temperature, 190 °C.
- Maximum pressure rating of cells, 16 bar/225 psi.
- Capable of testing aqueous or well fluids.

(i) Test results on a solvent-based ceramic filled epoxy

Panels were prepared using an airless spray in accordance with the manufacturer's instructions. The manufacturer's specification recommended the product for applications involving immersion in well fluids up to 150 °C. The product was tested at 150 °C in well fluids supplied by Amerada Hess from the Scott Field (North Sea). Permeation and corrosion occurred both in the gas and water phases of the test panel after only 3 days continuous service. Further testing in water only confirmed rapid breakdown at 100 °C after 1 week's immersion.

It was concluded that this system was unsuitable for immersion service at temperatures of 100 °C and above.

(ii) Test results on a solvent-free ceramic filled epoxy

The manufacture's specification recommended the product for applications involving immersion at temperatures up to 120 °C. The product was tested at both 100 °C and 120 °C, with blistering/dis-bondment and rapid breakdown after only one week's immersion of the test panels which were prepared in accordance with the manufacturer's instructions.

It was concluded that this system was unsuitable for immersion at 100 °C. Further testing has confirmed that the coating blisters at temperatures above 70 °C.

(iii) Test results on another modified phenol epoxy novolac system

This product, which has been proven in service and through independent testing by Statoil for its suitability under service conditions up to 120 °C, was tested to evaluate its suitability for applications on *unlagged* vessels. It showed borderline failure at 120 °C.

It was concluded that this system was unsuitable for immersion applications at temperatures above 120 °C on lagged vessels, and above 110 °C on unlagged vessels.

(iv) Test results on modified high-temperature system – Belzona 1591

The newly developed Belzona 1591 system was tested to the limits of the test cells both in lagged and unlagged modes. The panels were immersed in well fluids at temperatures of 150 °C and 185 °C for a period of 10 weeks, during which the cells were depressurised and pressurised to simulate operating conditions associated with oil and gas test separators. Inspection of the panels showed no deterioration of the coating system.

It was concluded that this coating system was suitable for applications involving aqueous solutions or well fluids at temperatures up to 185° C when lagged, and lower when unlagged.

In addition to the in-house testing of this modified high-temperature system (between 150 °C and 185 °C), independent testing was conducted by Shell Expro (UK) at a temperature of 130 °C and 30 bar pressure, together with other proprietary coating systems, and it was found to be the only material tested to withstand these conditions.

8.4 Practical application of the developed coating system

8.4.1 Oil and gas test separators

Material of construction – Carbon steel
Service conditions – Variable depending on well. Operation is between 80 and 135 °C, and pressure up to 100 bar.
Coating system – Modified high temperature epoxy novolac, Belzona 1591
Application date – March 1997
Specification – Surface prepared by grit blasting to SA 2.5 with a 75 mic. profile, after which Belzona coating was applied at a thickness of 800 microns and cured at 25 °C prior to service.

8.4.2 Waste water stripper tower

Material of construction – Carbon steel
Service conditions – Operating temperature of 147 °C, but decontaminated during shutdowns using steam at a temperature of 190 °C.
Coating system – Modified high temperature epoxy novolac, Belzona 1591
Application date – September 1998
Specification – Surface preparation by grit blasting to SA 2.5 with a 75 μ. profile, after which Belzona 1591 was applied at a thickness of 800 microns and cured at 25 °C prior to service.

Current installation list

Saga Petroleum, Shell, Halliburton, Amoco, BP, Kuwait Oil Company, Conoco, Chevron, Adco, Saudi Aramco, Petroleum Development Oman, Exxon Mobil.

8.5 Conclusions

The recent developments in cold-curing coating systems have revealed a means of formulating epoxy resin systems to increase the resistance to permeation of fluids/gases, thus increasing the scope of applications on process equipment up to and above temperatures of 185 °C. By using these coatings, design engineers have the option to downrate the basic materials of construction for new equipment and utilise the system to give resistance to corrosion, erosion, chemical attack, and bacterial and stress corrosion problems at temperatures up to 185 °C, dependent upon the chemicals involved.

Maintenance engineers now also have the option to up-rate existing equipment to cope with more demanding service conditions and replace existing coatings which may be subject to regular replacement due to shutdown requirements (e.g. steam cleaning or chemical washing).

9

The Field Signature Method (FSM) of corrosion monitoring

H. HORN, CorrOcean ASA, Trondheim, Norway and
D. MORTON, iicorr Ltd, Aberdeen, Scotland

9.1 Introduction

FSM-IT (Field Signature Method – Inspection Tool) is a new NDT technology for inspection and monitoring of metallic pipes and structures. The system is designed to monitor internal metal loss, or pitting due to corrosion or erosion with very high sensitivity and without operator variation. Wall changes, such as cracking, are also detected.

9.2 The FSM technology

The Field Signature Method (FSM) is based on feeding pulses of DC current through a selected section of the structure to be monitored. This current sets up an electrical field which is monitored by measuring the small potential differences between measuring pins on the surface of the object. The first measurement (signature) is unique to the geometry of the object. When corrosion occurs, the pattern of the electric field changes and is compared with the signature. Software is used to present the changes and indicates wall thickness reduction or localised corrosion. As sensitivity is related to detecting changes in the electrical field, absolute sensitivity *increases* as the defect develops.

9.3 The FSM principle

An electric field is set up across the area to be monitored, in this case a weld (Fig. 9.1).

Corrosion causes metal loss which causes increased resistance across the weld at that point, while a crack along the weld 'disturbs' the current in a similar manner (Fig. 9.2).

The resultant changes in the electric field are measured and converted back to metal loss figures.

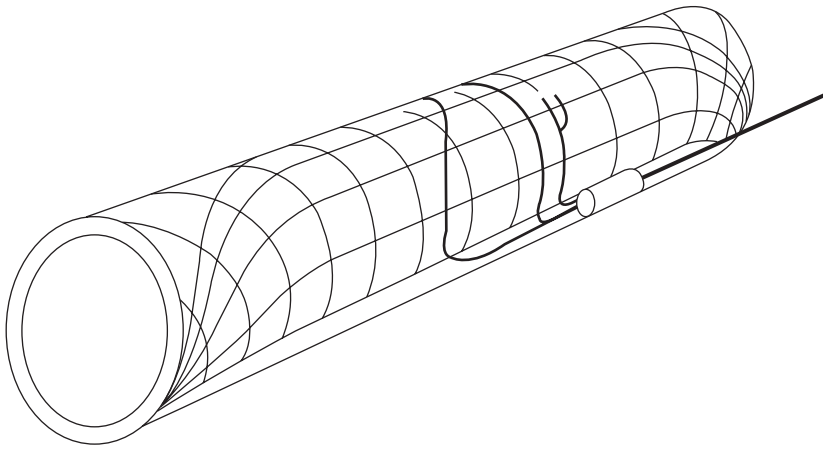

9.1 Electric field across area to be monitored.

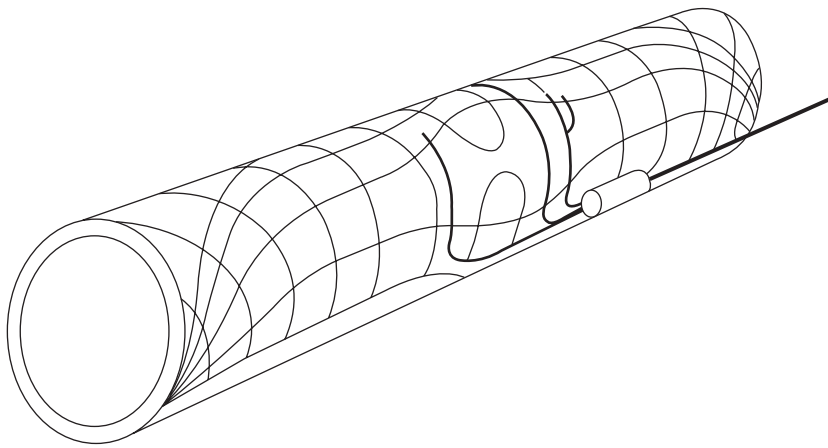

9.2 Metal loss due to corrosion causes increased resistance across the weld, while a crack along the weld 'disturbs' the current in a similar manner.

The main features of the FSM-IT are:

- Corrosion monitoring is done directly on the pipe wall, and therefore gives more direct and representative information than traditional intrusive probes or coupons.
- The system can detect and monitor different forms of corrosion, i.e. both general and pitting corrosion.
- The sensing electrodes (pin matrix) are non-intrusive and do not introduce any risk for leaks of possibly hot and aggressive fluids.
- It can be used for locations where access for traditional probes or NDT is

difficult, and in high temperatures (up to 400 °C), allowing corrosion monitoring during operation.
- Results are not significantly affected by the geometry of the monitored piece, or uneven surfaces. This means that Ts, bends and welds can be monitored directly for weld root corrosion.

The principles for the FSM technology were developed by researchers at SINTEF in Norway in the 80s. It was commercialized by the Norwegian company CorrOcean in 1991 and further developed for use on subsea oil and gas pipelines from 1994. FSM is now used at many locations worldwide, both top-side, underground and subsea. Systems are being operated under various environmental conditions from extreme heat in the desert to extreme cold. The project to adapt the technology for refineries and process plants was commenced in 1997, with financial support from Shell and Elf. FSM-IT now has well over 400 sensing matrices installed.

9.4 FSM equipment

The inspection system consists of a sensing matrix, a portable instrument and PC software. The sensing matrix is made up of a series of pins (electrodes) pin-brazed to the area to be inspected. This fixed pin type matrix provides a very high degree of repeatability in readings. Typically a matrix will consist of 28, 56 or 84 sensing pins in a predefined array. The pin brazing technique is an approved surface weld technique and can be applied at operating temperatures with no detrimental effect on the pipe.

The matrix includes minimal electronics in an interface that includes a unique identification tag for the location as well as microprocessor-controlled measurement circuitry. This equipment is left on the pipe, which means that the location identifies itself to the monitoring instrument to avoid confusion of data and measurement parameters.

The cabling length between the sensing pins and the instrument connection may vary, depending on the application. Generally the instrument connection point is situated at a location that provides safe and convenient access; typically, the cable can be from 3–10 metres for high temperature matrix and 30 m for low.

The portable instrument provides the interrogation of pin matrix and data storage. It will be certified for Zone 2 hazardous area operation and comes complete with extra battery, charger and carrying case. The instrument is menu driven via a touch screen/display and can interrogate up to 50 locations (measurements) before the battery needs re-charging or replacing. A typical interrogation period for one location is around 5 minutes. The instrument also provides self-diagnostic checks and checks the status of the sensing matrix when connected.

The stored data is downloaded to a PC set up with the proprietary FSM-

Trend software package, in a 'safe' environment. Results may be shown in *xy*-plots or 3D plots, and a 'time-lapse' function allows the various results to be shown in sequence to create a 'movie' effect.

New sets of measurements can be taken at different time intervals. This will depend on whether one can find reason to believe that there is an ongoing corrosion activity. The more often readings are taken, the more accurate the results will be, eliminating the uncertainty of noise, and allowing better filtering in the PC software.

Temperature compensation is obviously an issue for a technology where the conductivity of the material can affect the results. After 10 years of use, this problem has been extensively explored. The sensing matrix includes temperature sensors, and the software has a sophisticated temperature compensation algorithm. The area is typically insulated to avoid effects from changes in external temperature. The results are not affected by the hot environment itself or even temperature differentials in the monitored piece, as long as temperature conditions are relatively comparable between measurements. It is therefore standard operating procedure to take all measurements after the actual location has reached its operating temperature.

General sensitivity for the technique is 0.1% of the signal change, but in real life conditions using FSM-IT, 0.5% sensitivity is commonly given as 0.5% of the signal change. For uniform corrosion, the change of resistivity is proportional to the wall thickness reduction, leading to a sensitivity of 0.5% of the wall thickness for general corrosion.

For uneven corrosion, the correspondence in less linear. In a controlled test, the FSM-IT instrument successfully detected the start of pitting at 0.05 mm in a 10 mm thick plate. A corresponding test simulating weld groove damage showed the FSM detecting the weld groove starting at 0.25 mm in 19 mm wall thickness. When the groove reached its 12 mm maximum depth, sensitivity to actual changes had increased so that a change as small as 0.018 mm depth increase was detected.

9.5 Case studies

In recent years several FSM-IT matrices have been installed in various refineries onto pipes and vessels with different steel qualities, diameters, wall thickness and temperatures.

A European refinery monitors high temperature (380 °C) areas such as heater bends in the distillation unit. These areas can show high corrosion rates during processing of opportunity crude. The primary reasons for corrosion monitoring are economical (higher profits from processing opportunity crude, optimised inhibitor dosage and performance), but FSM-IT offered better insight into corrosion conditions due to inspection/monitoring during production. Monitoring during production also eliminated the cost of shutdowns

and repeatedly removing insulation for traditional inspection methods, and the fact that readings are taken at a distance means higher safety for operators.

A European chemical factory had corrosion/erosion problems in an inlet pipe, particularly weld corrosion. Traditional UT was seen to be unreliable because the uneven surfaces and varying wall thickness (not to mention the cramped space) made it a very challenging task for even the most experienced UT operator. Equipping the inlet with a sensing matrix allows the factory to regularly inspect for the onset of corrosion, with more intensive inspection if corrosion occurs. UT is also difficult to apply in high temperature.

The application of the FSM-IT system has since been developed by iicorr Ltd (formerly CorrOcean Ltd) within over 20 refineries worldwide, for monitoring the effects of high temperature Naphthenic acid corrosion, which is an increasing concern with the processing of high acid – opportunity crudes.

In addition iicorr have seen an increasing application of the technology in lower temperature locations i.e. monitoring of Hydrofluoric acid plant and Monel pipework.

10

Disbonding test methodology: Definition of representative test conditions – results of an industry joint research programme

L. COUDREUSE (CLI, France); B. CADILHAC (Total, France); C. DUMONTIER (CMP, France); R. KOERS (Shell, The Netherlands); G. RICCARDI (Nuovo Pignone, Italy); M. ROCHE (Total S.A., France); F. ROPITAL (IFP, France)

10.1 Introduction

In order to define a disbonding test procedure representative of actual service conditions, an industry join research programme has been performed at a European scale. A numerical approach has been used to calculate the hydrogen profiles both for laboratory test specimens and for actual reactors. It has been possible to establish relationships between the maximum amount of hydrogen at the interface and geometrical and exposure or service parameters. Laboratory test conditions representative of the actual situation in a reactor wall can be defined. An experimental testing programme has been conducted for one overlay condition. The results show a good correlation between the maximum hydrogen content at the interface and the disbonding test results. From both the numerical approach and experimental results, suggestions are proposed for a standardisation of the disbonding test procedure.

10.2 Background

The disbonding behaviour of welded or clad overlays has become a problem of great concern in the refinery industry. More and more specifications for hydrotreating reactors are asking for disbonding test qualification. Before 1996 there was not a standardised disbonding test, so that different procedures have been developed. It is difficult to compare results from different laboratories and there is no definition of what can be considered as an acceptable test result. Even the recent ASTM standard (ASTM G146-96) which indicates how to run a test (specimen preparation, test procedure, etc.) does not give indications on what has to be considered acceptable. It becomes necessary to know more about the representativity of a disbonding test in order to define reasonable test conditions.

An industry joint research programme has therefore been conducted at a European scale with the following objectives: (i) Numerical simulation of hydrogen profiles in test specimens and reactors; (ii) Experimental study of

the influence of test parameters on disbonding test results; (iii) Definition of representative test conditions.

10.3 The disbonding phenomenon

Disbonding is due to the conjunction of both hydrogen over-saturation and the presence of sensitive microstructure at the interface between a stainless steel welded or clad overlay and the base material. Over-saturation after cooling is a consequence of the higher hydrogen solubility and lower hydrogen diffusivity in the stainless steel. High hydrogen concentrations can be found in the stainless steel just near the interface [1].

In the case of welded overlays, parameters acting on the phenomena have been studied. It has been shown that disbonding depends on [2, 3]: (i) Materials parameters (base metal chemistry, stainless steel overlay chemistry), (ii) welding conditions (welding process, heat input, post weld heat treatment), and (iii) service parameters (temperature, hydrogen pressure, cooling rates).

For a given overlay process, disbonding depends on the maximum hydrogen content obtained at the interface after cooling down, which, in turn, depends on: Exposure condition (temperature, pressure), cooling rate, thicknesses of both overlay and base material, hydrogen diffusivity in both overlay and base material, and hydrogen solubility in both base material and overlay.

The disbonding tests developed to study the phenomena, which consist of autoclave exposures followed by cooling, are not representative of the actual situation of a reactor. Particularly specimen thicknesses and hydrogen charging conditions are not representative. Numerical calculations are then necessary to estimate the hydrogen profile, both in test specimens and in the wall of the reactor, and to determine if the maximum hydrogen contents obtained in the disbonding test specimens are representative of what can be achieved in the reactor wall.

10.4 Numerical simulation of hydrogen profiles

A numerical programme developed for thermal calculation, THER 2, has been adapted in order to make hydrogen diffusion calculations. Since hydrogen diffusivity and solubility laws are directly related to temperature, knowing the temperature and hydrogen diffusivity and solubility laws, it is possible to determine hydrogen concentration at any point in the structure. The objective of the numerical calculations performed was to establish a relationship between the maximum amount of hydrogen at the interface after cooling and the following parameters: exposure or service temperature, hydrogen pressure, cooling rate, and base material and overlay thickness. A screening design methodology approach has been used in order to minimise the number of calculations. According to the screening design methodology and to consider

second order interactions, 27 calculations have to be performed. The ranges of variation for the different parameters for simulation of test specimens and reactor walls are given in Table 10.1.

Calculations have been made for three combinations of solubility and diffusivity laws (Table 10.2).

From statistical analysis of the numerical simulations performed, relationships between the maximum hydrogen content at the interface and the studied parameters have been established, both for disbonding test specimens and reactor walls. In Figures 10.1(a) and (b), the maximum hydrogen content obtained with the numerical simulation versus the maximum hydrogen content obtained with the prediction formula have been plotted. The formula correlates very well with the numerical calculations.

For a specimen, the main parameters influencing the hydrogen profile are the cooling rate and the hydrogen pressure. Overlay thickness has only a very slight influence. For a reactor, the main parameter is the base material thickness. The influence of cooling rate is not so important as for test specimens.

From the established formula, it is possible to draw an abacus giving the maximum hydrogen contents as a function of several parameters. Examples of such abacuses are shown on Figures 10.2 and 10.3. From these it is possible to define equivalent conditions for a reactor and a specimen. Two examples of such equivalent conditions are given in Table 10.3. These examples show that in order to be representative of actual conditions for a reactor, it is necessary to decrease the severity of exposure conditions for a laboratory test specimen. If the temperature is kept equal to the service temperature, the hydrogen pressure has to be decreased.

Table 10.1 Range of variation of the studied parameters

	T(°C)	P(bar)	Cr (°C/h)	t_{ov}(mm)	t_{bm}(mm)
Test specimen	400/500	50/200	30/675	2/6	20/50
Reactor wall	350/550	50/200	5/100	4/10	50/400

Table 10.2 Combinations of solubility and diffusivity laws used for numerical calculations

		Base material	Overlay
Combination 1	D (m2/s)	$2.4\ 10^{-7}\exp(-2132/T)$	$7.1\ 10^{-8}\exp(-4555/T)$
	S (ppm√bar)	$33\ \exp(-3333/T)$	$8.93\ \exp(-650/T)$
Combination 2	D (m2/s)	$1\ 10^{-7}\exp(-1350/T)$	$6.7\ 10^{-7}\exp(-4555/T)$
	S (ppm√bar)	$23.6\ \exp(-3257/T)$	$8.93\ \exp(-650/T)$
Combination 3	D (m2/s)	$2.4\ 10^{-7}\exp(-2132/T)$	$7.1\ 10^{-8}\exp(-4555/T)$
	S (ppm√bar)	$42.7\ \exp(-3280/T)$	$14.8\ \exp(-1099/T)$

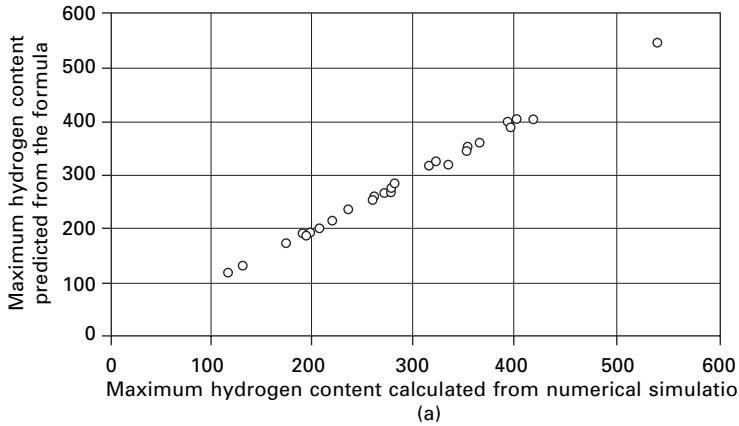

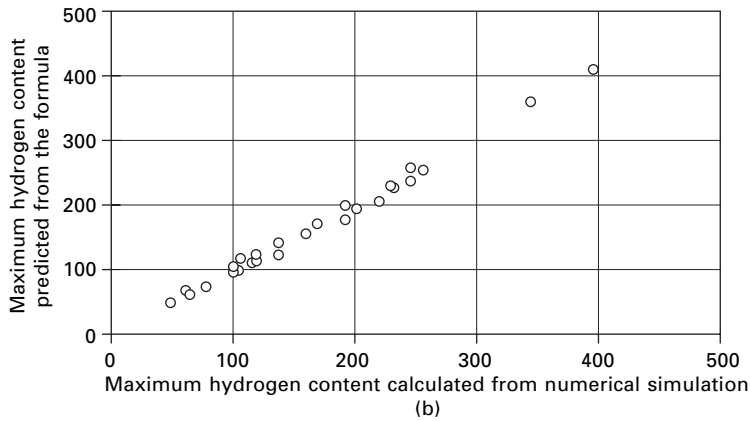

10.1 Comparison of maximum hydrogen contents predicted from statistical formula with maximum hydrogen content calculated from numerical approach: (a) disbonding test specimen; (b) reactor wall.

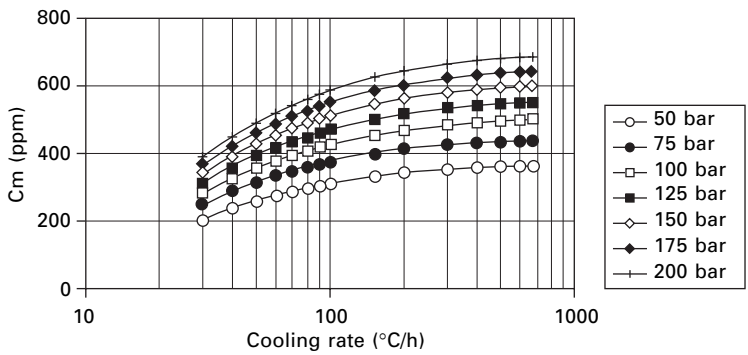

10.2 Maximum hydrogen content (cm) at the interface for a test specimen (thickness: 40 + 5 mm; *T* 475 °C).

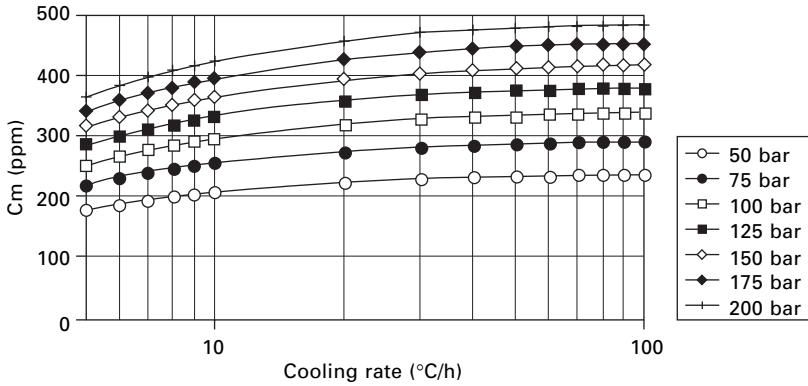

10.3 Maximum hydrogen content (Cm) at the interface for a reactor wall (thickness: 300 + 8 mm; *T* 475 °C).

Table 10.3 Examples of equivalent conditions for a reactor wall and a disbonding test specimen

Reactor wall					Representative test conditions				
t_{bm} (mm)	t_{ov} (mm)	T (°C)	pH_2 (bar)	Cr (°C/h)	t_{bm} (mm)	t_{ov} (mm)	T (°C)	pH_2 (bar)	Cr (°C/h)
300	8	475	150	10	40	5	475	75	100
150	5	450	150	50	40	5	450	75	80

The results presented so far have been obtained with Combination 1 [4] of solubility and diffusivity laws (Table 10.2). Calculations have been made for Combinations 2 and 3 in order to determine the influence of the diffusivity and solubility parameters. Results show that the choice of the combination of solubility and diffusivity laws strongly influences the amount of hydrogen obtained at the interface. This is particularly the case for Combination 2, where the differences between base materials and overlay have been maximised. This is illustrated on Fig. 10.4 where the maximum hydrogen content obtained from Combinations 1 and 2 are compared. The relationship between maximum hydrogen contents calculated from Combination 1 and 2 is a linear one. This means that whatever the choice of diffusivity and solubility laws (in the range of variation considered), definitions of equivalent testing conditions for laboratory tests will be similar.

10.5 Experimental approach

An experimental programme has been conducted to determine the influence of experimental parameters on disbonding test results. As for the numerical calculations, a screening design methodology was used. The experimental

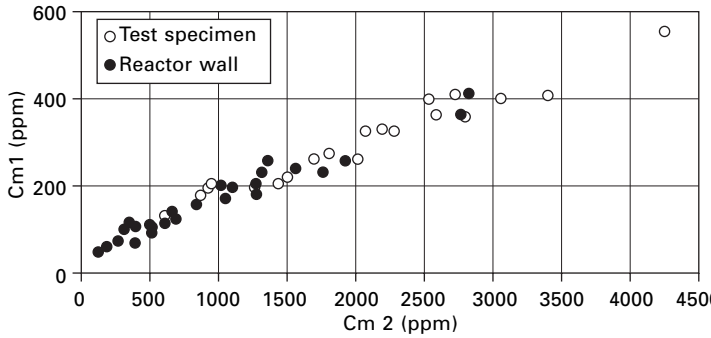

10.4 Relation between maximum hydrogen contents (Cm) calculated from Combination 1 (Cm 1) and Combination 2 (Cm 2) for solubility and diffusivity.

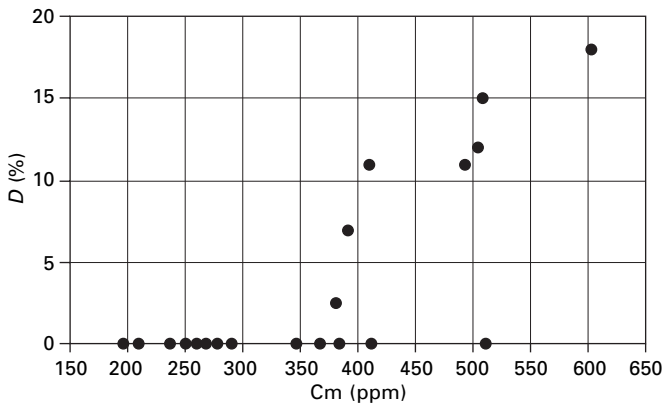

10.5 Relation between disbonding test results (*D*,%) and the predicted maximum hydrogen content (Cm) at the interface.

parameters considered were the following: Hydrogen pressure (50–200bar); temperature (400–500 °C); cooling rate (30–675 °C); base material thickness (20–50 mm). The overlay thickness has not been considered since it appears to be a second order parameter from the numerical calculations.

Tests have been conducted on a coupon prepared by a fabricator. The overlay procedure was representative of industrial practice. Only 6 of the 27 tested specimens gave disbonding. From such results it has been difficult to perform a statistical analysis; however, it has been found that disbonding occurrence depends mainly on cooling rate, pressure and temperature. Surprisingly, no influence of base material thickness has been observed. Figure 10.5 gives the amount of disbonding as a function of the calculated maximum hydrogen content at the interface. There is a correlation between the maximum amount of hydrogen and the occurrence of disbonding. For the

tested overlay, no disbonding was observed for maximum hydrogen contents below 375 ppm. For hydrogen contents higher than 400 ppm, the risk of disbonding is very high. For the lower cooling rate used (80 °C/h), even for the higher predicted hydrogen content (510 ppm) no disbonding was observed. This is probably due to the fact that for such a low cooling rate, the hypothesis of unidirectional diffusion is not valid, and that side diffusion influences the maximum hydrogen content at the interfaces

10.6 Conclusions – definition of representative test conditions

From numerical calculations, relationships have been established between maximum hydrogen content at the interface and geometrical and exposure or service parameters. It is possible to determine test conditions representative of actual situations, equivalent conditions being conditions giving the same maximum amount of hydrogen at the interface. Experimental results obtained for one overlay condition show that the disbonding test result is correlated with the predicted maximum hydrogen content at the interface.

From both numerical and experimental test results the following rules can be used for a standardised test procedure:

- Side overlay is not necessary since it is possible to correlate disbonding test results with calculated maximum amounts of hydrogen.
- The following specimen sizes seem suitable: Cylindrical (diam. 70/80 mm) or Parallelipedic (100 × 50 mm); thickness: 45/50 mm.
- The cooling rate for disbonding tests has to be accelerated to avoid a problem with sides degassing. Cooling rates between 100 and 200 °C seem appropriate.
- The exposure temperature can be kept equal to the service temperature.
- The hydrogen pressure has to be adapted, depending on the size of the reactor. Lower hydrogen pressures have to be used for thinner reactors.

10.7 References

1. H. Okada, K. Naito, J. Watanabe, K. Onishi, and R. Chiba: *Current Solutions to Hydrogen Problems in Steels*, ed. C.G. Interrante and G.M. Pressouyre, ASM, 1982, p. 349
2. A. Vignes, R. Palengat and P. Bocquet: *Interaction of Steels with Hydrogen in Petroleum Industry Pressure Vessel Service*: ed. M. Prager, The Material Properties Council Inc., 1993, p. 139
3. G.M. Pressouyre, J.M. Chaiilet and G. Valette: ibid [1], p. 331
4. K. Smit and P.F. Ivens: ibid [2]; p. 205

Index

acetate replication 27
acid storage section of alkylation units 66
  see also HF alkylation units
assessment procedures
  fired heaters 24–30
  hydrogen attack 44–5
  pipework 39–40
  reactor vessels 31–3
  see also risk assessment
austenitic stainless steel 86

Brinell hardness 58

carbon steel 57–63
  after-service examinations 59–60
  corrosion rate 76–7
  in-service examinations 58–9
  overlaid carbon steel 86
  in process equipment 86
  residual element content 68–9
  sulfide corrosion rates 62–3
  ultrasonic testing 58
carbon transfer reaction 1, 2, 4
carburisation 1, 2–9
  inner-wall 27–8
  internal oxidation equation 7
  occurrence of failures 4–5
  oxide scale failure 5–6, 10
  suppression by adsorbed sulfur 7
Catalytic Reformer Units (CRUs) 18–45
  design life 19
  fired heaters 23–30
  heat exchangers 40–3
  high-temperature hydrogen attack 43–5
  pipework 36–40
  reactor vessels 30–6
  risk assessment 20–3
CCR (Continuous Catalyst Regeneration) units 12–16
cementite destruction 60
circumferential welds 40
coating systems 87–94
  cold-curing coatings 87, 94
  epoxy resin 83–4, 89–90
  formulated glass flake unsaturated polyester 87
  in HF alkylation units 70–1
  high-temperature resistant 90–93
  modified high-temperature 91–4
  modified phenol epoxy novolac 90–1, 92
  thermo-setting polyurethane resin 88–9
  thermo-setting unsaturated polyester 87
  vinyl ester 88
cold-curing coatings 87, 94
Continuous Catalyst Regeneration (CCR) units 12–16
corrosion monitoring 95–9
corrosion rates
  carbon steel 76–7
  and flux measurements 53
  furnace tubes 62–3
  storage tanks 80
  sulfide corrosion 62–3
  and water concentration 82
costs of risk assessment 20
cracking
  and hydrogen concentration 53
  nozzle cracking 34–5, 43
  Type IV cracking in pipework 38–9
creep cavitation damage 27

CRUs *see* Catalytic Reformer Units

decoking 6
design life *see* life and integrity
disbonding test methodology 100–6
drying section of alkylation units 66
duplex stainless steel 86

electron probe microanalysers (EPM) 59, 60
embrittlement of hydrogen 65
energy dispersive spectrometers (EDS) 59–60
epoxy resin coatings 83–4, 89–90
ethylene production 5

ferritic radiant tubes 29
Field Signature Method (FSM) technology 95–9
  equipment 97–8
  principles 95–7
fired heaters 23–30
  assessment procedures
    at shutdown 26–30
    prior to shutdown 24–6
  degradation mechanisms 24
  life and integrity 23–4
  tube design 24
  tube metal temperature 25
  tube wall thickness 25
flux measurement 50–6
  confidence guidelines 50–2
  derivation of hydrogen activity conversion 53–6
formulated glass flake unsaturated polyester coatings 87
FSM *see* Field Signature Method (FSM) technology
furnace tubes 57, 62–3
  see also carbon steel

gas oil storage tanks 83
gaskets 70
gasoline storage tanks 80–1

heat exchangers 40–3
  nozzles 43
  in sour water systems 73, 74
heavy fuel oil storage tanks 83
HF alkylation units 64–72
  corrosion problems by section 65–8
  hydrogen embrittlement 65
  leak prevention 69
  protective coatings tests 70–1
  residual element content 68–9
  spiral gaskets 70
  stripper section 67
  surface corrosion 64–5
high-temperature hydrogen attack 43–5
high-temperature resistant coatings 90–93
hydrocarbons, carbon transfer reaction 1
hydrofluoric acid (HFA) 47, 64
  see also HF alkylation units
hydrogen
  concentrations and cracking 53
  derivation of activity conversion 53–6
  disbonding phenomenon 101
  embrittlement 65
  flux measurement 50–6
  high-temperature hydrogen attack 43–5
  numerical simulation of hydrogen profiles 101–4
  permeation and detection 47–50

identification of risk drivers 22
inner-wall carburisation 27–8
inspection programmes *see* assessment procedures; risk assessment
internal oxidation equation 7
iron fluorides 64–5
isostripper fractioning section of alkylation units 66–7

leak prevention 69
life and integrity
  of Catalytic Reformer Units (CRUs) 19
  of fired heaters 23–4
  of furnace tubes 57
  of pipework 36–9
  of reactor vessels 30–1
LPG processing section of alkylation units 67

metal dusting 1–2, 9–16
  in ferritic radiant tubes 29
  mechanisms 9–12
  oxide scale protection 12
  platformer units failure 12–16

of steel and nickel-based materials 11–12
mild steel corrosion in distillates 81–2
modified high-temperature coatings 91–3
modified phenol epoxy novolac coatings 90–1, 92
monitoring 95–9

Nelson curves 44
neutralization section of alkylation units 67–8
nickel-based materials, metal dusting 11–12
nitrogen content of crude oil 73–4
nozzle cracking 34–5, 43
numerical simulation of hydrogen profiles 101–4

objectives of risk assessment 20
oil and gas test separators 93
overlaid carbon steel 86
oxide scale failure 5–6, 10, 12

pipework 36–40
  assessment procedures
    at shutdown 40
    prior to shutdown 39–40
  life and integrity 36–9
  transfer pipework 39
  Type IV cracking 38–9
platformer units failure 12–16
polyester coating systems 83–4, 87
post-weld heat treatment (PWHT) 38
prefractionating section of alkylation units 65
process vessels 86–94
  coating systems 87–94
  construction materials 86–7
protective coatings *see* coating systems

qualitative risk assessment (level 1) 20–1, 22–3
quantitative risk assessment (level 3) 21–2

reaction section of alkylation units 66
reactor vessels 30–6
  assessment procedures
    at shutdown 32–3
    prior to shutdown 31–2
  in cold-shell service 30
  in hot-shell service 30–1
  life and integrity 30–1
  nozzle cracking 34–5, 43
redox potential 77–8
regeneration section of alkylation units 66
residual element content of carbon steel 68–9
risk assessment 20–3
  costs 20
  decisions on actions 22
  identification of risk drivers 22
  objectives 20
  qualitative analysis (level 1) 20–1, 22–3
  quantitative analysis (level 3) 21–2
  semi-quantitative analysis (level 2) 21
  see also assessment procedures

scanning electron microscopes (SEM) 59
seam welds 39
semi-quantitative risk assessment (level 2) 21
sensing matrix 97–8
shell plate thickness 80–1
solvent-based ceramic filled epoxy 92
solvent-free ceramic filled epoxy 92
sour gas 47
sour water systems 73–8
  cooling water temperature 74
  heat exchangers 73–4
  main corrodent 75
  redox potential 77–8
spiral gaskets 70
stainless steel
  corrosion potential 78
  in process equipment 86
steel
  corrosion potential 78, 81–2
  metal dusting 11–12
  see also carbon steel
storage tanks 79–85
  coating systems 83–4
  corrosion rate 80
  gas oil 83
  gasoline 80–1
  heavy fuel oil 83

mild steel corrosion in distillates 81–2
shell plate thickness 80–1
stress analysis 39–40
sulfide corrosion rates 62–3
sulfur content of crude oil 73–4
surface corrosion 64–5

thermo-setting polyurethane resin coatings 88–9
thermo-setting unsaturated polyester coatings 87
thermodynamics 1–2
transfer pipework 39
transmission electron microscopy (TEM) 59–60
tube design 24
tube metal temperature 25
tube wall thickness 25
Type IV cracking 38–9

ultrasonic testing 58

vinyl ester coatings 88

waste water stripper towers 93
water concentration 82